

Appendix D–FIB-54 Tests

Table of Contents

D.1 Summary	214
D.1.1 Introduction	214
D.2 Girder Design and Construction.....	218
D.2.1 Test Girder Classification.....	218
D.2.2 Test Girder Design	221
D.2.3 Girder Construction.....	231
D.2.4 Material Properties	241
D.3 Test Setup and Procedures	245
D.3.1 Data Collection during Fabrication	245
D.3.2 Load Test Setup and Procedures	246
D.3.3 Coordinate System.....	248
D.4 Instrumentation.....	250
D.4.1 Types and Descriptions	250
D.4.2 Strain Gage Coordinates.....	257
D.5 Results and Discussion: Fabrication.....	265
D.5.1 Strain Data	265
D.5.2 Crack Data.....	287
D.5.3 Prestress Loss	301
D.5.4 Variable Comparison and Discussion.....	302
D.5.5 Summary and Conclusions	304
D.6 Results and Discussion: Load Tests	308
D.6.1 Failure Modes.....	308
D.6.2 Load Test Results	311
D.6.3 Confinement Reinforcement and Bearing Plates.....	335
D.6.4 Variable Comparisons	345
D.6.5 Code Comparisons.....	352
D.7 Summary and Conclusions.....	356

List of Figures

Figure 1–I-Girder highway bridge	215
Figure 2–Cross-section 54-in. deep Florida I-Beam	215
Figure 3–End region reinforcement.	216
Figure 4–FIB-54 end region reinforcing detail (FDOT 2009b)	217
Figure 5–Labeling scheme	218
Figure 6–Specimen labels and graphical descriptions	220
Figure 7–Cross-section of FIB-54.....	221
Figure 8–Strand layout and prestressing details	222
Figure 9–Strand bond and shielding patterns.....	223
Figure 10–Reinforcement for girder H	225
Figure 11–Reinforcement for girder V	226
Figure 12–Reinforcement for girders W and F.....	227
Figure 13–Reinforcement for girder D	228
Figure 14–Reinforcement and bearing plate details.....	229
Figure 15–Confinement reinforcement schemes	230
Figure 16–Cast-in-place deck reinforcement.....	230
Figure 17–Girder orientation during fabrication.....	232
Figure 18–Tension pattern and wire break locations	233
Figure 19–Girder H reinforcement A) Specimen HC and B) Specimen HU.....	233
Figure 20–Girder V reinforcement A) Specimen VC and B) Specimen VU.....	234
Figure 21–Girder W reinforcement A) Specimen WN and B) Specimen WB	234
Figure 22–Girder F reinforcement A) Specimen FN and B) Specimen FB	234
Figure 23–Girder D reinforcement A) Specimen DC and B) Specimen DM	235
Figure 24–Concrete placement and internal consolidation phase 1	235
Figure 25–Concrete placement phase 2	236
Figure 26–Girder finished surface	236
Figure 27–Girders covered with tarps.....	237
Figure 28–Strand release patterns	238
Figure 29–Test girder lifted by crane.....	239
Figure 30–Girder resting on dunnage above stressing bed	239
Figure 31–Girder H on truck prior to transit.....	240
Figure 32–Deck construction A) reinforcement and B) formwork.....	240
Figure 33–Concrete placement A) unloading and B) placement with bucket	241
Figure 34–Test setup.....	247
Figure 35–Test setup at A) bearing and B) load point.....	248
Figure 36–Test specimen and load frame A) top of girder and B) end of girder.....	248
Figure 37–Coordinate system relative to load and supports	249
Figure 38–MS gage A) before protective covering and B) with protective cover and label	251
Figure 39–XS gage installation.....	251
Figure 40–ES gage A) vertical and B) horizontal orientation.....	252
Figure 41–V gage (view from above).....	253
Figure 42–Wire harness and plywood bulkhead.....	253
Figure 43–S gage A) on top of bottom flange and B) close-up	254
Figure 44–LVDT placement and labels	254
Figure 45–LVDT and support frame	255
Figure 46–Girder H and V strands monitored by LVDT	255
Figure 47–Wood frame and LVDTs	256
Figure 48–Girder W, F, and D strands monitored by potentiometer	256
Figure 49–Aluminum brackets and linear potentiometers on strands.....	257

Figure 50–Load cells below hydraulic actuators	257
Figure 51–Girders H and V strand cutting stages	266
Figure 52–Transverse strain HC	266
Figure 53–Flange displaced shapes for specimen HC	267
Figure 54–Shear and moment during release, lifting, storage (prestressing not shown)	269
Figure 55–Girders W and F strand cutting stages	270
Figure 56–Girders W and F strand bond patterns	271
Figure 57–Bearing plate strain	271
Figure 58–Flange displaced shapes specimens FN and FB	273
Figure 59–Displaced shapes specimen WB and WN	274
Figure 60–WB Confinement reinforcement strain at 2 in. and 9 in. from end of girder	275
Figure 61–WN Confinement reinforcement strain at 2 in. and 9 in. from end of girder	276
Figure 62–FB confinement reinforcement strain at 2 in. and 9 in. from end of girder	278
Figure 63–FN Confinement reinforcement strain at 2 in. and 9 in. for end of girder	279
Figure 64–Confinement reinforcement average strain at prestress release	279
Figure 65–Forces in reinforcement and plates after prestress transfer	282
Figure 66–Strain gages for measuring transfer length	285
Figure 67–Transfer length in girders H and V	285
Figure 68–Transfer length in girder F	286
Figure 69–Web splitting and flange splitting cracks	288
Figure 70–Girder H and V cracks prior to load tests	291
Figure 71–Flange splitting crack intersecting outer strand	292
Figure 72–Web splitting cracks in specimens H and V	293
Figure 73–Maximum crack widths in girders H and V	294
Figure 74–Flange splitting crack data in girders H and V	295
Figure 75–Girders W, F, and D web and flange splitting cracks	297
Figure 76–End of bottom flange covered by portion of steel bulkhead	298
Figure 77–Girder F flange splitting cracks in A) specimen FN and B) specimen FB	299
Figure 78–Flange splitting cracks in girders W, F, and D	299
Figure 79–Maximum crack widths in girders W, F, and D	300
Figure 80–Web splitting cracks in girders W, F, and D	300
Figure 81–Girder D flange splitting cracks in A) specimen DC and B) specimen DM	301
Figure 82–Web-shear failure	309
Figure 83–Lateral-splitting failure A) bottom view and B) side-end view	309
Figure 84–Lateral-splitting failure mechanics	310
Figure 85–Bond-shear failure A) bottom view and B) side view	311
Figure 86–Specimen HC load test summary A) shear-displacement and B) crack pattern	312
Figure 87–HC after load testing (cracks shown blue; spalling in brown)	314
Figure 88–Close-up of web crushing and spalling	314
Figure 89–Cracks at end of HC after testing	315
Figure 90–Specimen HU load test summary A) shear-displacement and B) crack pattern	316
Figure 91–Bottom and end of HU after testing	317
Figure 92–Bottom view of splitting cracks in HU	317
Figure 93–Specimen VC load test summary A) shear-displacement and B) crack pattern	318
Figure 94–VC after load test	320
Figure 95–Specimen VU load test summary A) shear-displacement and B) crack pattern	321
Figure 96–Bottom view of splitting cracks in VU	322
Figure 97–Specimen WN load test summary A) shear-displacement/slip and B) crack pattern	323
Figure 99–Specimen WB load test summary A) shear-displacement/slip and B) Crack pattern	325
Figure 100–Specimen FN load test summary A) shear-displacement/slip and B) crack pattern	327
Figure 101–Strut and tie behavior specimen FN	329

Figure 102–Longitudinal splitting cracks on bottom of specimen FN (release cracks shown black; final cracks shown blue)	329
Figure 103–Confinement reinforcement strain specimen FN	330
Figure 104–Specimen FB load test summary A) shear-displacement/slip and B) crack pattern	331
Figure 105–Specimen DC load test summary A) shear-displacement/slip and B) crack pattern	333
Figure 106–Specimen DM load test summary A) shear-displacement/slip and B) crack pattern	335
Figure 107–Strain gage placement girders W, F, and D	336
Figure 108–Confinement stress at shear = 375 kip	337
Figure 109–Confinement stress at ultimate capacity	337
Figure 110–Transverse (x-x) stress profiles at bearing plate centerline	340
Figure 111–Strain gage placement girders H and V	341
Figure 112–Specimens HC and VC confinement reinforcement and bearing plate transverse (x-x) forces due to maximum applied load	342
Figure 113–Bearing plate stress due to applied load	343
Figure 114–Bearing plate force due to applied load	344
Figure 115–Percent of transverse force due to applied loads carried by bearing plate.....	344
Figure 116–Percent of transverse force carried by bearing plate in WB and FB.....	345
Figure 117–Maximum superimposed shear.....	345
Figure 118–Girder D bottom flange cracking A) specimen DC with limited bottom flange cracking in front of bearing and B) specimen DM with severe bottom flange cracking in front of bearing	349
Figure 119–Relationship between strand quantity and end region capacity	350
Figure 120–Comparison of FB (left) and WB (right) (release cracks shown black; final cracks shown blue).....	351

List of Tables

Table 1–Test girder and specimen variables.....	219
Table 2–Specified material properties	231
Table 3–Construction and testing chronology	231
Table 4–Tested concrete compressive strengths	242
Table 5–Prestressing steel properties	243
Table 6–Grout strength for NASP tests	243
Table 7–NASP Test Results.....	243
Table 8–Steel reinforcement properties	244
Table 9–Load test chronology.....	246
Table 10–Instrumentation types and labels.....	250
Table 11–Specimen HC strain gage coordinates	258
Table 12–Specimen HU strain gage coordinates	259
Table 13–Specimen VC strain gage coordinates	260
Table 14–Specimen VU strain gage coordinates	261
Table 15–Specimen WN strain gage coordinates	261
Table 16–Specimen WB strain gage coordinates.....	262
Table 17–Specimen FN strain gage coordinates	262
Table 18–Specimen FB strain gage coordinates	263
Table 19–Specimen DC strain gage coordinates	263
Table 20–Specimen DM strain gage coordinates.....	264
Table 21–Girders H and V fabrication chronology.....	265
Table 22–Tensile strain girders H and V	269
Table 23–Girders W and F fabrication stages.....	270
Table 24–Confinement reinforcement strain after prestress transfer	280
Table 25–Confinement and plate forces	283
Table 26–Girders H and V construction events and inspection dates.....	290
Table 27–Recommended action for web splitting cracks (Tadros et al. 2010).....	294
Table 28–Girders W, F, and D construction events and inspection dates.....	296
Table 29–Prestress losses girders F and W	301
Table 30–Prestress losses girder H, V, and D	301
Table 31–Transverse forces in W and F specimens.....	339
Table 32–Maximum superimposed shear	346
Table 33–Variable comparisons.....	347
Table 34–Material properties for capacity calculations	352
Table 35–Experimental moments and nominal moment capacities.....	353
Table 36–Experimental shear and nominal shear capacities.....	354

D.1 Summary

Confinement reinforcement is placed near the end of pretensioned concrete I-girders to enclose prestressing strands in the bottom flange. Experimental and analytical test programs were conducted to investigate the function of confinement reinforcement and to provide the basis for a confinement reinforcement design model. Five 54-in. deep Florida I-Beam (FIB-54) girders were fabricated and load tested in the experimental program. Each end of each girder had a different combination of variables, which resulted in ten unique test specimens. Variables included: presence or absence of embedded steel bearing plates, quantity and configuration of confinement reinforcement, strand bond pattern, strand quantity, and quantity of horizontal and vertical end region reinforcement. Data were collected during and after prestress transfer to evaluate the effects of test variables on bottom flange cracking. Load tests were then conducted on each specimen (end) to determine the effects of test variables on girder behavior and capacity. Specimens were loaded in three-point bending at a shear span-to-depth ratio of 2.0. Failure modes in the test program included web-shear, bond-shear, and lateral-splitting. Primary outcomes of the research include an improved understanding of the function of confinement reinforcement during prestress transfer and at ultimate load, and an improved understanding the interaction between confinement reinforcement and the other end region variables.

D.1.1 Introduction

Of the almost 12,000 bridges in Florida's public road system, approximately half utilize prestressed concrete as the structural system (FHWA, 2010). Simple-span pretensioned concrete I-girders are the most common type of prestressed concrete structures, and are ubiquitous in Florida's highway system (Figure 1). In 2009, the Florida Department of Transportation (FDOT) introduced the Florida I-Beam (FIB) (Figure 2) for use in highway bridges. The FIB girders "were developed to be more efficient to fabricate, safer to construct, and more cost effect when compared to the [previously] used prestressed beams" (FDOT 2009a).



Figure 1–I-Girder highway bridge

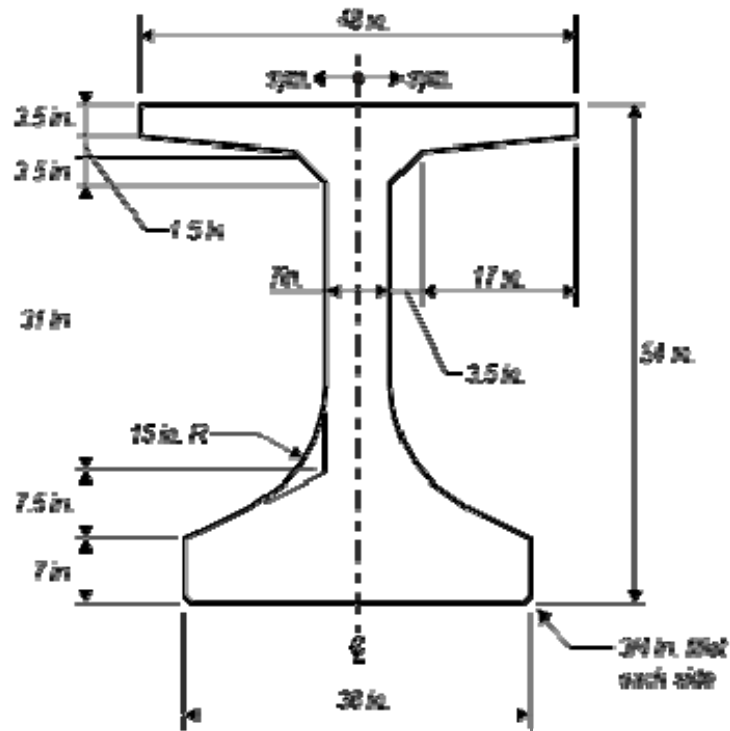


Figure 2–Cross-section 54-in. deep Florida I-Beam

To further improve the efficiency of FIB girders, it is desirable to investigate the feasibility of reducing reinforcement placed in the end region (Figure 3). End region reinforcement is specified by FDOT standard details (Figure 4), which are based on historic FDOT details, code requirements, and constructability considerations (Nolan 2009; Fallaha 2009). There is particular incentive to investigate confinement reinforcement, which is placed in the bottom flange around prestressing strands (Figure 3). The current use of confinement reinforcement is limited by the following:

- Confinement reinforcement approximately doubles the amount of time required to place reinforcement in I-girders (Magus 2010).
- Code provisions governing confinement reinforcement are based on limited experimental data. The interaction of confinement reinforcement and other end region design variables has not been studied.
- Code provisions governing confinement reinforcement are prescriptive and do not provide a rational model for design.

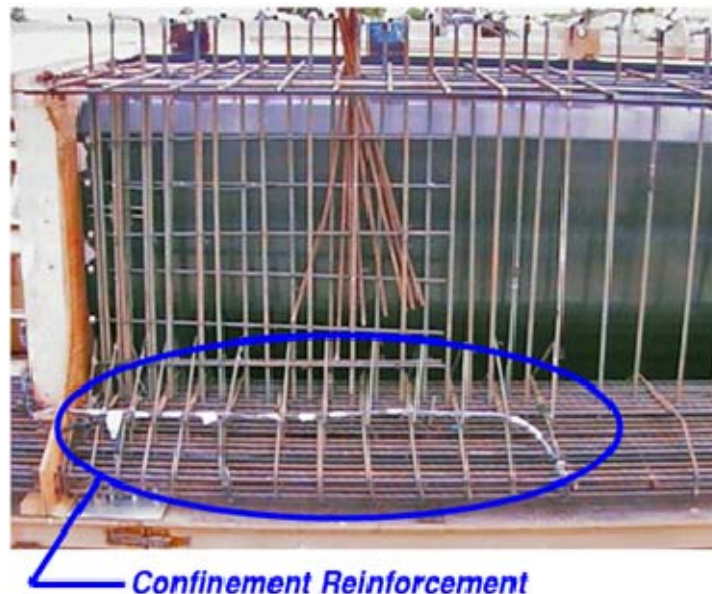


Figure 3–End region reinforcement.

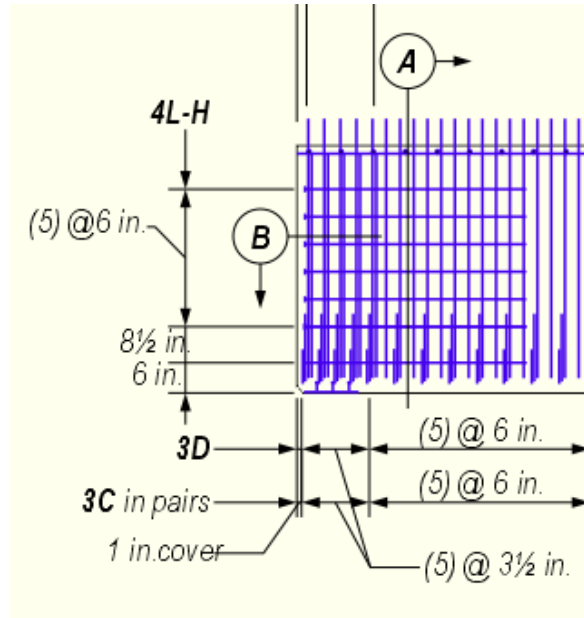


Figure 4–FIB-54 end region reinforcing detail (FDOT 2009b)

Previous research (see Appendix A) has focused on the effects of confinement reinforcement but does little to address its function. For purposes of this document, the “function” of confinement reinforcement is defined as how, why, where, and when confinement reinforcement acts in the end region structure.

Research presented in this document made use of analytical and experimental methods to investigate the function of confinement reinforcement. Interaction between confinement reinforcement and other end region variables was also considered. One goal of the research was to provide a rational model for the design of confinement reinforcement. Experimental results coupled with a rational model may justify a reduction in the quantity of reinforcement in the end region, thereby improving the efficiency of pretensioned I-girders.

In addition to having sufficient strength pretensioned I-girders must also satisfy serviceability requirements. Bottom flange splitting cracks are a particular serviceability concern in girders with relatively slender bottom flanges such as the FIB. Accordingly, development of a serviceability design model for the bottom flange of FIB girders was part of the research program. Such a model can improve the efficiency of FIB girders by giving engineers a tool for designing bottom flanges that are less prone to splitting cracks.

D.2 Girder Design and Construction

Five 54 in. deep Florida I-Beam (FIB-54) girders were fabricated and tested to evaluate the effects of end region detailing on girder behavior and capacity. Variables in the test program included: quantity of horizontal and vertical mild reinforcement in the end region, quantity or lack of confinement reinforcement, strand debonding pattern, and presence or lack of embedded steel bearing plates. This chapter presents details of the girders, construction procedures, and material properties. The labeling convention used to identify the different girders and specimens is also presented.

D.2.1 Test Girder Classification

Each end of each girder had a unique combination of variables. Because of the unique detailing, each end will be referred to as a separate “specimen” in this document. Figure 5 presents the nomenclature used to label specimens and girders. The first letter in the label identifies the girder and the second letter is used to designate the end. Both letters combine to form a specimen label. Letters used in the labels describe the key variables associated with each girder and specimen. A complete description of variables is contained in Table 1. Schematic representations of each specimen and the associated variables are shown in Figure 6.

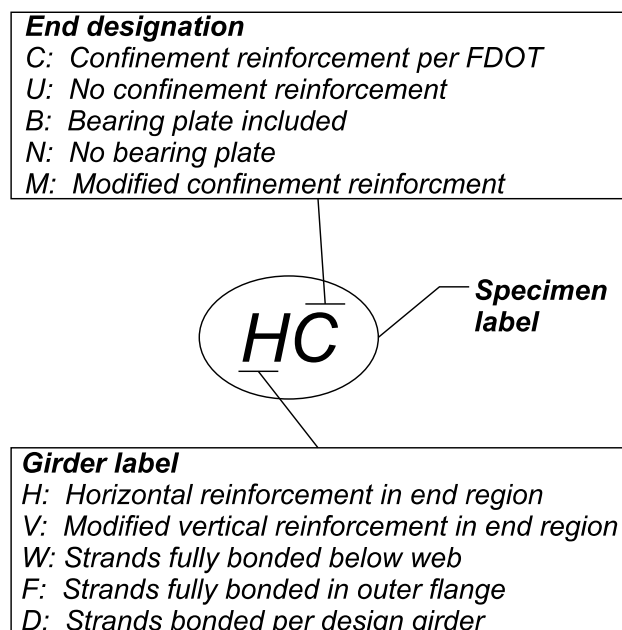


Figure 5–Labeling scheme

Table 1–Test girder and specimen variables

Test Girder	Specimen	Bearing plate	Mild reinforcement		Strand bond pattern	Confinement reinforcement	Phase
			Vertical	Horizontal			
H	HC	Yes	FDOT	Yes	Design	FDOT	1
	HU	Yes	FDOT	Yes	Design	No	1
V	VC	Yes	Mod	No	Design	FDOT	1
	VU	Yes	Mod	No	Design	No	1
W	WN	No	FDOT	No	Web	Mod	2
	WB	Yes	FDOT	No	Web	Mod	2
F	FN	No	FDOT	No	Flange	Mod	2
	FB	Yes	FDOT	No	Flange	Mod	2
D	DC	Yes	FDOT	No	Design	FDOT	2
	DM	Yes	FDOT	No	Design	Mod	2

FDOT: Detailed per FDOT design standards
 Mod: Detailed with modifications to FDOT design standards
 Web: Fully bonded strands placed below web
 Flange: Fully bonded strands placed in outer portion of flange
 Design: Strand pattern based on prototype design

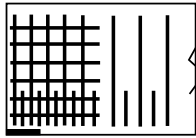
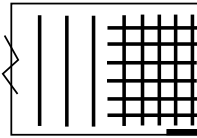

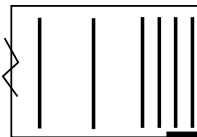
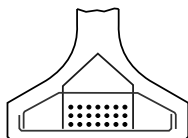
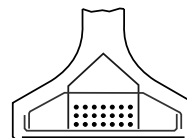
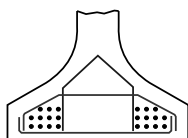
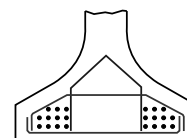

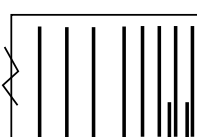
	<i>End 1</i>	<i>End 2</i>
<i>Girder H</i>	<p><i>HC</i></p> 	<p><i>HU</i></p> 
<i>Girder V</i>	<p><i>VC</i></p> 	<p><i>VU</i></p> 
<i>Girder W</i>	<p><i>WN</i></p> 	<p><i>WB</i></p> 
<i>Girder F</i>	<p><i>FN</i></p> 	<p><i>FB</i></p> 
<i>Girder D</i>	<p><i>DC</i></p> 	<p><i>DM</i></p> 

Figure 6–Specimen labels and graphical descriptions

Girders were constructed in two phases. The final column in Table 1 notes the construction phase for each test girder. Phase 1 girders were constructed at Dura-Stress Inc. in Leesburg, FL in August of 2010. Phase 2 girders were constructed at Standard Concrete Products in Tampa, FL in February of 2012.

Meetings were held with the FDOT, the project sponsor, prior to each construction phase to solicit input on test variables. Variables in phase I include the presence or lack of confinement

reinforcement and quantity of mild steel reinforcement in the end region. Variables tested in phase II include confinement reinforcement configuration, the presence or lack of steel bearing plates, and the strand bond pattern.

D.2.2 Test Girder Design

Test girder prototype design was based on girders used in an existing bridge in Clay County, FL, which had the FIB-54 cross-section (Figure 7) and spanned approximately 120 ft. The strand pattern and reinforcement for the prototype girder were designed based on these conditions. Due to laboratory space restrictions, the test girder length was reduced to 49.5 ft. The shorter length, however, still allowed for evaluation of the end region detailing, which was the primary focus of the research program.

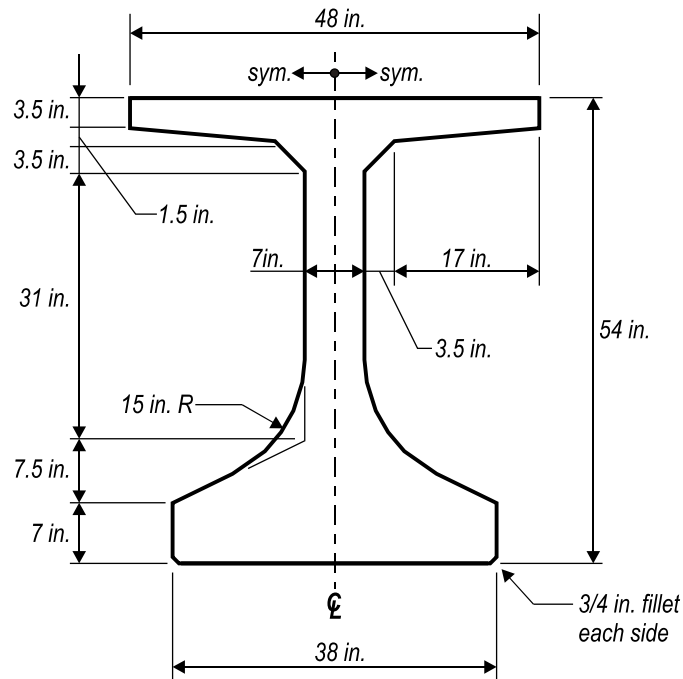


Figure 7–Cross-section of FIB-54

The prototype design called for (52) 0.6-in. diameter prestressing strands in the bottom flange and (4) 3/8-in. diameter strands in the top flange (Figure 8) using the strand bond pattern designated as “design pattern” in Figure 9. While strand bond patterns were varied among the specimens as indicated in Figure 9, the strand diameter, positions, and total prestress force were constant. The design pattern had six partially shielded strands and seven fully shielded strands.

Fully shielded strands in the test girders correspond to locations in the prototype with shielding lengths of 20 ft or 35 ft. Because test girders were shorter than the prototype, these shielding lengths resulted in fully shielded strands in the test girders.

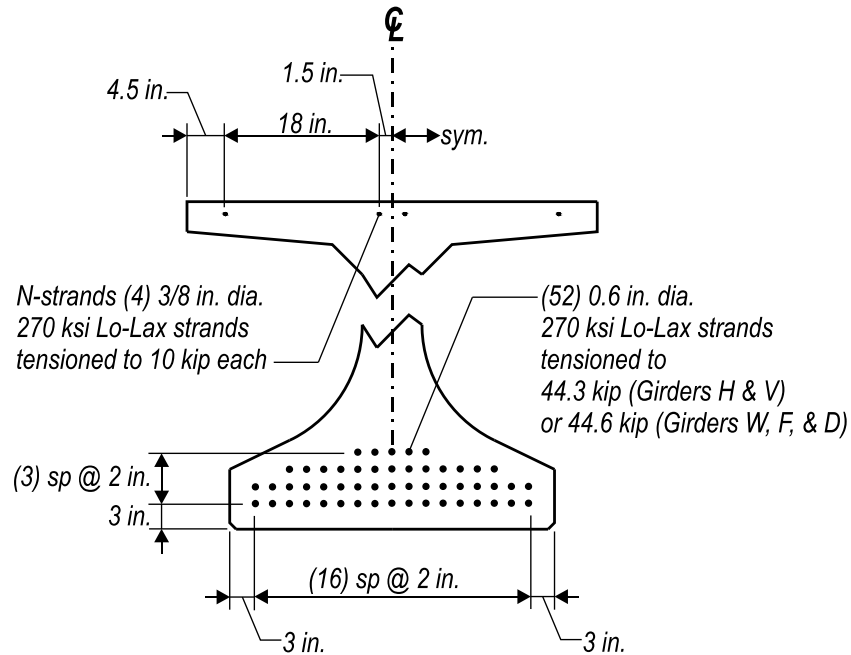


Figure 8—Strand layout and prestressing details

Some strands in Figure 9 are denoted at “Shielded entire length”. This designation is not strictly accurate for girders W, F, and D. All strands in these girders were bonded to the concrete for at least 18 in. at the girder center span. This was done for safety reasons so that the strands would be restrained from dangerous whipping movements during release of prestress forces. Bonding at the center 18 in. did not affect the end regions where load tests were conducted.

The “web pattern” and “flange pattern” (Figure 9) were designed to test the effect of strand placement on end region behavior and capacity. These patterns were created by partially shielding strands in select locations. Both patterns violate current AASHTO LRFD requirements for quantity and placement of shielding, but were useful for research purposes. The two outermost strands in each pattern were fully bonded so that confinement reinforcement could be secured to these strands during fabrication.

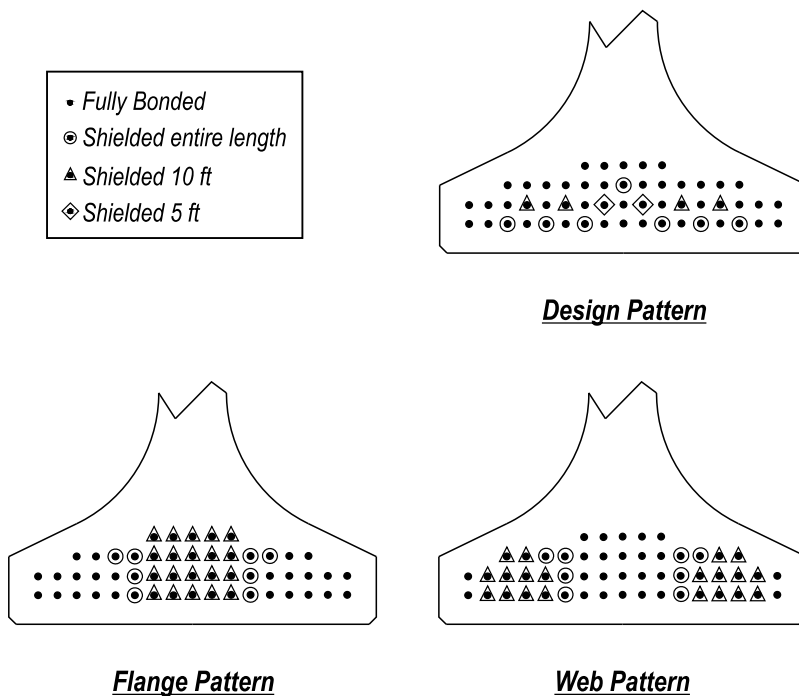


Figure 9–Strand bond and shielding patterns

Mild reinforcement details (Figure 10 through Figure 13) were based on the prototype girder and on FDOT Florida-I 54-Beam Interim Standard Details (FDOT, 2008, 2010). Bar labels are similar to those used in FDOT standards. The numeric portion of each label indicates the size of bar (i.e. 5A is a #5 bar). Reinforcement bending and bearing plates details are shown in Figure 14. The different types of bars will be described in the following paragraphs.

5A. Bars placed longitudinally in the top flange and were continuous for the entire length of the girder. Splices of 5A bars were at least 36 in. long.

BP. Galvanized steel bearing plates with headed studs embedded in the concrete at the girder bearing. Plates in girders H and V had eight studs, whereas plates in girders W, F, and D had six studs. Changes in stud quantity and width were made to follow the FDOT bearing plate detail which changed after girders H and V were constructed. Changes to the FDOT bearing plate detail were unrelated to the current research program.

3C, 4C, 3D, 4E and 4F. Bars placed in the bottom flange as confinement reinforcement around the prestressing strands. Both FDOT and modified confinement schemes were used in the test program and are shown in Figure 15. The FDOT confinement scheme used #3 bars and the modified scheme used #4 bars. Fewer bars were used in modified scheme and all bars were

placed directly above the bearing. The D and E bars in the modified scheme did not splice at the cross-section centerline as did the C bars in the FDOT scheme.

7G and 8G. Bars placed longitudinally in the top flange. These bars were included to control cracking in the top flange after prestress transfer, and are not specified in FDOT standards. The G bars did not extend into the end regions where load testing took place. Girders H and V had #7 G bars. Girders W, F, and D had #8 G bars.

5K and 5Ks. Bars were placed vertically in the web with hooks top and bottom. These bars protruded through the top flange to help develop composite action with the cast-in-place deck. They also acted as shear reinforcement. The bottom hook on 5K bars was 16 in. long to assist in constructability. The bottom hook on 5Ks bars was only 6 in. long. To eliminate any incidental confinement effects from the bottom hooks, 5Ks bars were used in lieu of 5K bars within the end region.

4L and 4L-H. Bars were placed horizontally in the end region of girder H. The 2008 FIB details specify that 4L bars extend beyond the girder end and hook into a cast-in-place end diaphragm. Test girders did not have end diaphragms. In the absence of a diaphragm to anchor the 4L bars, 4L-H bars with headed anchors were used in the web and bottom flange where development was critical. The 4L bars did not have headed anchors and were placed in the top flange. For reasons unrelated to the experimental program the 2010 FDOT standard detail eliminated the use of end diaphragms and horizontal bars in the end region. Girders W, F, and D were designed using the 2010 detail and did not have 4L or 4L-H bars.

4M. Bars placed transversely in the top flange.

N-Strands. Strands placed in the top flange. These strands are sometimes called “dormant” strands. Their primary purpose is to support mild reinforcement during fabrication. They also provide a nominal amount of crack control to the top flange at prestress transfer.

5Y. Vertical bars bundled with 5Ks and 5Z bars at girder ends. These bars are used to control web splitting cracks that form due to prestressing.

5Z. Bars placed vertically within the end region to control web splitting cracks.

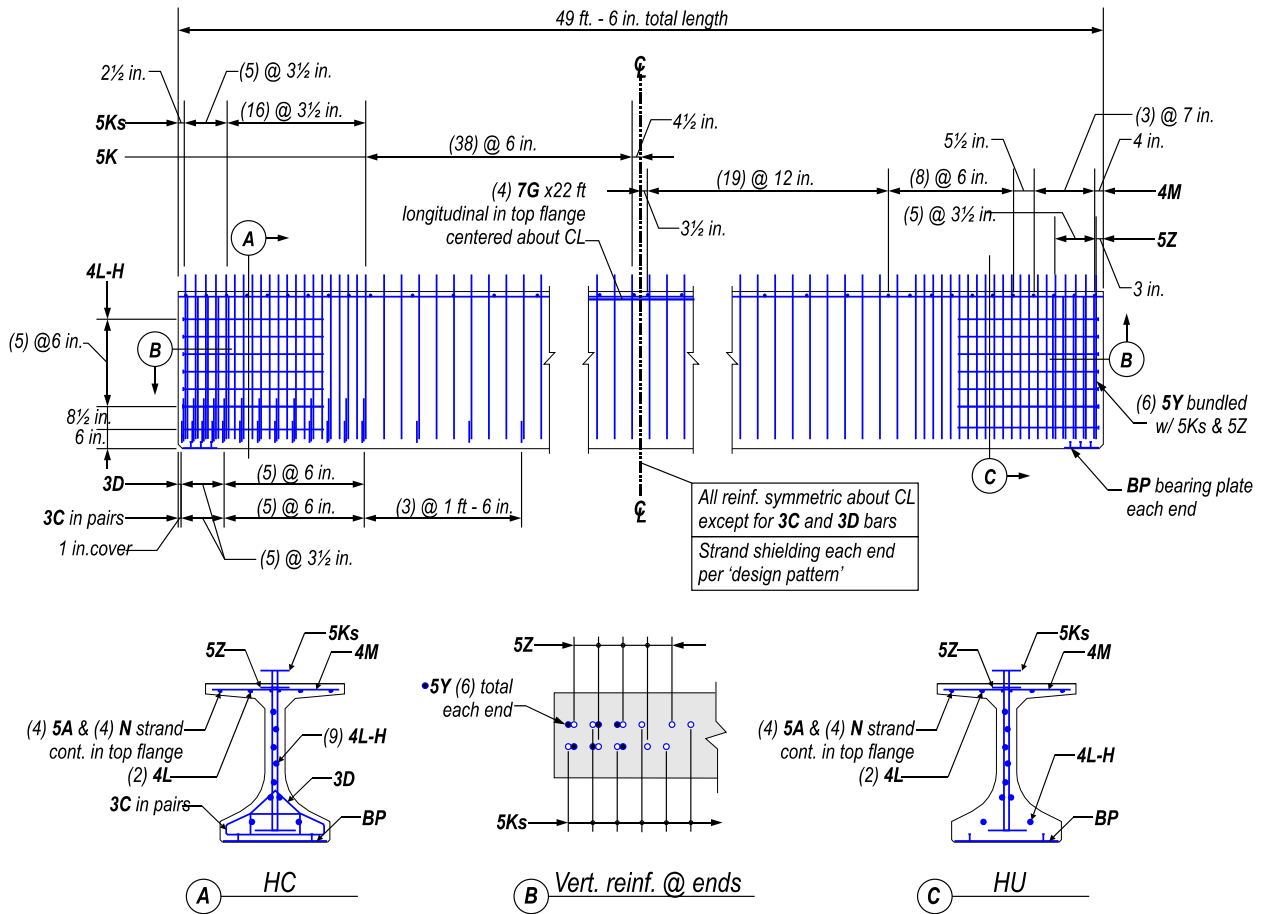


Figure 10–Reinforcement for girder H

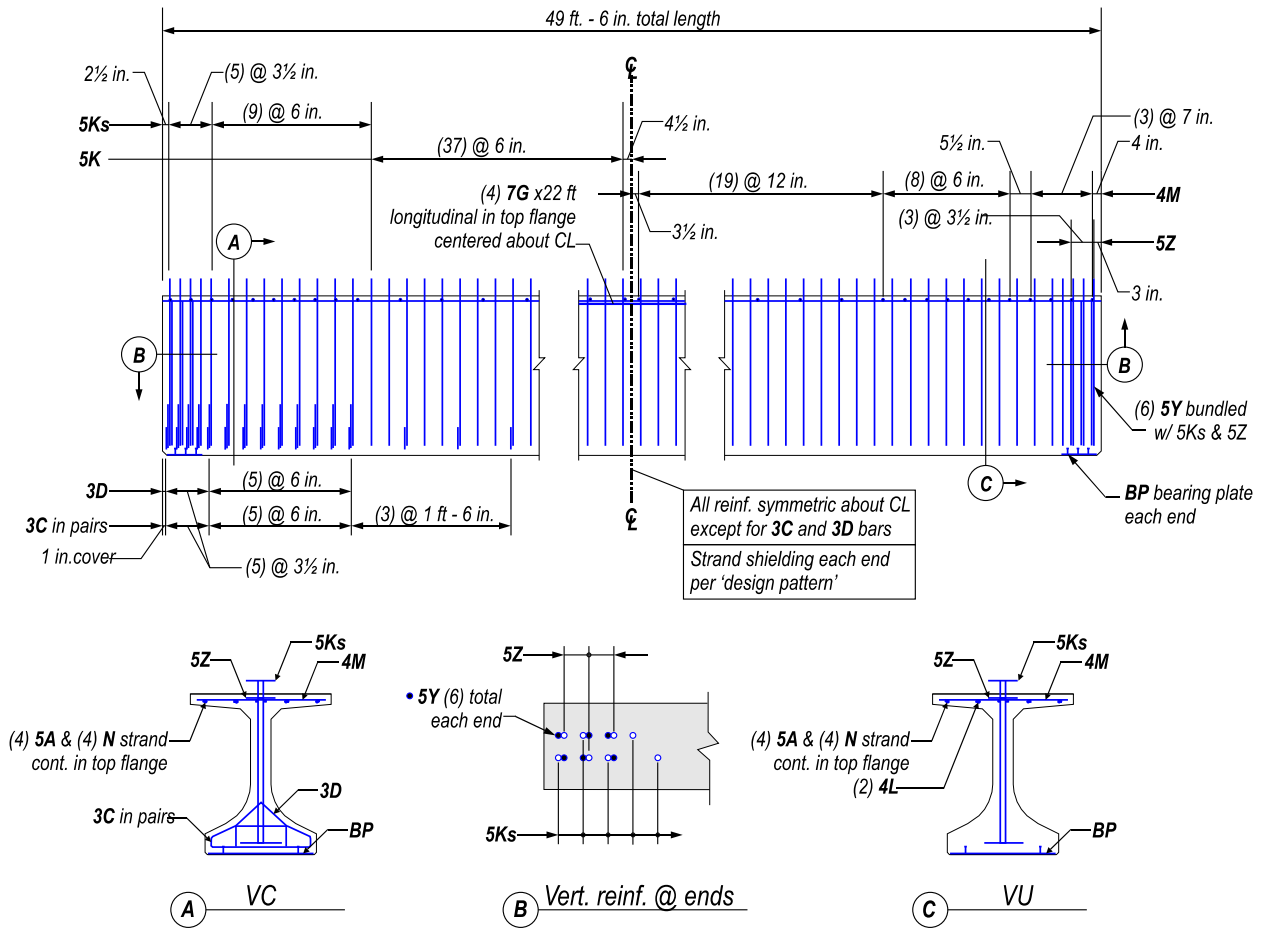


Figure 11–Reinforcement for girder V

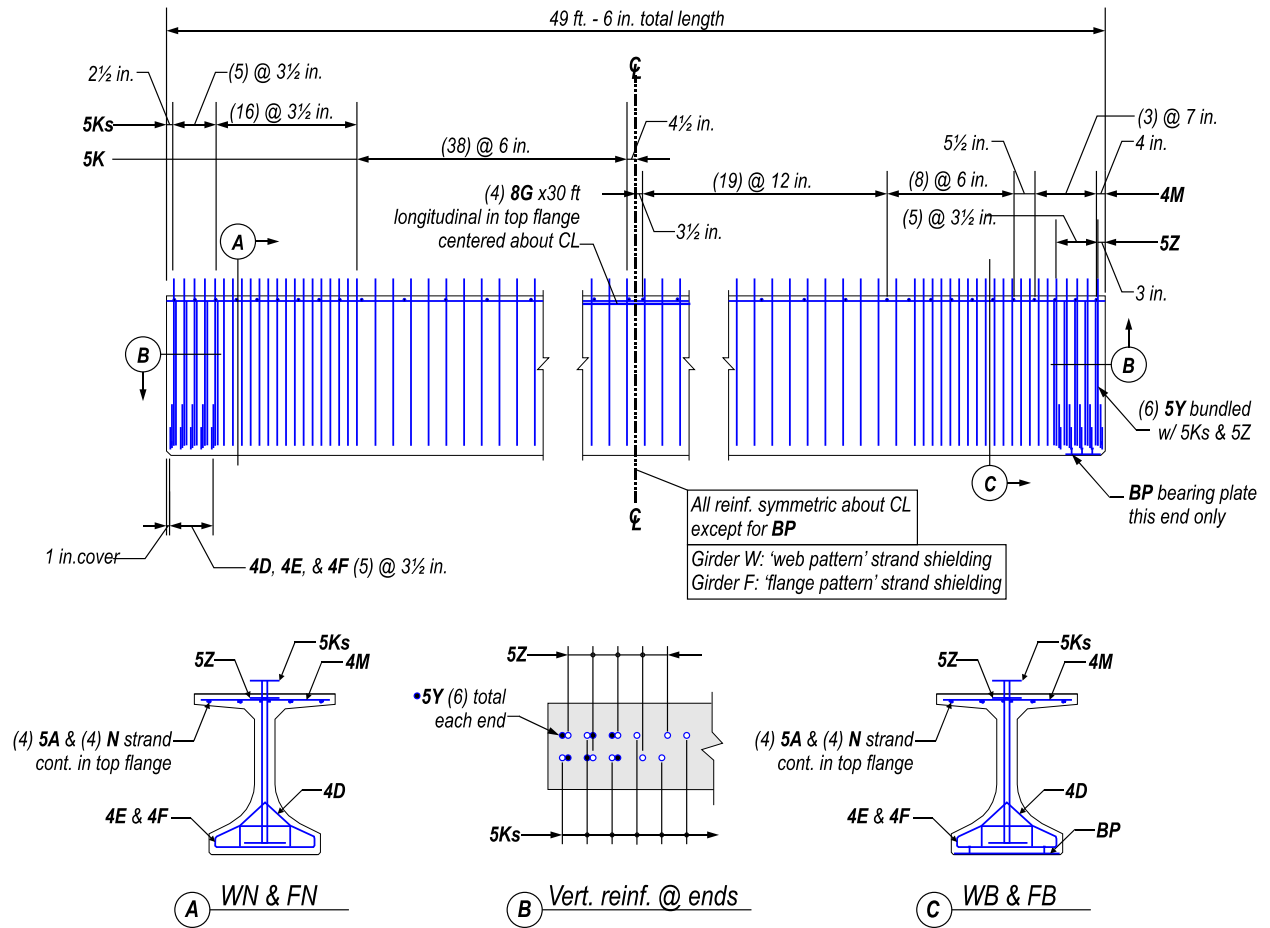


Figure 12—Reinforcement for girders W and F

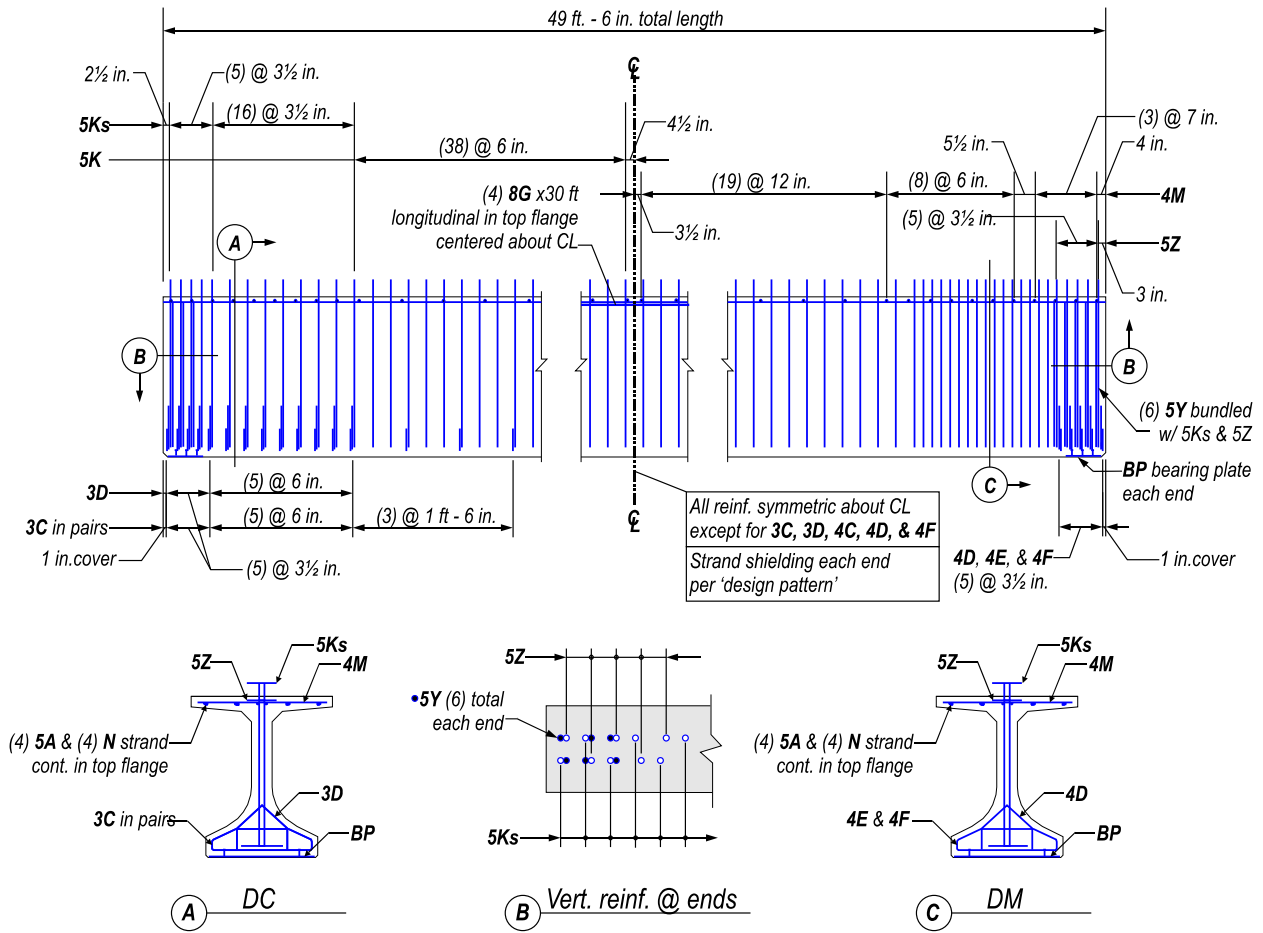


Figure 13—Reinforcement for girder D

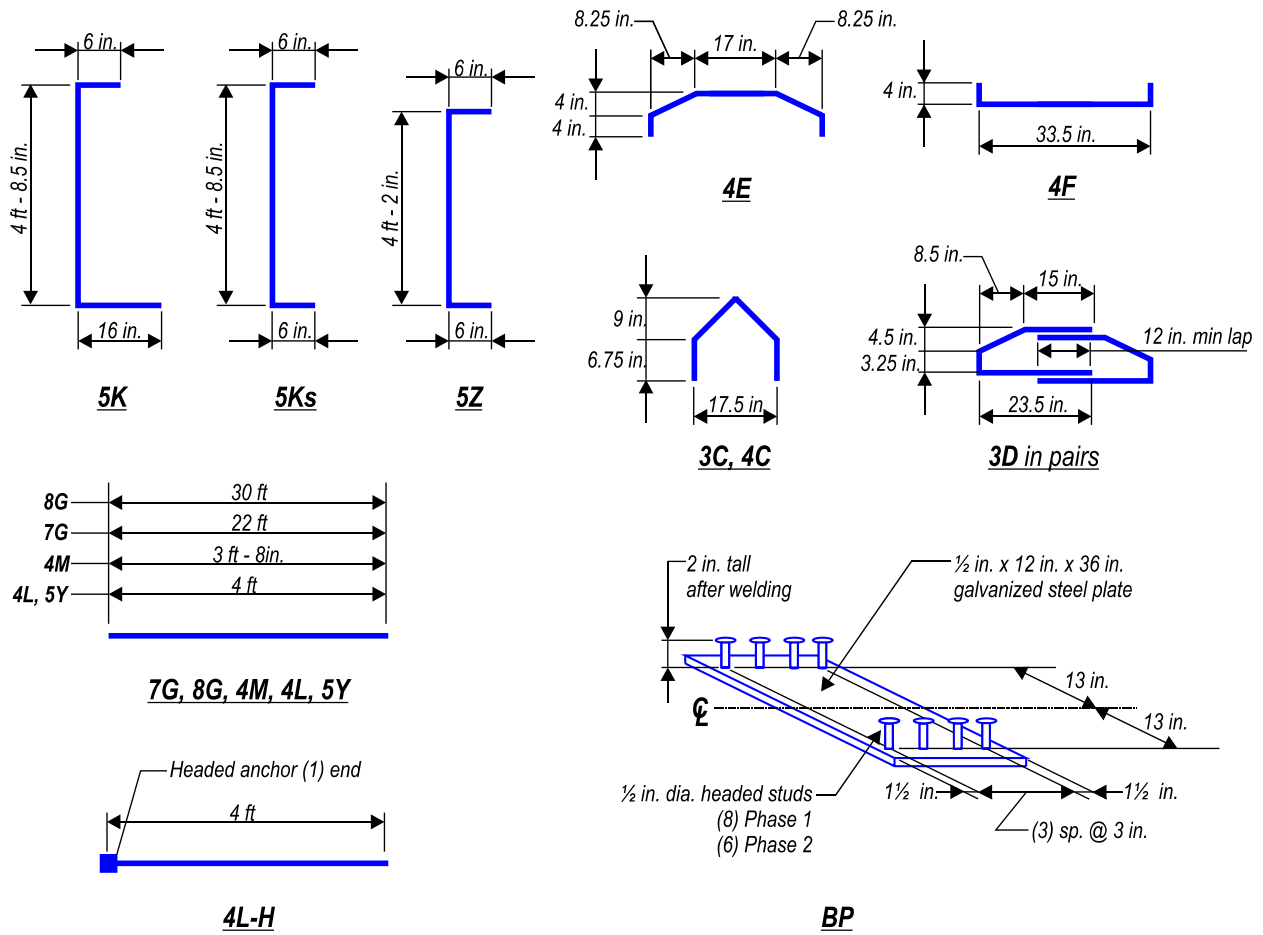


Figure 14–Reinforcement and bearing plate details

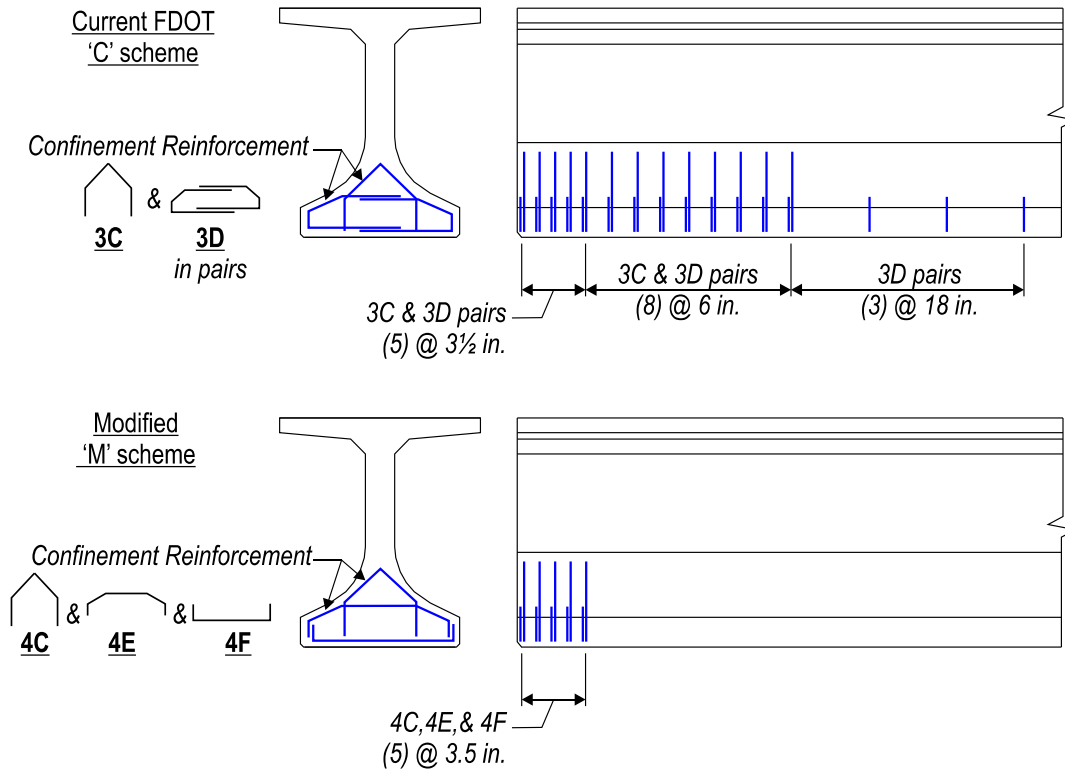


Figure 15–Confinement reinforcement schemes

Cast-in-place concrete slabs were built on top of the test girders to mimic a bridge deck. The slab was 8-in. thick, 48-in. wide and was reinforced longitudinally and transversely (Figure 16).

Specified material properties matched FDOT standards. Specifications are listed in Table 2. Tested material properties will be discussed in a later section.

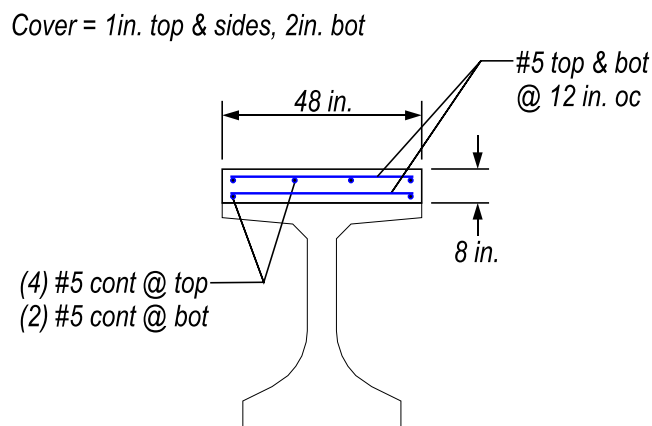


Figure 16–Cast-in-place deck reinforcement

Table 2–Specified material properties

Material	Specification
Girder Concrete	FDOT class VI 8500 psi 28-day compressive strength 6000 psi compressive strength at prestress transfer
Deck Concrete	FDOT class II 4500 psi 28-day compressive strength
Prestressing Strand	ASTM A416 270 ksi ultimate strength Low relaxation
Mild Reinforcement	ASTM A615 60 ksi yield strength

D.2.3 Girder Construction

Girders H and V were fabricated at Dura-Stress, Inc. in Leesburg, FL during the first phase of construction. Girders W, F, and D were fabricated in the second phase at Standard Concrete Products in Tampa, FL. The fabrication process was similar for both phases. Differences are specifically noted in the text in this section. Table 3 presents a summary of the construction events and dates for both phases.

Table 3–Construction and testing chronology

Event	Phase 1 Date	Phase 2 Date
Strands tensioned	August 30, 2010	February 13, 2012
Concrete poured	September 1, 2010	February 17, 2012
Concrete exceeds release strength	September 3, 2010	February 20, 2012
Forms removed	September 7, 2010	February 20, 2012
Prestress released	September 8, 2010	February 21, 2012
Moved to storage	September 8, 2010	February 22, 2012
Trucked to FDOT laboratory	February 23, 2011	April 30, 2012
Deck cast	April 6, 2011	May 7, 2012
Load testing	May 9, 2011 to May 17, 2011	May 23, 2012 to June 1, 2012

Fabrication began with the placement prestressing strands and form bulkheads. Plywood bulkheads were used during phase one. Holes were cut in the plywood for strands to pass through. Steel bulkheads were used in phase two. The steel bulkheads were installed in segments after the strands were tensioned.

A hydraulic jack was used to tension the strands. Jacking force was determined from pressure in the hydraulic line and was verified by measuring strand elongation. Girders were oriented on stressing beds as shown in Figure 17. Dormant strands in the top flange were tensioned first followed by strands in the bottom flange. The same tensioning pattern (Figure 18) was used for both phases.

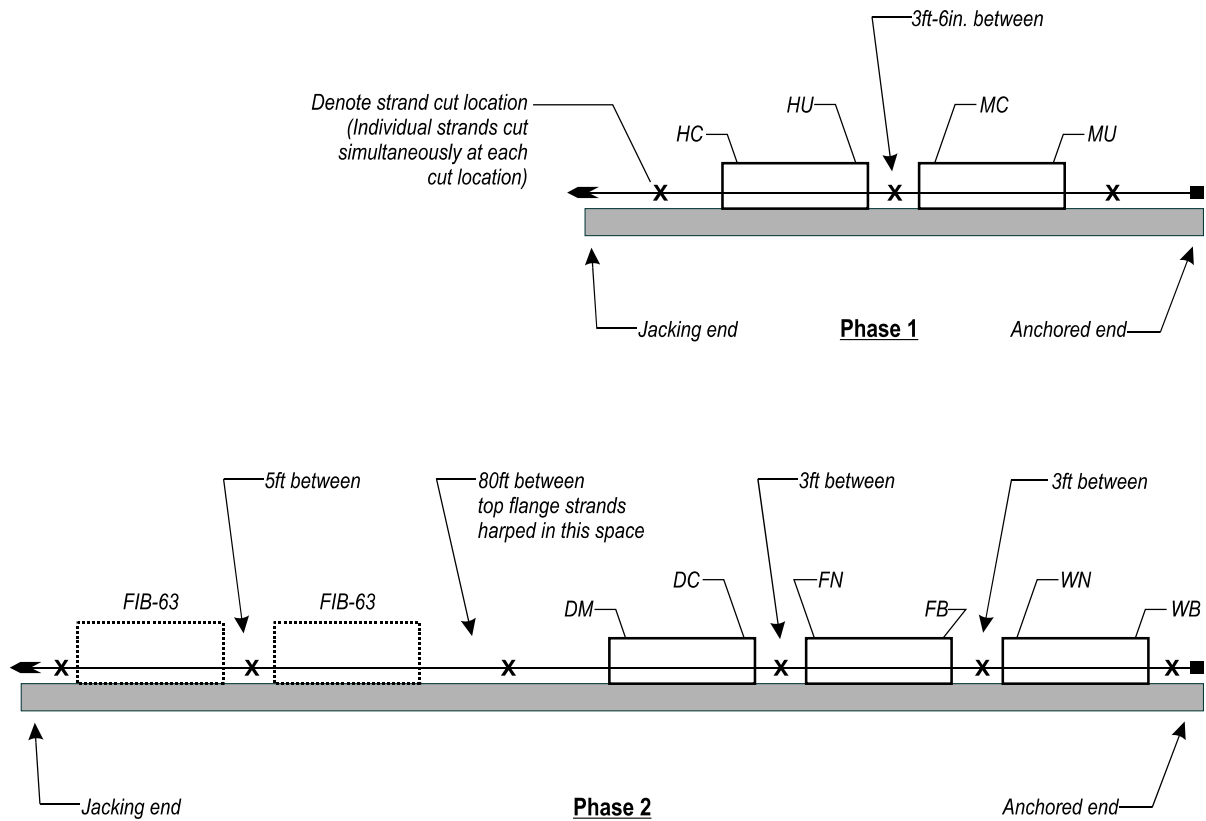


Figure 17–Girder orientation during fabrication

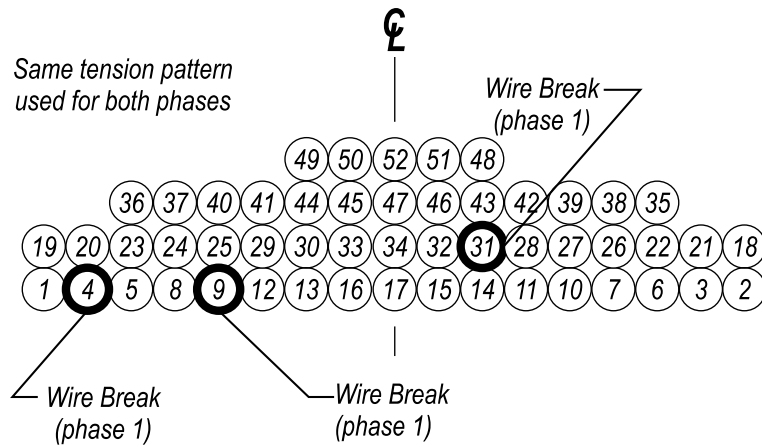


Figure 18–Tension pattern and wire break locations

Wire breaks occurred in three different strands during phase one (Figure 18). The wire breaks did not occur inside the test girders so the strand cross-section within the girders was not compromised. The jacking force of the strands with broken wires could not be checked by the elongation method, however the jacking force as determined by pressure in the hydraulic line was still within the specified range. No wires broke during the second construction phase.

After tensioning, mild steel reinforcement was placed. Select bars were instrumented with strain gages prior to placement in the girders. Figure 19 through Figure 23 show the reinforcement in each specimen.

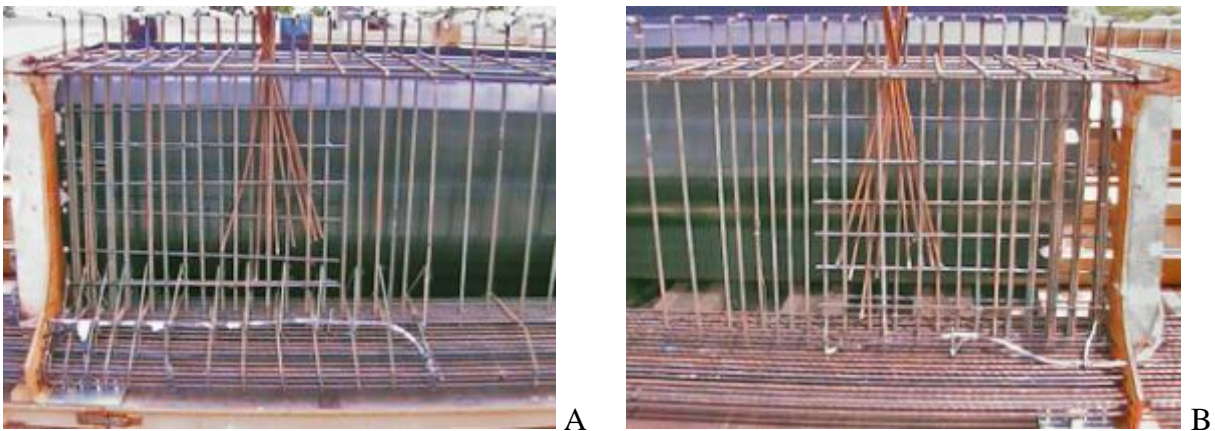
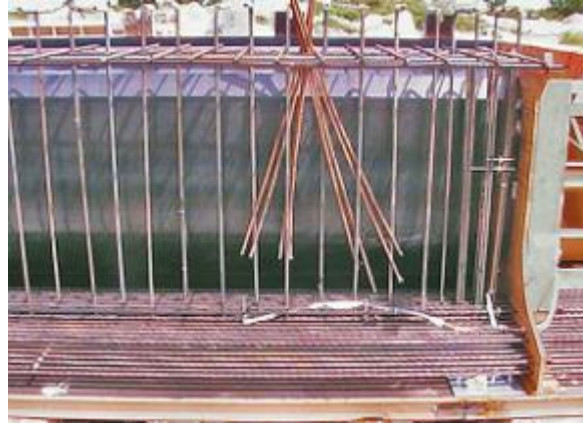


Figure 19–Girder H reinforcement A) Specimen HC and B) Specimen HU



A



B

Figure 20–Girder V reinforcement A) Specimen VC and B) Specimen VU



A



B

Figure 21–Girder W reinforcement A) Specimen WN and B) Specimen WB



A



B

Figure 22–Girder F reinforcement A) Specimen FN and B) Specimen FB

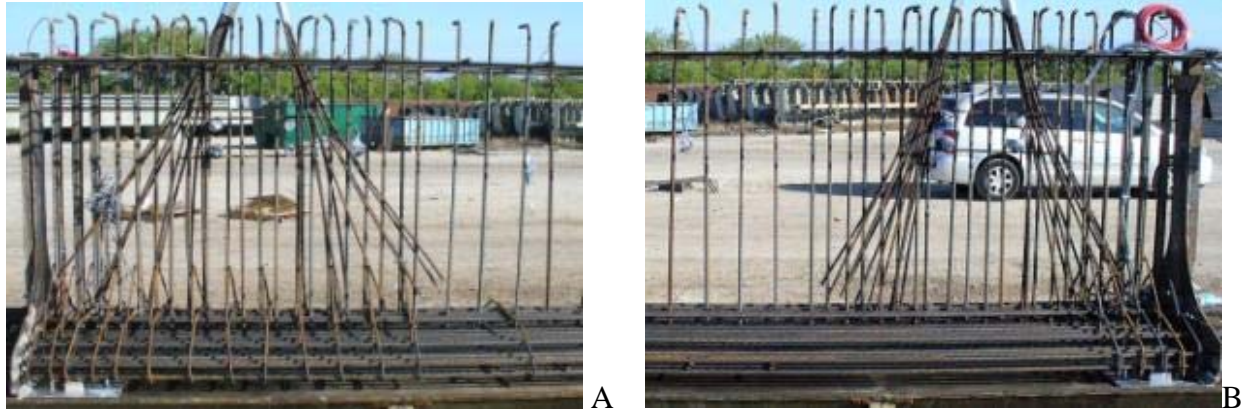


Figure 23–Girder D reinforcement A) Specimen DC and B) Specimen DM

Concrete was mixed at on-site batch plants. For phase one girders, concrete was placed in two lifts and was consolidated with internal and external vibrators after each lift (Figure 24). The internal vibrator was only used on the north side of the web to keep the vibrator away from internal strain gages which were primarily placed on the south side. A self-consolidating concrete mix was used for phase two (Figure 25) and vibration was not necessary. Test cylinders were taken by the fabricators and by the research team from each batch of concrete. The top surface of each girder was raked to intentionally roughen the surface (Figure 26). Girders were covered with heavy tarps during curing (Figure 27).



Figure 24–Concrete placement and internal consolidation phase 1



Figure 25–Concrete placement phase 2



Figure 26–Girder finished surface



Figure 27–Girders covered with tarps

Forms were removed six days after casting during phase one and three days after casting during phase two. Prestress was transferred to the girders the day after form removal. The time between form removal and prestress transfer was used to install bonded foil strain gages and to connect the data acquisition system.

Two 4x8 field cured cylinders were tested on the day of prestress transfer. The average compressive strength was 6880 psi for phase one and 7320 psi for phase two. Both values are above the specified release strength of 6500 psi.

Flame cutting was used in both phases to release the prestressing strands. Individual strands were cut simultaneously at points shown in Figure 17. Dormant strands in the top flange were cut first, followed by the bottom strands, which were cut from the outside-in and from bottom-to-top (Figure 28). This release pattern was selected because it is relatively easy to execute and because it is typical of precast girders in Florida. Strand cutting was stopped intermittently at multiple stages to obtain strain readings from the vibrating wire strain gages and to check the girders for cracking.

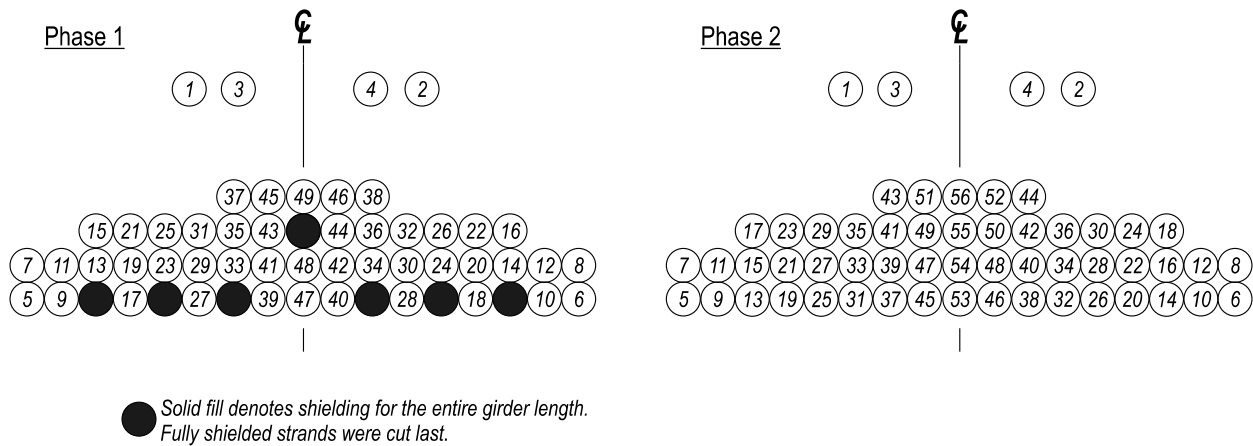


Figure 28—Strand release patterns

For safety reasons, the fully shielded strands in phase one were cut last and were released by a single cut between girders H and V. In some cases the fully shielded strands completely slipped out of the girders upon release. This was not an issue in phase two because each strand was at least partially bonded to each girder.

The girders in both phases shifted slightly (less than 1 in.) along the length of the stressing bed multiple times during prestress transfer. Movement events always corresponded to strand cuts. A more pronounced shift occurred during phase one as the final bonded strand was cut. Just after the final bonded strand was cut, girders H and V each slid approximately 2 ft. along the stressing bed. After sliding, the gap between girders was approximately 7 ft-6in.

To investigate changes in strain due to lifting (Figure 29), girders H and V were lifted by crane immediately after prestress transfer was completed. Girders were supported by the crane momentarily and then placed on dunnage on the stressing beds (Figure 30). Strain data were collected during lifting and as girders were placed on dunnage. After the data were collected, the girders were taken to a storage yard to await shipping. Girders were examined for cracking periodically while in they were held in storage at the prestress fabrication facilities.



Figure 29–Test girder lifted by crane



Figure 30–Girder resting on dunnage above stressing bed

Girders were trucked to the Marcus H. Ansley FDOT structures laboratory in Tallahassee, FL for deck construction and load testing. Strain gages were used to monitor strain

in girder H (phase one) during transport. Figure 31 shows girder H being transported. The black box on top of the girder in the picture housed the data acquisition system.



Figure 31–Girder H on truck prior to transit

After unloading of the test girders in Tallahassee, forms were constructed and reinforcement was placed for the concrete deck. Wood forms were affixed to the top flange of the girders using pipe clamps (Figure 32). Concrete was prepared by a local ready mix plant.

Cast-in-place decks were poured inside the lab. Concrete was transported from the mix truck to the girders via a bucket and crane (Figure 33). Concrete was consolidated using hand-held and form-mounted vibrators. After consolidation and screeding, the decks were troweled to a smooth finish. Cylinders of the concrete were taken for material testing.



A



B

Figure 32–Deck construction A) reinforcement and B) formwork

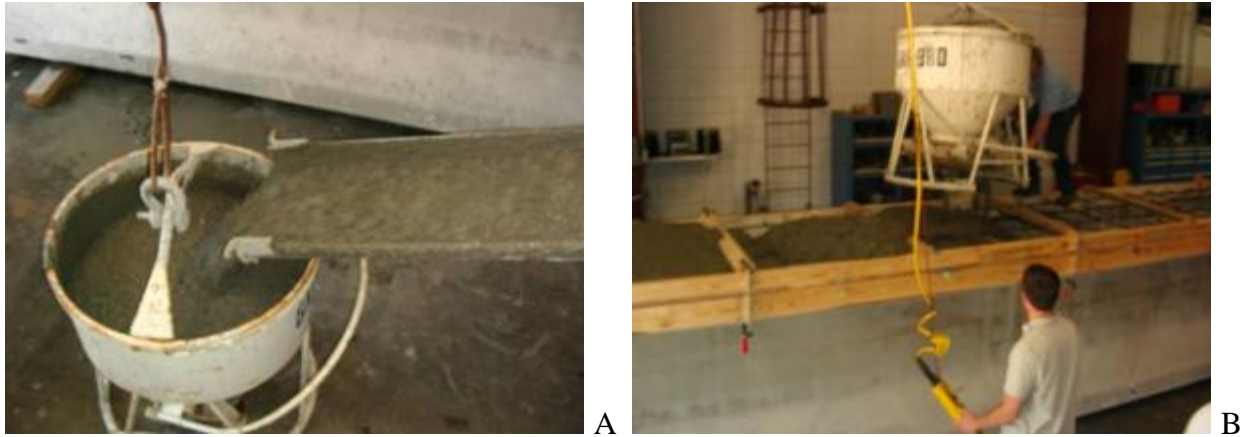


Figure 33–Concrete placement A) unloading and B) placement with bucket

D.2.4 Material Properties

Concrete, mild steel, and prestressing strand were detailed to match FDOT specifications. FDOT class VI concrete ($f'c = 8500$ psi) was specified for the girders, and FDOT class II concrete ($f'c = 4500$ psi) for the deck. Concrete compressive strength was tested using both 4x8 and 6x12 cylinders. Table 4 presents the tested concrete strengths.

Prestressing strands were Grade 270 low-relaxation, conforming to ASTM A416. Tested strand properties are shown in Table 5.

Bond capacity of phase one prestressing strands was tested in accordance with the proposed standard recommended by the North American Strand Producers (NASP 2009). This test method consists of pull-out tests of strand samples embedded in mortar. The method places tight requirements on flow and strength of the mortar. Flow must be between 100 and 124, and the strength at the time of the pull-out tests must be between 4500psi and 5000psi. The pull-out tests must be conducted between 22 and 26 hours after mixing and placing the grout. In spite of efforts to create a grout that would meet specifications, the grout used in the NASP tests failed to achieve the required strength. Table 6 lists the grout strengths. Low grout strength was the only deviation from the test method. Flow of the grout was 107.5. Table 7 lists results of the NASP tests. Because the grout strength was less than the value specified by the method, results from NASP tests are conservative when compared to tests that strictly meet the grout strength requirements.

Table 4–Tested concrete compressive strengths

Material	Cast date	Test date	Average strength (psi)	Sample size	Testing agent*	Cure Method
Phase 1 Girder Concrete	8-31-10	9-3-10	6400	(2) 4x8 cylinders	1	Wet
		9-8-10	6940	(2) 4x8 cylinders	1	Field
		9-8-10	6880	(3) 6x12 cylinders	2	Field
		9-29-10	9185	(3) 4x8 cylinders	1	Wet
		9-29-10	8235	(3) 6x12 cylinders	2	Field
		9-28-10	8790	(3) 4x8 cylinders	3	Wet
		5-10-11	10,950	(4) 6x12 cylinders	4	Wet
		5-17-11	11,610	(3) 4x7 cores girder FH	4	Core
		5-18-11	10,510	(3) 4x7 cores girder MH	4	Core
Phase 1 Deck Concrete	4-6-11	5-4-11	6615	(3) 6x12 cylinders	4	Field
		5-18-11	6950	(3) 6x12 cylinders	4	Field
Phase 2 Girder Concrete	2-17-12	2-20-12	7050	(2) 4x8 cylinders	1	Wet
		2-21-12	7330	(2) 4x8 cylinders	1	Field
		3-02-12	8790	(2) 4x8 cylinders	1	Wet
		3-16-12	8250	(3) 6x12 cylinders	2	Wet
		3-16-12	9210	(3) 4x8 cylinders	1	Wet
		5-30-12	10,520	(3) 6x12 cylinders	4	Field
Phase 2 Deck Concrete	5-7-12	5-30-12	6400	(9) 6x12 cylinders	4	Field
* 1. Tested by girder fabricator 2. Tested by FDOT State Materials Office 3. Tested by FDOT District Office 4. Tested by FDOT Structures Research Center						

Table 8 presents the tested material properties for mild steel reinforcement. All reinforcement was ASTM A615 grade 60, with the exception of the 4L-H headed bars placed in girder H. The supplier of the headed bars provided reinforcing bars that met ASTM A706. During phase one the #3 bars came from two separate suppliers; Table 8 presents values from both suppliers.

Table 5–Prestressing steel properties

Material	Stress at 1% elongation	Ultimate stress	Elongation at ultimate stress	Testing agent*
Phase 1 Prestressing Strand	259 ksi	285 ksi	5.47%	1
	271 ksi	284 ksi	4.59%	2
Phase 2 Prestressing Strand	261 ksi	287 ksi	5.38%	1
	259 ksi	285 ksi	NA	2
* 1. Strand supplier 2. FDOT State Materials Office (average of 4 samples)				

Table 6–Grout strength for NASP tests

Time of test (Time zero at mixing of grout)	Grout Strength* (average of (3) cubes)
22 hr	4210 psi
23 hr	4380 psi
24 hr	4030 psi
25 hr	4280 psi
26 hr	4340 psi
* Test method requires a strength between 4500 and 5000 psi	

Table 7–NASP Test Results.

Test Number	Load at 0.1 in. strand slip
1	22.08 kip
2	22.80 kip
3	24.09 kip
4	22.93 kip
5	22.98 kip
6	22.57 kip
Average	22.91 kip

Table 8–Steel reinforcement properties

Material	Yield Stress	Ultimate Stress	Elongation at Ultimate Stress	Testing agent*
Phase 1 #4 Headed rebar	68.8 ksi	90.8 ksi	19%	1
	64.6 ksi	89.6 ksi	18%	2
Phase 1 #3 confinement rebar	72.9 ksi	114.8 ksi	11%	1
	78.6 ksi	121.3 ksi	9%	1
	69.5 ksi	106.2 ksi	9%	2
Phase 1 #5 vertical rebar	66.1 ksi	100.7 ksi	17%	1
	68.6 ksi	105.7 ksi	9 %	2
Phase 2 #3 confinement rebar	73.6 ksi	113.3 ksi	12%	1
	85.2 ksi	115.4 ksi	12%	2
Phase 2 #4 confinement rebar	70.0 ksi	109.1 ksi	11%	1
	76.4 ksi	106.8 ksi	11%	2
Phase 2 #5 vertical rebar	64.5 ksi	103.2 ksi	11%	1
	63.2 ksi	103.5 ksi	13%	2
* 1. Rebar supplier 2. FDOT State Materials Office (average of 2 samples minimum)				

D.3 Test Setup and Procedures

D.3.1 Data Collection during Fabrication

Strain and crack data were collected during various stages of fabrication including: prestress transfer, lifting, storage, trucking, and deck construction. This section describes the procedures used to collect data during each stage of construction.

Data from strain gages were monitored and logged using a computerized data acquisition system powered by portable generators. Data from vibrating wire strain gages were monitored using an electronic readout box and logged manually. Crack data were collected through visual observation and using a microscope. Instrumentation details are presented in Chapter D.5.

Prestress transfer. Data were collected from each girder during prestress transfer. Prior to transfer girders were examined for cracks and null readings were taken from all gages. For girders H and V, the acquisition system and generator were secured to the top of the girders. For girders F, W, and D the acquisition system was placed in a van adjacent to the stressing bed. Strand cutting was paused at various times during prestress transfer to allow for visual evaluations and to take readings from the vibrating wire gages. Visual evaluations and vibrating wire readings were also conducted after prestress transfer was complete. Crack widths were measured by microscope at few locations on each specimen. Crack locations were marked with a crayon or marker and documented by photograph.

Lifting. Data were collected during lifting of girders H and V only. Immediately following the conclusion of prestress transfer, girder H and V were lifted by crane, held in place for approximately four minutes, and then placed onto dunnage. Strain data were collected throughout this process. The data acquisition systems and generators were strapped to the top of the girders to secure them during lifting. Vibrating wire gage readings were taken and visual crack evaluations were conducted during each step.

Storage. All girders received periodic visual evaluations while they were in storage at the precast facilities. Cracks were marked then documented by photograph. Crack widths were measured by microscope at few locations on each specimen. Dates of visual evaluations are listed in Table 3. Vibrating wire gage data were also collected while the girders were in storage.

Trucking. Internal and external strain gages were used to monitor concrete strains in girder H during trucking from the precast facility to the laboratory. The data acquisition system

and generator were strapped to the top of the girder to secure them during transport. Vibrating wire readings were taken before and after trucking. A visual evaluation was given to all girders upon arrival at the laboratory.

Deck construction. All girders were visually evaluated for cracks before and after construction of the cast-in-place decks. Vibrating wire gage readings were also taken before and after deck construction.

Material properties. Samples of reinforcement, strand, and concrete were taken during each construction phase and were tested to determine the associated material properties. Documentation regarding material properties was also obtained from the supplier of each material.

D.3.2 Load Test Setup and Procedures

Load tests were conducted at the FDOT M. H. Ansley Structures Research Center in Tallahassee, FL. Test dates are listed in Table 9. Load tests were conducted on both ends of each girder. After the first end was tested, the supports and load point were moved and the opposite end was tested.

Table 9–Load test chronology

Specimen	Service load test	Ultimate strength test
HC	May 11, 2011	May 11, 2011
HU	May 9, 2011	May 10, 2011
VC	May 13, 2011	May 13, 2011
VU	May 17, 2011	May 17, 2011
WN	May 23, 2012	May 23, 2012
WB	May 25, 2012	May 25, 2012
FN	May 29, 2012	May 29, 2012
FB	May 30, 2012	May 30, 2012
DC	May 31, 2012	May 31, 2012
DM	June 1, 2012	June 1, 2012

For purposes of this document each end will be referred to as a separate specimen. Each specimen was loaded at least twice. The first loading simulated the service load. The simulated service load was approximately 300kip and was determined from the prototype girder that was used as a basis for the test girder designs. Once the service load was reached, the load was held constant and cracks were identified and marked. After the cracks were marked the load was removed. The second loading determined the specimen’s ultimate strength. A load-displacement

plot was monitored real-time during the ultimate load test. Load was applied until it was apparent from the load-displacement plot that a peak load had been reached. Cracking was documented after the ultimate load test was complete.

Load and support geometry are shown in Figure 34. Each support consisted of a 10 in. x 32 in. reinforced bearing pad. Pads were “Type E” pads constructed according to FDOT design interim design standards (FDOT 2009d). The bearing pad at the near support was centered below the embedded steel bearing plate (Figure 35). Load was applied to the specimen using side-by-side hydraulic actuators. The load rate was controlled by adjusting a pump that pressurized the hydraulic system. The combined load rate varied from 0.1 kip/sec to 0.6 kip/sec, with the typical rate being approximately 0.4 kip/sec. Load was spread from the actuators to the girders through steel plates and a 10 in. x 30 in. reinforced neoprene bearing pad. A reaction frame was used to transmit load from the actuators to the strong floor (Figure 36).

Load, displacement, strand slip, and strain data were continuously collected during the service and ultimate load tests. Strain from the vibrating wires strain gages was collect at discrete points during load testing. Concrete samples were tested in conjunction with the load tests to determine compressive strength at the time of load testing.

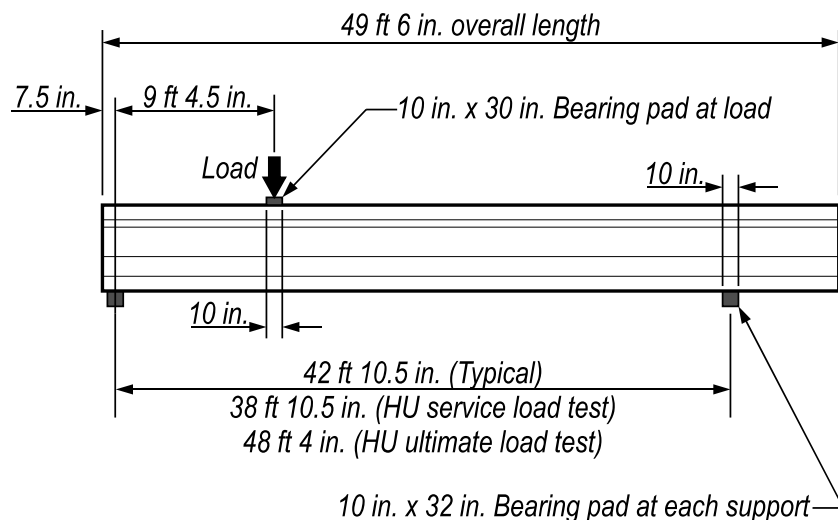


Figure 34—Test setup

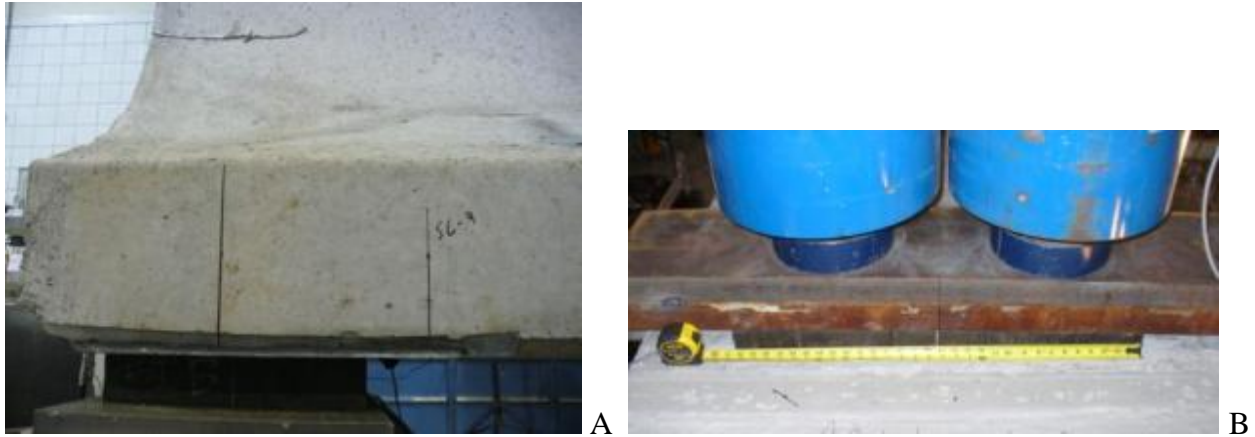


Figure 35–Test setup at A) bearing and B) load point



Figure 36–Test specimen and load frame A) top of girder and B) end of girder.

D.3.3 Coordinate System

A consistent coordinate system is used throughout this document. The system is used to define instrumentation locations and to identify the direction of strains, stress, and forces. The origin for the coordinate system is placed at the centerline of the cross-section, at the bottom of the girder, and at the girder end (Figure 37). The z-direction is vertical, the x-direction is

horizontal across the width of the girder, and the y-direction is horizontal along the span length. The support nearest the origin is denoted as the near support, and the opposite end is denoted as the far support.

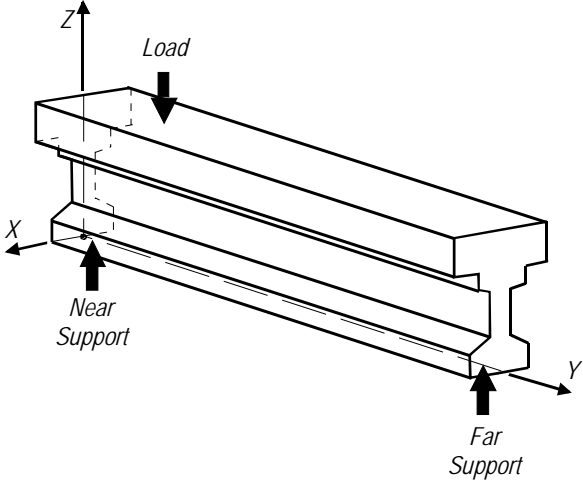


Figure 37–Coordinate system relative to load and supports

D.4 Instrumentation

Strain, displacement, force, and crack data were collected during fabrication and load testing. This chapter describes the instrumentation used to collect data and the labeling scheme that was used to identify the various instruments.

D.4.1 Types and Descriptions

Data were collected using load cells, LVDTs, linear potentiometers, variable resistance strain gages and vibrating wire strain gages. Table 10 lists the different types of instrumentation and the associated labels. With the exception of the vibrating wire strain gages, all data were logged electronically. Vibrating wire gage data were logged manually from an electronic readout box.

Table 10–Instrumentation types and labels

Label	Type	Placement
MS	Foil strain gage	Reinforcement and bearing plates
XS	Foil strain gage	Concrete surface
ES	Embedded strain gage	Concrete interior
V	Vibrating wire strain gage	Concrete interior
S	Foil strain gage	Concrete surface
R	Foil strain rosette	Concrete surface
L	Linear variable displacement transducer (LVDT)	Load point, supports, and strands
P	Linear potentiometer	Strands
--	Load Cell	Load point

MS strain gages were attached to select mild reinforcement and to bearing plates prior to placement in the test girders (Figure 38). MS gages had a gage length of 5mm and were used to monitor strain during prestress transfer and load testing.

XS strain gages (Figure 39) were attached to the surface of test girders immediately after formwork was removed. These gages were used to measure concrete strains during prestress transfer, lifting, and trucking. XS gages had a 60mm gage length.

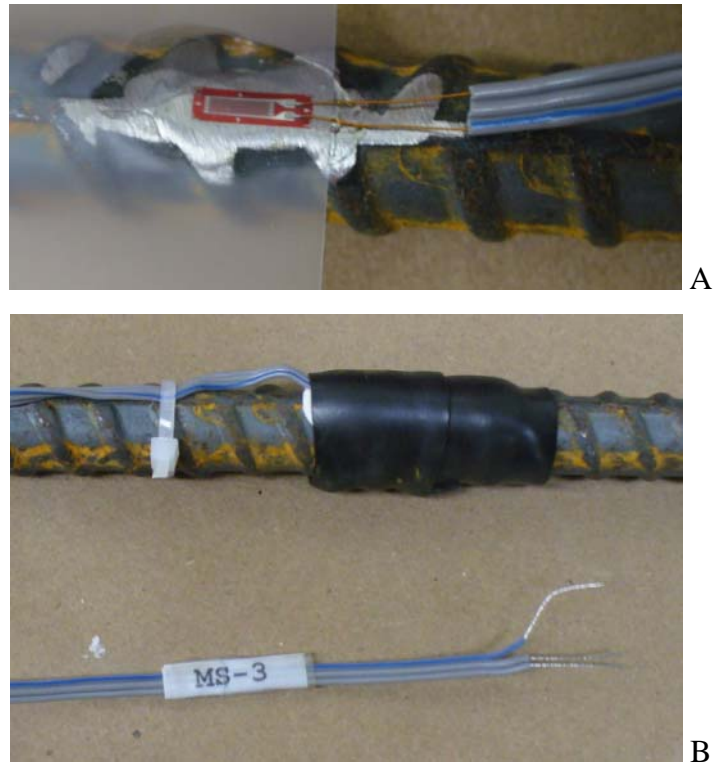


Figure 38–MS gage A) before protective covering and B) with protective cover and label



Figure 39–XS gage installation

ES gages were embedded in the test girders and were used to monitor concrete strain during all phases of fabrication and load testing. ES gages had a gage length of 60mm. Figure 40 shows ES gage installations prior to concrete placement.

V series gages were vibrating wire strain gages which were embedded in the test girders. These gages had a gage length of 152mm and were used to measure concrete strain during all phases of fabrication and load testing. Figure 40 shows a V series gage installation prior to

concrete placement. Because vibrating wire gages do not experience electronic drift over time, they were particularly useful in monitoring long term prestress losses.

Wire leads were collected into harnesses after all internal instrumentation (MS, ES, and V series gages) had been placed in the girders. Harnesses in girders F and V were routed to the ends of the girders and exited through holes in the wood bulkheads (Figure 42). Harnesses in girders F, W, and D were routed to the top of the girders. Wire harnesses were covered with a rubber sleeve and duct tape to protect the wires during concrete casting. A label was placed at the end of each wire lead for identification purposes.

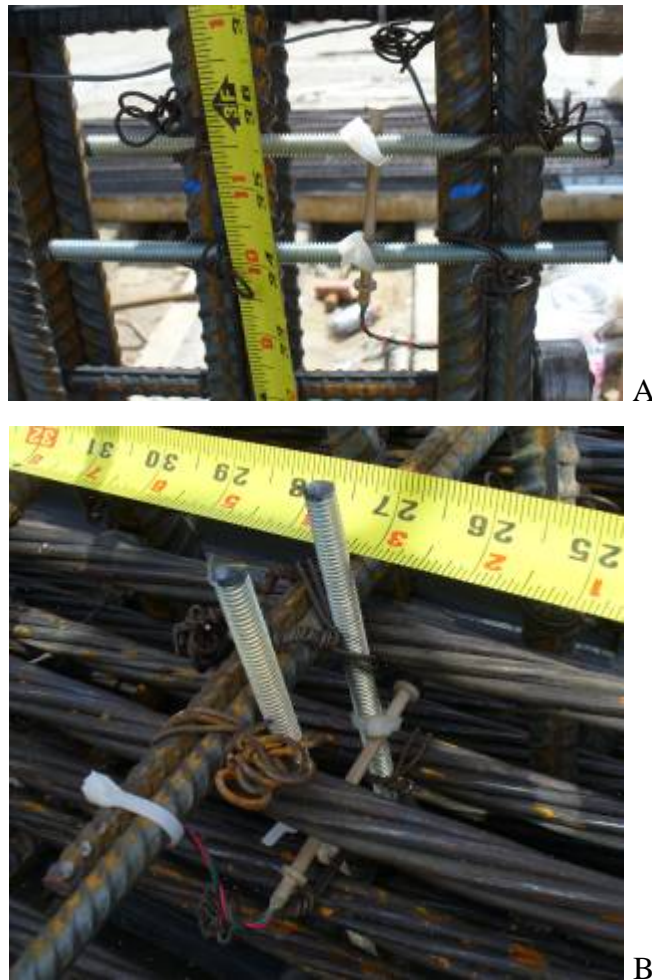


Figure 40–ES gage A) vertical and B) horizontal orientation



Figure 41–V gage (view from above)



Figure 42–Wire harness and plywood bulkhead

Prior to load testing S and R series strain gages were installed at discrete locations on girder surfaces (Figure 43). These gages had 60mm gages lengths. R series gages were strain rosettes built-up from three individual strain gages.

L series instruments were LVDTs used to monitor vertical displacement during load tests. Labels and locations of the LVDTs measuring vertical displacement are shown in Figure 44. LVDTs were mounted to fixed support structures as shown in Figure 45.

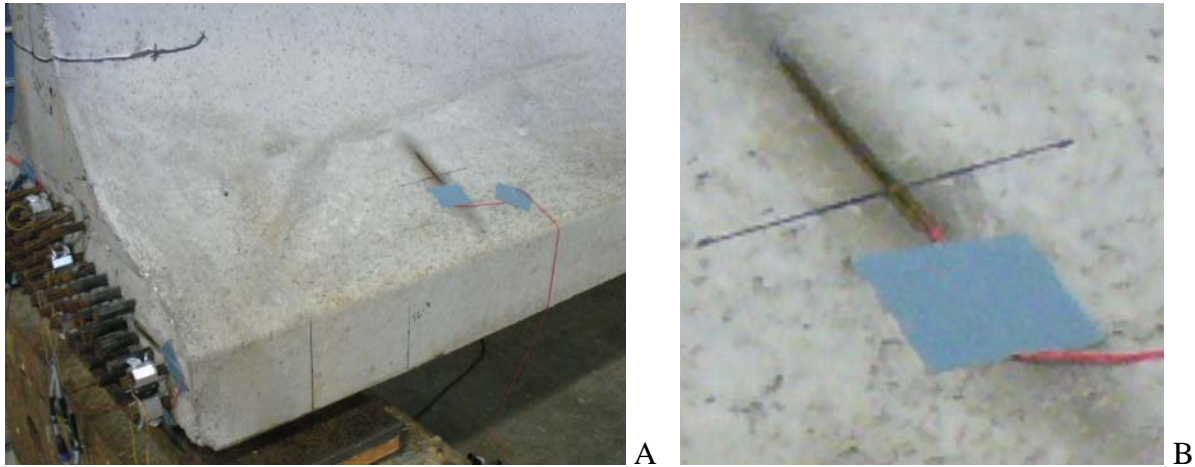


Figure 43—S gage A) on top of bottom flange and B) close-up

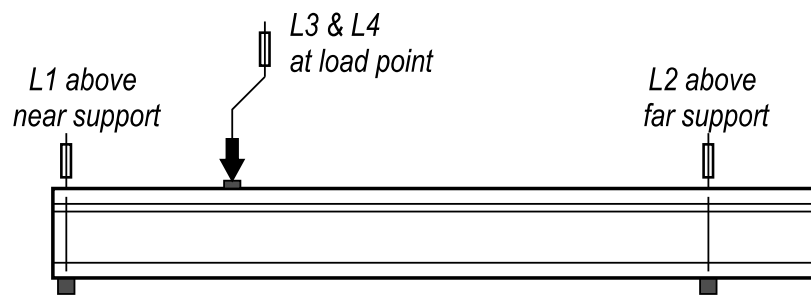


Figure 44—LVDT placement and labels



Figure 45–LVDT and support frame

LVDTs were also used to monitor strand slip for girders H and V. Monitored strands are shown in Figure 46. LVDTs for monitoring strand slip were mounted to a wooden bracket affixed to the girder end (Figure 47). This setup was unreliable because cracking in the concrete caused the LVDT frame to shift during load testing.

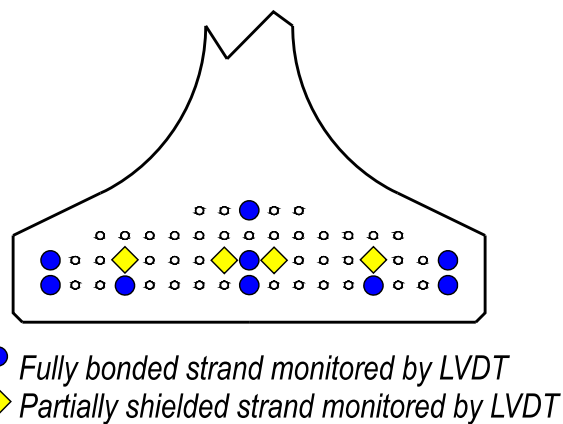


Figure 46–Girder H and V strands monitored by LVDT



Figure 47–Wood frame and LVDTs

Rather than LVDTs, P series variable resistant potentiometers were used to measure strand slip for girders F, W, and D. Instrumented strands are shown in Figure 48. P series instruments were mounted directly to the strands using custom-machined aluminum brackets and set-screws (Figure 49). This setup did not have the problems associated with the wooden frame used for girders H and V.

Load cells (Figure 50) were used to measure the force applied during the load tests. A hydraulic system was used to apply the loads, and a pressure transducer was used to measure pressure in the hydraulic line during testing. Both force and pressure data were logged electronically, along with displacement and strain data from the other instruments.

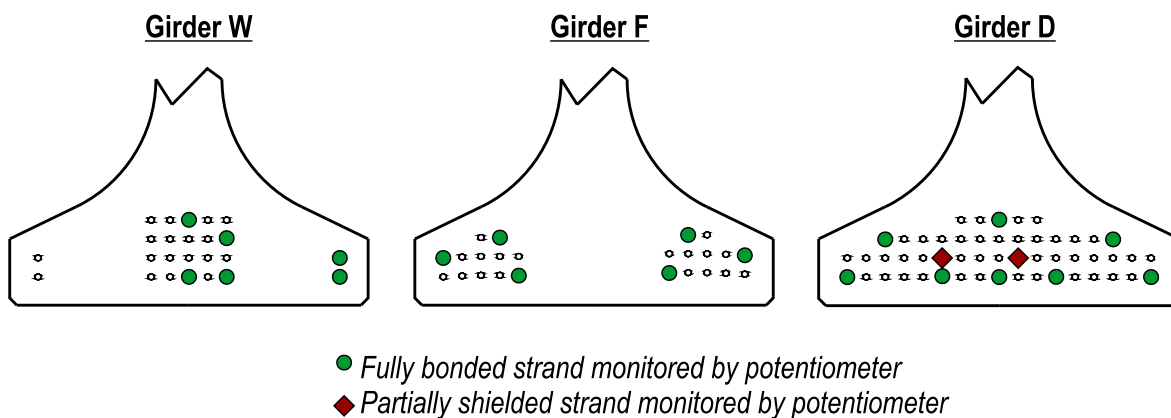


Figure 48–Girder W, F, and D strands monitored by potentiometer

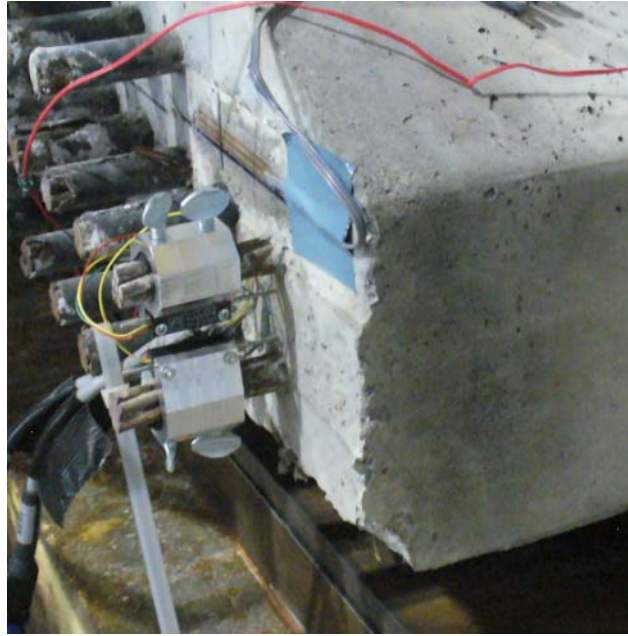


Figure 49–Aluminum brackets and linear potentiometers on strands



Figure 50–Load cells below hydraulic actuators

D.4.2 Strain Gage Coordinates

Figures in this document that present strain data typically also contain information regarding the location of gage(s) from which the data were collected. Information in the figures gives a general idea of the gage orientation and position but doesn't always give specific coordinates. Table 11 through Table 20 give specific coordinates of gages referenced in this document. Coordinates are based on the system defined in Figure 37.

Table 11–Specimen HC strain gage coordinates

Instrument	X (in.)	Y (in.)	Z (in.)	Orientation	Reference(s)
XS3	0	0	12	X	Figure 52, Figure 53, and Table 22
XS5	-19	18	6	Y	Figure 66 and Figure 67
XS6	-19	30	6	Y	Figure 66 and Figure 67
XS7	-19	36	6	Y	Figure 66 and Figure 67
XS8	-19	42	6	Y	Figure 66 and Figure 67
XS9	-19	48	6	Y	Figure 66 and Figure 67
XS10	-19	54	6	Y	Figure 66 and Figure 67
XS11	19	18	6	Y	Figure 66 and Figure 67
XS12	19	54	6	Y	Figure 66 and Figure 67
ES2	-3	27	8	X	Figure 52, and Table 22
ES3	-3	47	8	X	Figure 52, and Table 22
MS1	-0.5	2	0.5	X	Figure 110
MS2	0	13	0.5	X	Figure 110
MS10	0	2	10	X	Figure 110
MS14	0	2	2	X	Figure 110
MS15	-1	2	16	X-Z	Figure 110
MS20	0	8	10	X	Figure 110
MS24	-13	8	2	X	Figure 110
MS25	-1	9	16	X-Z	Figure 110
MS30	0	22	10	X	Figure 110
MS34	0	22	2	X	Figure 110
MS35	-1	22	16	X-Z	Figure 110
MS40	0	66	10	X	Figure 110
MS44	0	66	2	X	Figure 110
MS45	-1	67	16	X-Z	Figure 110
MS51	0	2	0	X	Figure 110
MS52	0	13	0	X	Figure 110
V1	-1	292	7.5	X	Table 30

Table 12–Specimen HU strain gage coordinates

Instrument	X (in.)	Y (in.)	Z (in.)	Orientation	Reference(s)
XS3	0	0	12	X	Figure 53, and Table 22
XS5	-19	18	6	Y	Figure 66 and Figure 67
XS6	-19	30	6	Y	Figure 66 and Figure 67
XS7	-19	36	6	Y	Figure 66 and Figure 67
XS8	-19	42	6	Y	Figure 66 and Figure 67
XS9	-19	48	6	Y	Figure 66 and Figure 67
XS10	-19	54	6	Y	Figure 66 and Figure 67
XS11	19	18	6	Y	Figure 66 and Figure 67
XS12	19	54	6	Y	Figure 66 and Figure 67
ES2	3	27	8	X	Figure 52, and Table 22
ES3	3	48	8	X	Figure 52, and Table 22
MS1	0	2	0.5	X	Figure 110
MS2	0	13	0.5	X	Figure 110
MS51	0	2	0	X	Figure 110
MS52	0	13	0	X	Figure 110

Table 13–Specimen VC strain gage coordinates

Instrument	X (in.)	Y (in.)	Z (in.)	Orientation	Reference(s)
XS3	0	0	12	X	Figure 53, and Table 22
XS5	-19	18	6	Y	Figure 66 and Figure 67
XS6	-19	30	6	Y	Figure 66 and Figure 67
XS7	-19	36	6	Y	Figure 66 and Figure 67
XS8	-19	42	6	Y	Figure 66 and Figure 67
XS9	-19	48	6	Y	Figure 66 and Figure 67
XS10	-19	54	6	Y	Figure 66 and Figure 67
XS11	19	18	6	Y	Figure 66 and Figure 67
XS12	19	54	6	Y	Figure 66 and Figure 67
ES2	-3	29	8	X	Figure 52, and Table 22
ES3	-3	48	8	X	Figure 52, and Table 22
MS1	-0.5	2	0.5	X	Figure 110
MS2	0	13	0.5	X	Figure 110
MS10	0	2	10	X	Figure 110
MS14	0	2	2	X	Figure 110
MS15	-1	3	16	X-Z	Figure 110
MS20	0	8	10	X	Figure 110
MS24	-13	8	2	X	Figure 110
MS25	-1	8	16	X-Z	Figure 110
MS30	0	22	10	X	Figure 110
MS34	0	22	2	X	Figure 110
MS35	-1	22	16	X-Z	Figure 110
MS40	0	64	10	X	Figure 110
MS44	0	64	2	X	Figure 110
MS45	-1	64	16	X-Z	Figure 110
MS51	0	2	0	X	Figure 110
MS52	0	13	0	X	Figure 110
V1	-1	297	7.5	X	Table 30

Table 14–Specimen VU strain gage coordinates

Instrument	X (in.)	Y (in.)	Z (in.)	Orientation	Reference(s)
XS3	0	0	12	X	Figure 53, and Table 22
XS5	-19	18	6	Y	Figure 66 and Figure 67
XS6	-19	30	6	Y	Figure 66 and Figure 67
XS7	-19	36	6	Y	Figure 66 and Figure 67
XS8	-19	42	6	Y	Figure 66 and Figure 67
XS9	-19	48	6	Y	Figure 66 and Figure 67
XS10	-19	54	6	Y	Figure 66 and Figure 67
XS11	19	30	6	Y	Figure 66 and Figure 67
XS12	19	54	6	Y	Figure 66 and Figure 67
ES2	3	27	8	X	Figure 52, and Table 22
ES3	3	48	8	X	Figure 52, and Table 22
MS1	0	2	0.5	X	Figure 110
MS2	0	13	0.5	X	Figure 110
MS51	0	2	0	X	Figure 110
MS52	0	13	0	X	Figure 110

Table 15–Specimen WN strain gage coordinates

Instrument	X (in.)	Y (in.)	Z (in.)	Orientation	Reference(s)
MS10	-1	2.5	17.5	XZ	Figure 61 and Figure 106
MS11	0	2.5	10	X	Figure 61 and Figure 106
MS12	0	2	2	X	Figure 61 and Figure 106
MS20	-1	9	18	XZ	Figure 61 and Figure 106
MS21	0	9	10	X	Figure 61 and Figure 106
MS22	0	10	2	X	Figure 61 and Figure 106
MS30	-1	16.5	17.5	XZ	Figure 61 and Figure 106
MS31	0	16.5	10	X	Figure 61 and Figure 106
MS33	0	16	2	X	Figure 61 and Figure 106Figure 106
V1	0	276	10	X	Table 30

Table 16–Specimen WB strain gage coordinates

Instrument	X (in.)	Y (in.)	Z (in.)	Orientation	Reference(s)
MS3	0	0.5	0.5	X	Figure 59 and Figure 106
MS4	0	7.5	0.5	X	Figure 59 and Figure 106
MS5	0	13.5	0.5	X	Figure 59 and Figure 106
MS10	1.5	2.5	18	XZ	Figure 60 and Figure 106
MS11	0	2	10.5	X	Figure 60 and Figure 106
MS12	0	2	2	X	Figure 60 and Figure 106
MS20	1.5	9	18	XZ	Figure 60 and Figure 106
MS21	0	9	10.5	X	Figure 60 and Figure 106
MS22	0	8	2	X	Figure 60 and Figure 106
MS30	1.5	16	18	XZ	Figure 60 and Figure 106
MS31	0	15.5	10.5	X	Figure 60 and Figure 106
MS33	0	15	2	X	Figure 60 and Figure 106

Table 17–Specimen FN strain gage coordinates

Instrument	X (in.)	Y (in.)	Z (in.)	Orientation	Reference(s)
XS1	19	14.5	6.25	Y	Figure 68
XS2	19	23	5.25	Y	Figure 68
XS3	19	30	6.25	Y	Figure 68
XS4	19	121	6.5	Y	Figure 68
XS5	19	128	6	Y	Figure 68
XS6	19	135.5	6.5	Y	Figure 68
XS7	19	142.5	6.5	Y	Figure 68
MS10	-1	2	18	XZ	Figure 63 and Figure 106
MS11	0	2	10.5	X	Figure 63 and Figure 106
MS12	0	3	2	X	Figure 63 and Figure 106
MS20	-1	9	18.5	XZ	Figure 63 and Figure 106
MS21	0	9	10.5	X	Figure 63 and Figure 106
MS22	0	7	2	X	Figure 63 and Figure 106
MS30	-1	16	18.5	XZ	Figure 63 and Figure 106
MS31	0	15.5	10.5	X	Figure 63 and Figure 106
MS33	0	14.5	2	X	Figure 63 and Figure 106
V1	0	276	10.25	X	Table 29

Table 18–Specimen FB strain gage coordinates

Instrument	X (in.)	Y (in.)	Z (in.)	Orientation	Reference(s)
XS1	19	14	5.5	Y	Figure 68
XS2	19	22	6	Y	Figure 68
XS3	19	29.5	5.25	Y	Figure 68
XS4	19	119	6	Y	Figure 68
XS5	19	127	6.25	Y	Figure 68
XS6	19	135	6	Y	Figure 68
XS7	19	142	6.25	Y	Figure 68
MS3	0	0.5	0.5	X	Figure 58
MS4	0	7	0.5	X	Figure 58
MS5	0	13.5	0.5	X	Figure 58
MS10	0.5	2	17	XZ	Figure 62 and Figure 106
MS11	0	2	10	X	Figure 62 and Figure 106
MS12	0	1.5	2	X	Figure 62 and Figure 106
MS20	1	9	18	XZ	Figure 62 and Figure 106
MS21	0	8.5	10	X	Figure 62 and Figure 106
MS22	0	7.5	2	X	Figure 62 and Figure 106
MS30	0.5	16.5	17.5	XZ	Figure 62 and Figure 106
MS31	0	16	10	X	Figure 62 and Figure 106
MS33	0	14	2	X	Figure 62 and Figure 106

Table 19–Specimen DC strain gage coordinates

Instrument	X (in.)	Y (in.)	Z (in.)	Orientation	Reference(s)
MS3	0	3	0.5	X	Figure 106
MS4	0	9	0.5	X	Figure 106
MS5	0	15	0.5	X	Figure 106
MS10	1	2	18	XZ	Figure 106
MS11	0	1.5	10.5	X	Figure 106
MS12	0	2	3	X	Figure 106
MS20	1	9	18	XZ	Figure 106
MS21	0	9	10	X	Figure 106
MS22	0	8.5	3	X	Figure 106
MS30	2	16	18	XZ	Figure 106
MS31	0	16.5	10.5	X	Figure 106
MS33	0	16	3	X	Figure 106
V1	0	276	10	X	Table 30

Table 20–Specimen DM strain gage coordinates

Instrument	X (in.)	Y (in.)	Z (in.)	Orientation	Reference(s)
MS3	0	2.5	0.5	X	Figure 106
MS4	0	8	0.5	X	Figure 106
MS5	0	15	0.5	X	Figure 106
MS10	3	2.5	18	XZ	Figure 106
MS11	0	2.5	10	X	Figure 106
MS12	0	3	2.5	X	Figure 106
MS20	3	9.5	18	XZ	Figure 106
MS21	0	9	10.5	X	Figure 106
MS22	0	8	2.5	X	Figure 106
MS30	3	16	18.5	XZ	Figure 106
MS31	0	16	10	X	Figure 106
MS33	0	15	2.5	X	Figure 106

D.5 Results and Discussion: Fabrication

Strain and crack data were collected during multiple stages of fabrication including prestress transfer, lifting, storage, trucking, and deck placement. Data were collected to analyze the effects of fabrication events on end region behavior. The effects of end region detailing, particularly confinement reinforcement, were also of interest. Strain data are presented and discussed first followed by crack data.

D.5.1 Strain Data

D.5.1.1 Concrete Strain

Concrete strain data were primarily collected from girders H and V. These girders had the same strand shielding pattern, instrumentation scheme, material properties, and timing of construction events. To facilitate review of the strain-time history, the strand flame-cutting sequence is divided into the stages shown in Table 21. Stages A through D listed in Table 21 are graphically depicted in Figure 51.

General trends in the strain-time history for specimen HC (Figure 52) are representative of the other specimens in girders H and V. Any differences between the specimens were in the strain magnitudes, which are discussed later.

Table 21–Girders H and V fabrication chronology

Stage	Event
A	strands 1-4 cut
B	strands 5-12 cut
C	strands 13-32 cut
D	strands 33-49 cut
E	All bonded strands cut, girder resting on bed
F	Girder held aloft by lifting loops
G	Girder resting on dunnage

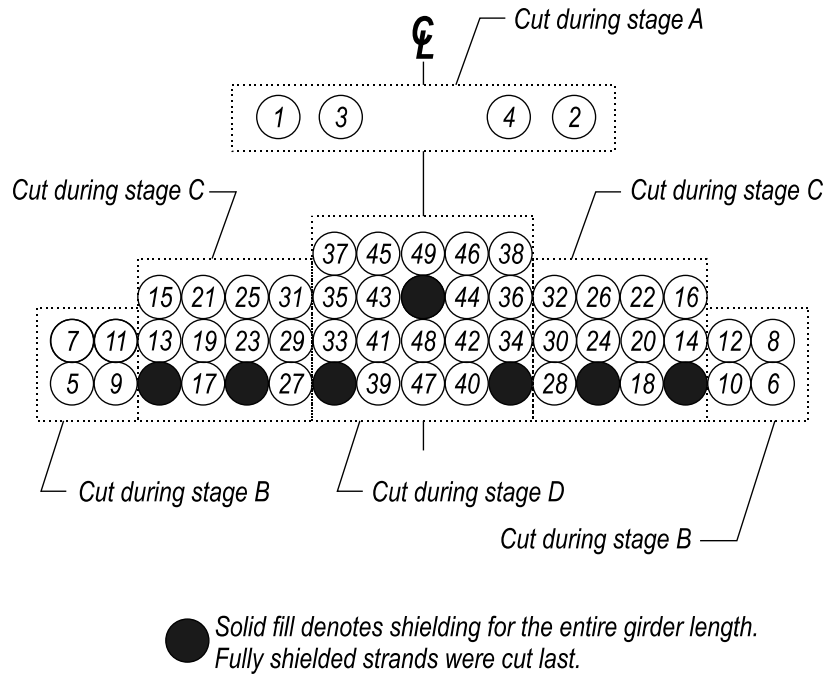


Figure 51–Girders H and V strand cutting stages

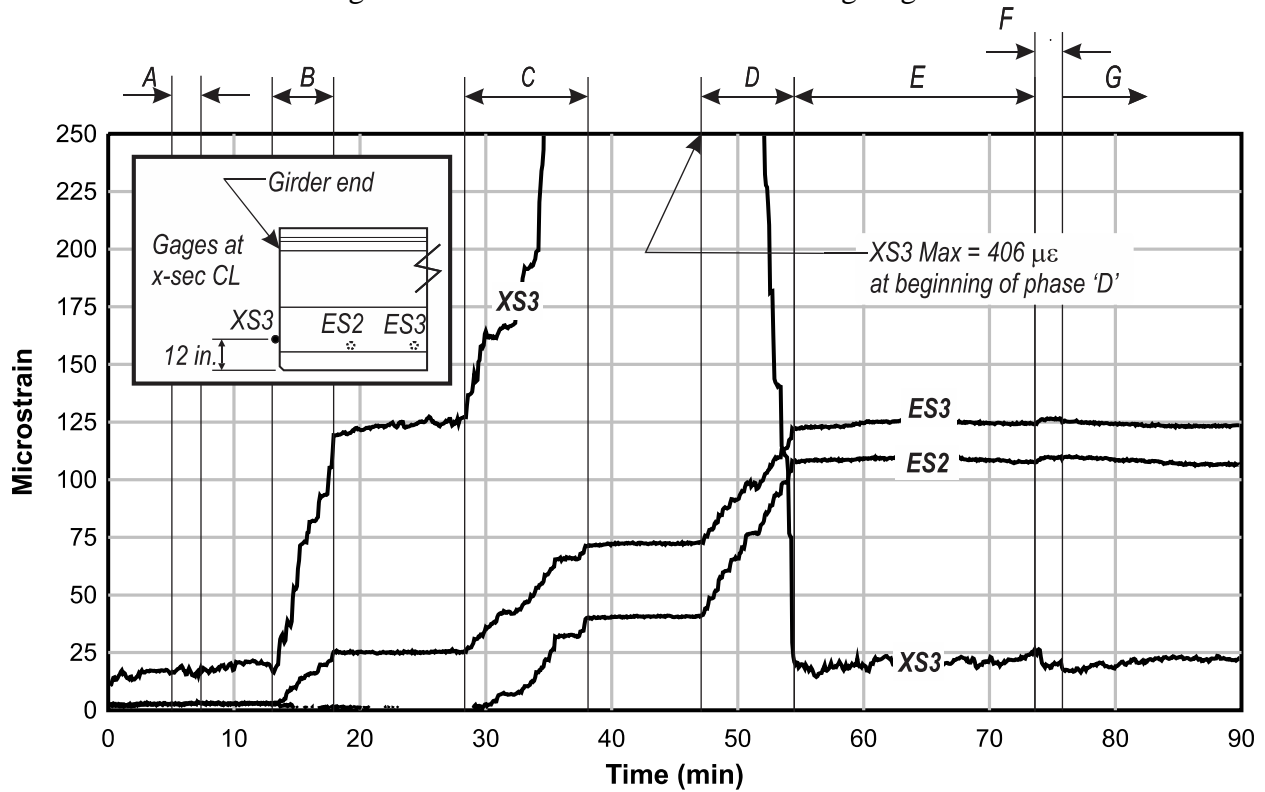


Figure 52–Transverse strain HC

Strands in the top flange were the first to be cut; this stage is denoted A in Figure 52. Data indicate that the transverse strain change was negligible when the top strands were cut. Cutting the bottom strands (stages B, C, and D) had significant impact on transverse tensile strain. The largest measured transverse tensile strain in specimen HC was 406 microstrain reported by gage XS3. This gage was located on the end of the girder, at the cross-section centerline, 3in. above the strands. The maximum strain occurred at the beginning of stage D after all strands in the outer flange had been cut and before any of the strands below the web had been cut. For this chapter, strands in the outer portion of the flange are referred to as “outer strands” and strands below the web are referred to as “inner strands”.

Transverse strain at gage XS3 decreased as inner strands were cut during stage D. The strain-time history from gage XS3 can be understood by considering the strand release pattern (Figure 51) and the resulting deformed shapes (Figure 53). As the outer strands were cut during stage B, the outside edges of the bottom flange deformed as shown in Figure 53. This deformed shape corresponded with the formation of tensile strains at the location of XS3. After the inner strands were cut, deformation of the bottom flange was more uniform and the tensile strain at XS3 was partially relieved. Once all of the strands were cut (stage E), the reported tensile strains at XS3 settled to approximately 25 microstrain.

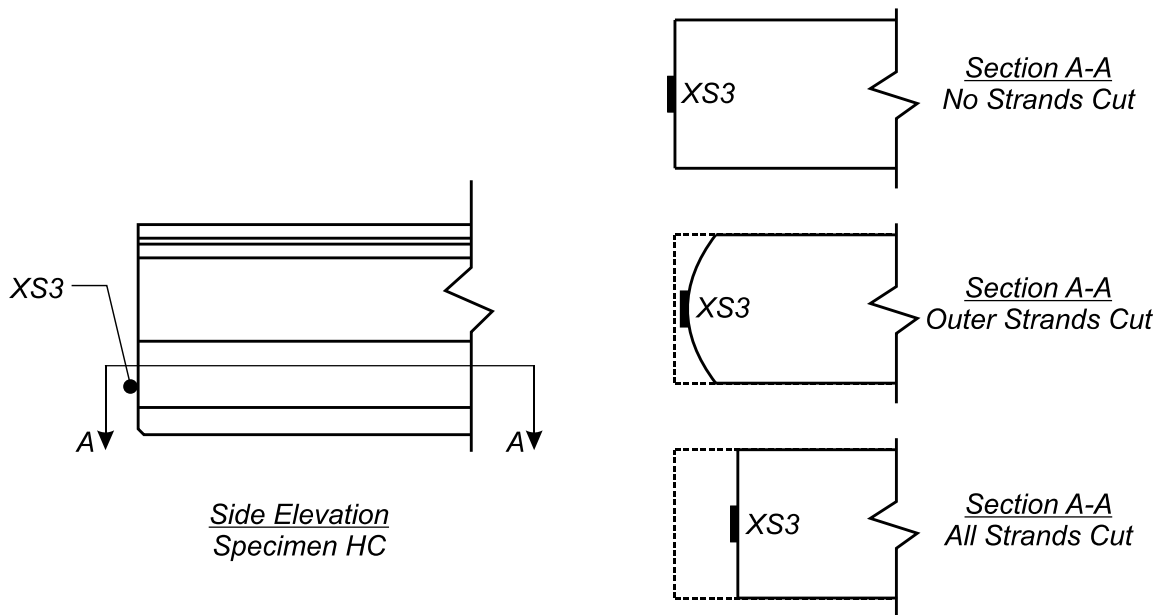


Figure 53–Flange displaced shapes for specimen HC

Concrete strain was monitored for all specimens in girders H and V using gages placed at the same location as XS3 on specimen HC. Results from these gages are summarized in Table 22. While the overall behavior of the other specimens in girder H and V were similar to that shown in Figure 52, the magnitudes of the reported strains differed.

Several observations can be made from the strain data in Table 22. First, although cracks were not visually observed during prestress transfer, the strain magnitudes suggest that cracks had likely formed in each specimen, with the possible exception of specimen VC. Expected rupture strain for the concrete used in the specimens is approximately 132 microstrain. This value of expected rupture strain was derived from empirical equations for concrete elastic and rupture moduli from ACI 318 (2011). Second, the average maximum tensile strain in the unconfined specimens (HU and VU) was 3.4 times greater than the average maximum tensile strain in the confined specimens (HC and VC). Cracks forming in the unconfined ends would not have been impeded by confinement reinforcement, resulting in greater maximum transverse strains than in the confined ends. Finally, the average concrete tensile strain during stage E (all strands cut) was 2.6 times greater in the specimens without confinement reinforcement. The presence of confinement reinforcement significantly reduced the concrete tensile strain at the end of specimens HC and VC relative to specimens HU and VU.

Internal concrete strain gages (ES2 and ES3 in Figure 52) reported increases in tensile strain as prestress force was transferred. In contrast to gage XS3, the tensile strain reported by these gages increased as the inner strands were cut during stage D. Based on this observation and the location of the internal gages, it is concluded that the bending behavior captured by gage XS3 only occurred at or near the end of specimen HC. ES gages in HU, VC, and VU confirmed similar behavior in those specimens. In each specimen strain magnitudes reported by ES gages (Table 22) suggest that concrete near the internal gages remained linear-elastic (i.e. no cracking) during prestress transfer.

Confinement reinforcement did not affect the magnitude of concrete strain at the ES gages. Similar strain magnitudes were reported by specimens with and without confinement reinforcement (Table 22). Gages ES2 and ES3 were placed approximately 2ft and 4ft from the specimen ends, respectively. It is concluded that confinement reinforcement only affected concrete strain at the end of the test specimens.

Stage F on Figure 52 denotes lifting of girder H. Figure 54 shows the supports conditions, loading, shear, and moment diagrams for the girders before, during, and after lifting. The change in support conditions had negligible effect on strain in the end region. None of the gages in the end region of girders H or V reported more than a 25 microstrain change during lifting and placement on dunnage.

Table 22–Tensile strain girders H and V

Gage	Strain in specimens with confinement reinforcement (microstrain)		Strain in specimens without confinement reinforcement (microstrain)	
	HC	VC	HU	VU
X3 maximum tensile strain	406	177	724	1258
X3 Stage E (all strands released)	25	15	60	45
ES2 Stage E	109	113	100	135
ES3 Stage E	125	88	111	105

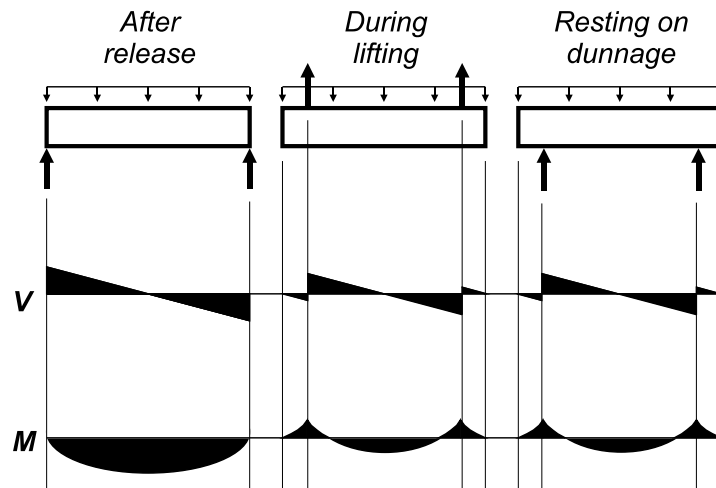


Figure 54–Shear and moment during release, lifting, storage (prestressing not shown)

D.5.1.2 Confinement Reinforcement and Bearing Plate Strain

Girders W and F were fabricated during phase 2 and had the same material properties, instrumentation scheme, and timing of construction events. Instrumentation was designed to

capture confinement reinforcement and bearing plate behavior. To facilitate discussion of data, strand cutting events were broken into the stages listed in Table 23. Strand cutting events listed in Table 23 are keyed to the strand cutting pattern shown in Figure 55.

The strand bond patterns in girders W and F (Figure 56) had significant influence on the observed strain behavior. Girder W had fully bonded strands placed primarily below the web and partially shielded strands placed in the outer portion of the flange. Girder F had fully bonded strands in the outer portion of the flange and partially shielded strands below the web.

Three strain gages were placed on the bearing plates in specimens FB and WB. Gages were oriented to monitor the transverse (x-x) strain during prestress transfer. Gage locations and strain data are shown in Figure 57. Gage MS3 in specimen FB malfunctioned during prestress transfer and data from this gage is not shown in figure.

Table 23–Girders W and F fabrication stages

Stage	Event
J	strands 1-4 cut
K	strands 5-30 cut
L	Pause
M	strands 30-56 cut
N	all strands cut

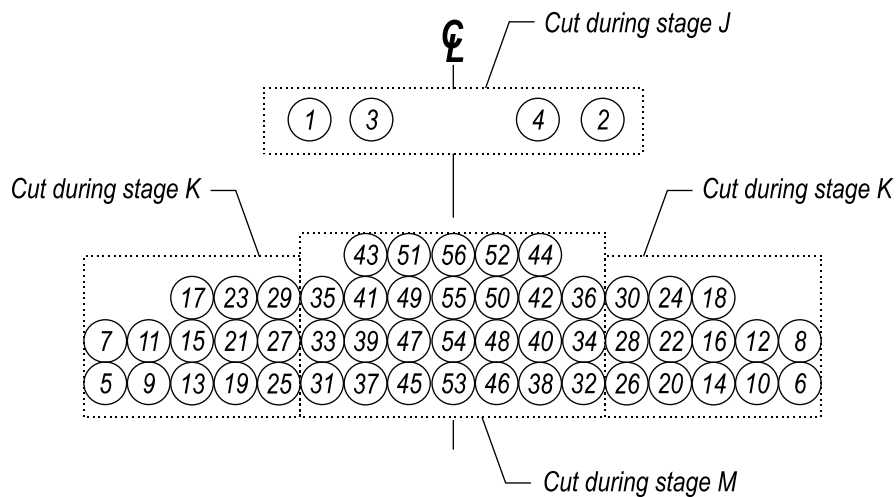


Figure 55–Girders W and F strand cutting stages

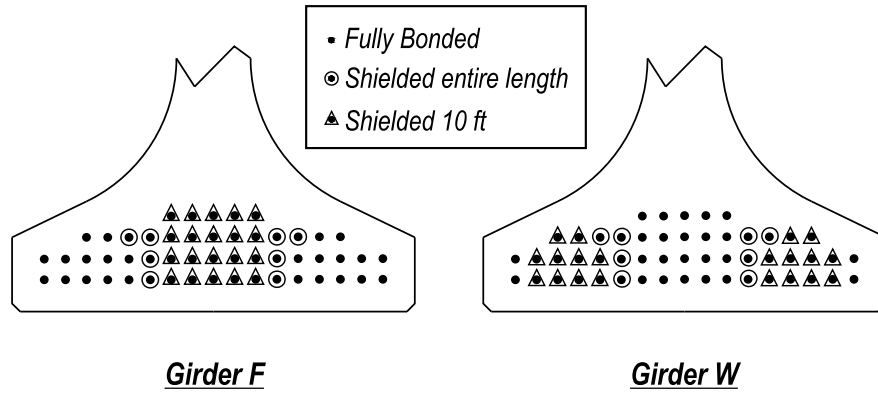


Figure 56–Girders W and F strand bond patterns

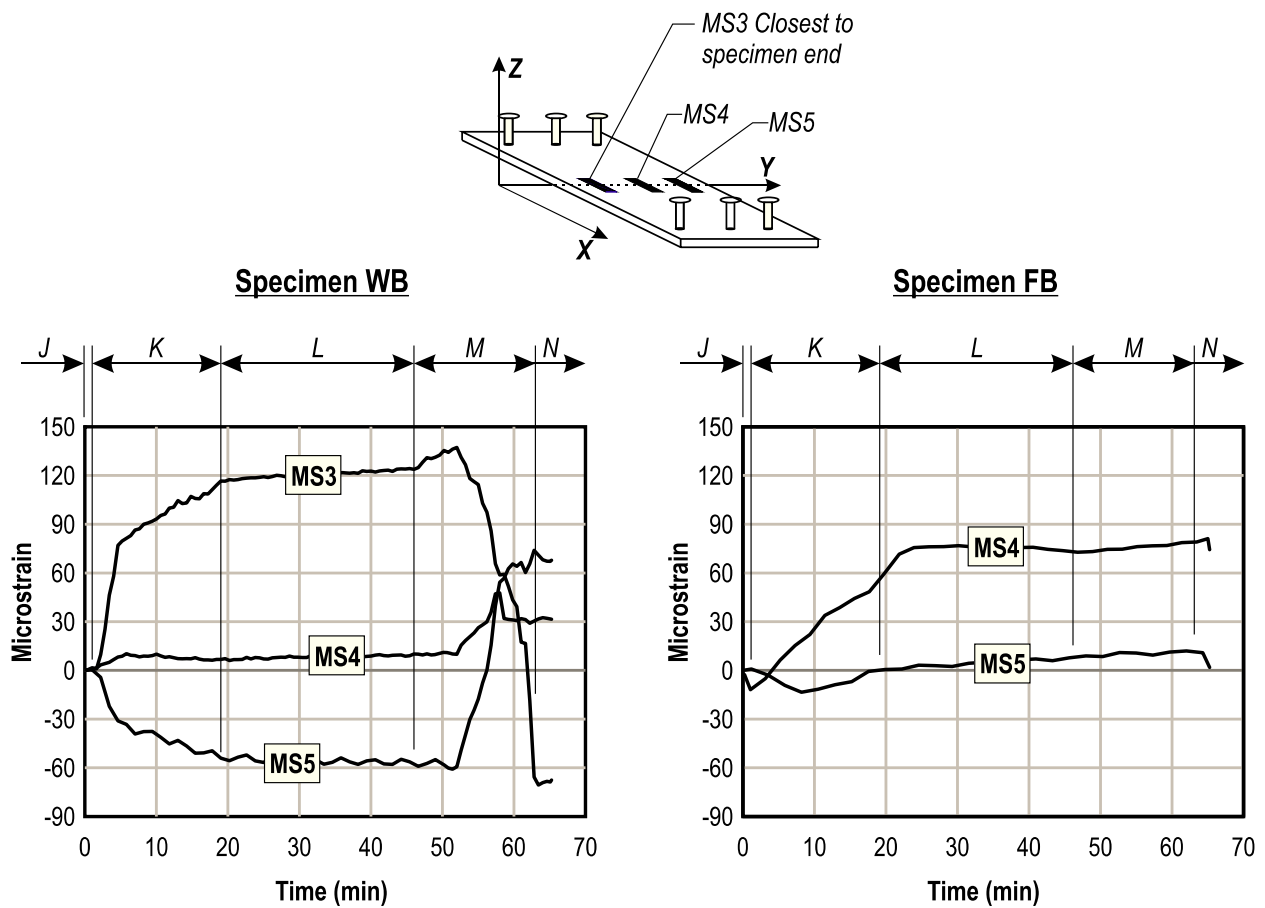


Figure 57–Bearing plate strain

Strain at MS4 in specimen FB grew in tension as the outer strands were cut during stage K. Outer strands were fully bonded in specimen FB and caused the flange and plate to bend as shown in Figure 58. Strain in the plate was fairly constant after stage K. This is because no

strands were cut during stage L and because the strands released during stage M were shielded in specimen FB. The difference in strain between gages MS4 and MS5 indicates in-plane bending of the plate due to the eccentric prestress force.

Data from gages on the plate in specimen WB also indicate in-plane bending during and after strand cutting. The direction of plate bending in specimen WB changed when the strands below the web were cut during stage M. This behavior is attributed to the strand bond pattern in specimen WB, which placed a few fully bonded strands in the outer portion of the flange and many fully bonded strands below the web. This pattern is thought to have caused the deformations and internal forces shown schematically in Figure 59. Release of the outermost strands at the beginning of stage K led to tension in the bearing plate at MS3 and compression in the bearing plate at MS5. The strain sense in the bearing plate reversed after the inner strands were released during stage M. After all strands were released (stage N) the bearing plate was in compression at MS3 and tension at MS5. The net strain in the plate after all strands were cut was approximately 32 microstrain tension, as calculated from the average of gages MS3, MS4, and MS5. The average strain from these gages is also equal to the strain reported at MS4, indicating that the strain reported by MS4 is also a reasonable measure of net strain.

Transverse forces in the bearing plates were calculated by multiplying the net bearing plate strains by the plate cross-sectional area and elastic modulus. Assuming that the net bearing plate strain is equal to the strain at MS4 (center of plate) the net plate strain at stage N was 32 microstrain tension for specimen WB and 79 microstrain tension for specimen FB. Accordingly, net tensile stresses in the plates were 0.9ksi, and 2.3ksi, and the net tensile forces in the plates were 5.2kip and 13.6kip for specimens WB and FB, respectively.

Select confinement reinforcement assemblies were instrumented with strain gages to monitor confinement reinforcement strain during prestress transfer. A confinement assembly is defined as the reinforcing bars placed together at the same y-ordinate (Figure 60). One strain gage was placed on each of the three reinforcement layers in each assembly.

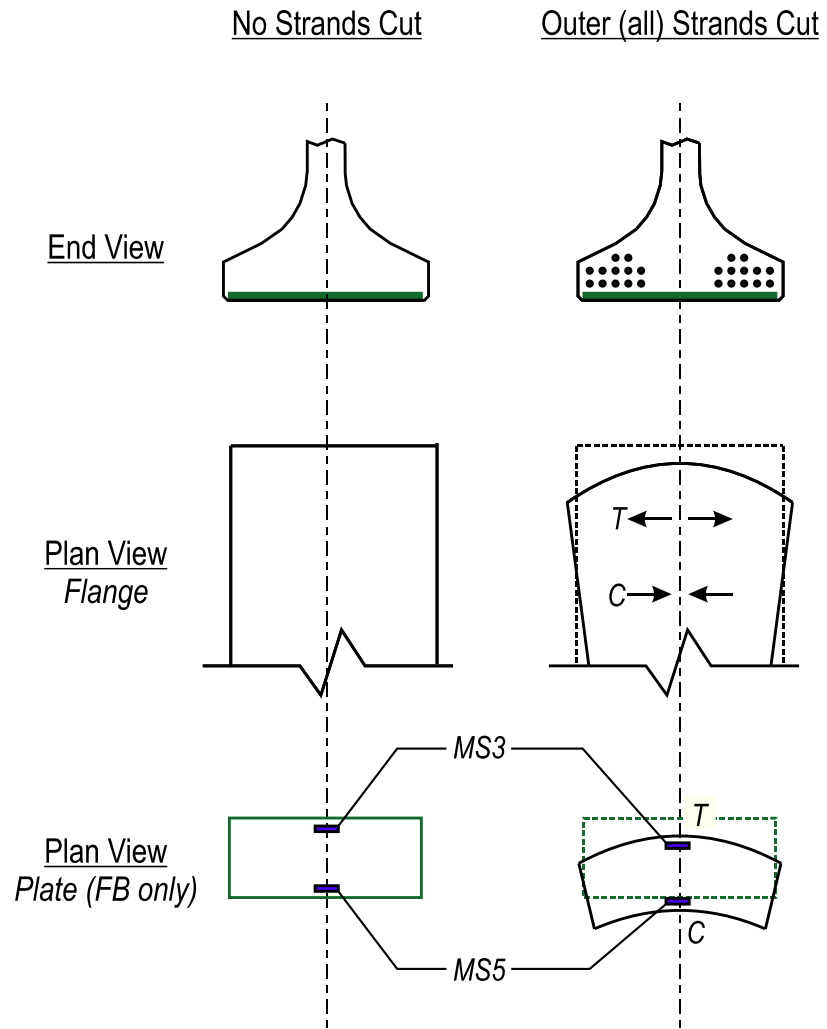


Figure 58–Flange displaced shapes specimens FN and FB

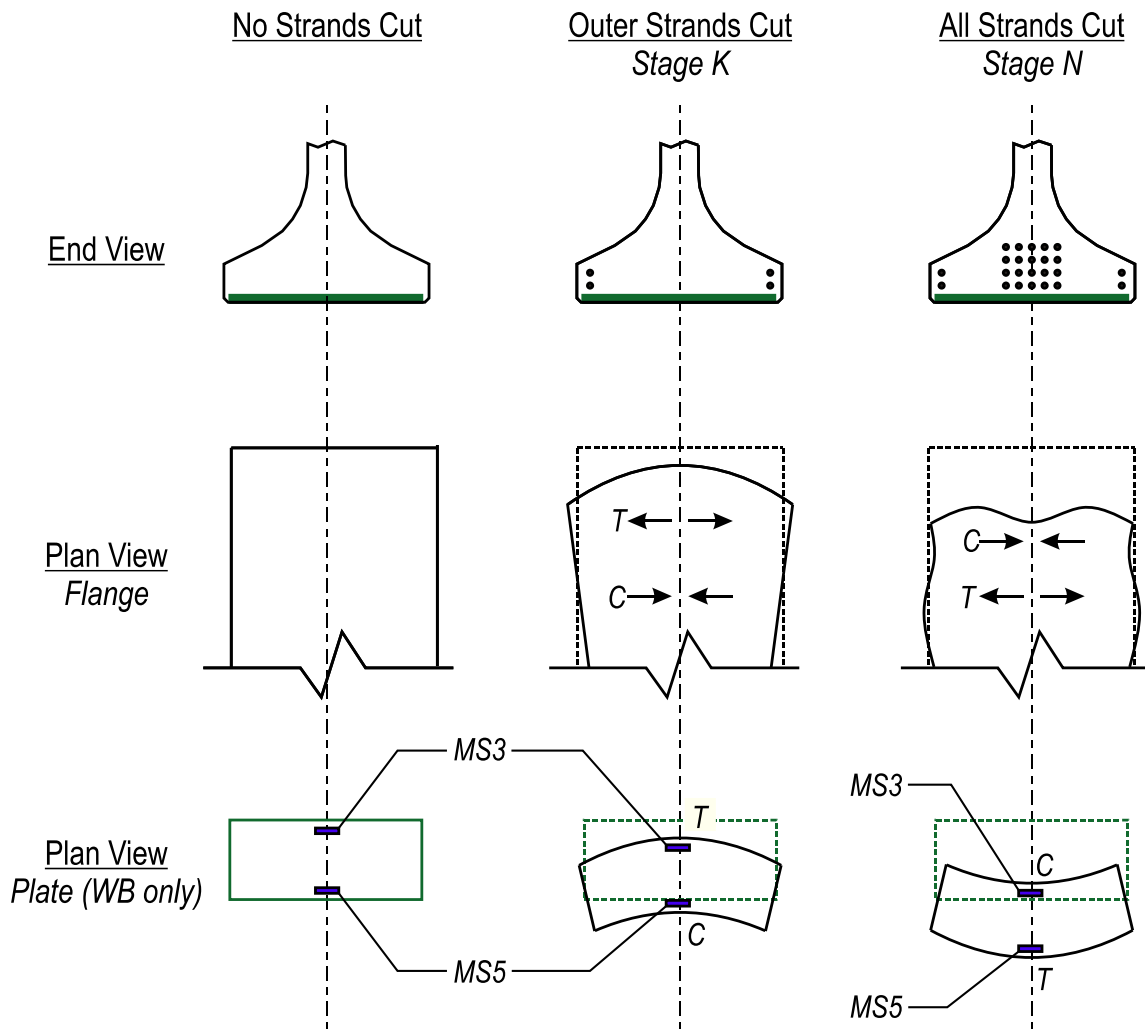


Figure 59–Displaced shapes specimen WB and WN

Figure 60 shows confinement reinforcement strain from specimen WB. Reinforcement nearest to the end of the girder ($y=2\text{in.}$) was initially in tension due to release of the outermost strands during stage K. The strain later became compressive as the inner strands were released during stage M. This strain behavior is similar to the bearing plate strain in WB and is also attributed to flange bending behavior described in Figure 59. Confinement reinforcement placed 9in. from the end had very little strain until the innermost strands were released at the end of stage M. General strain behavior from the confinement assembly at 9 in. is representative of the strain behavior reported by gages on the confinement assembly placed 15 in. from the end (not shown).

Specimen WN had the same strand bond pattern as WB. The only significant difference in strain data between WN (Figure 61) and WB was that the confinement reinforcement located 2in. from the end of specimen WN did not move all the way into compression during stage M. This difference may have been due to the absence of a bearing plate in specimen WN. Without a bearing plate there was less confinement in specimen WN and tensile strains were not relieved during stage M.

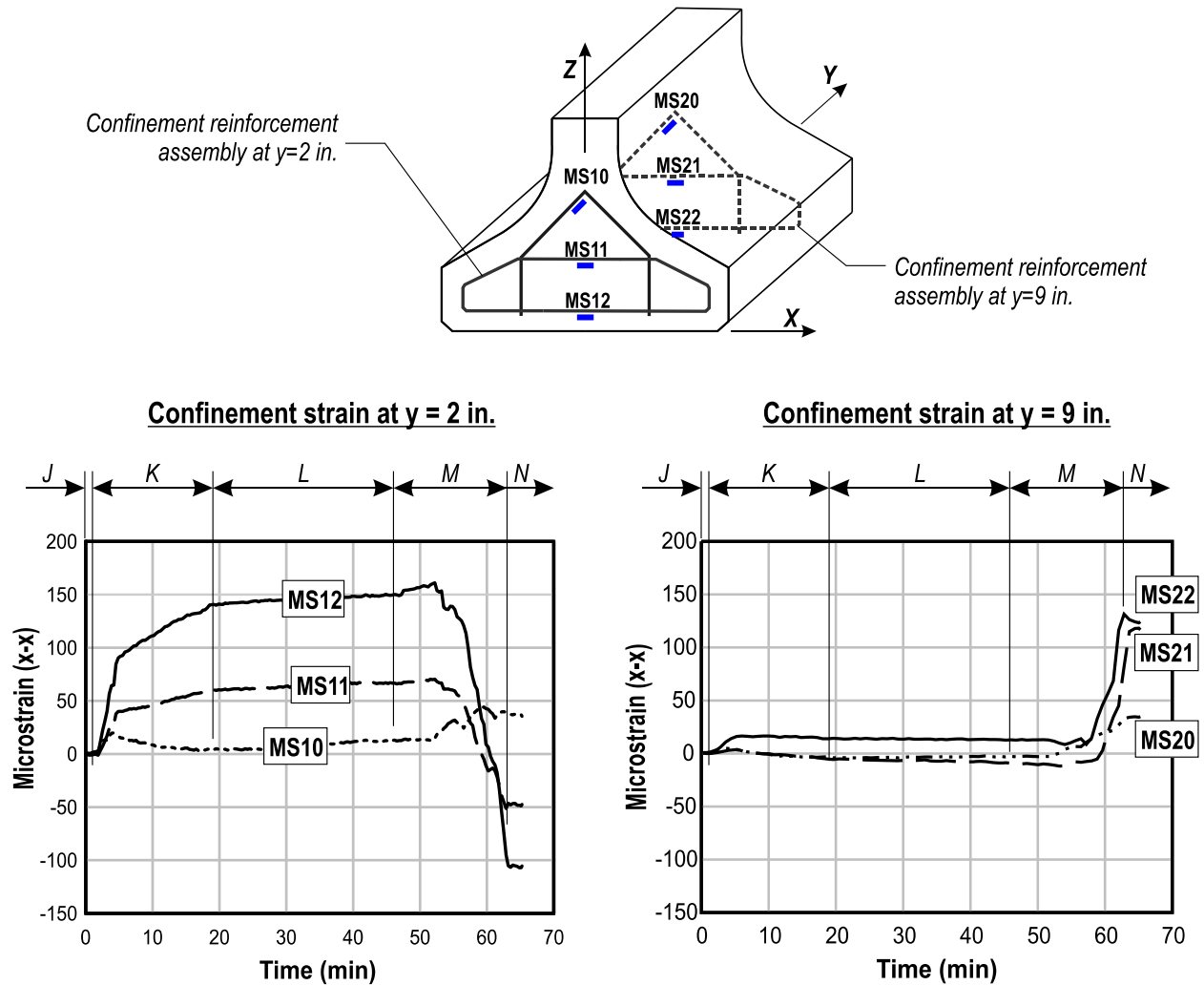


Figure 60–WB Confinement reinforcement strain at 2 in. and 9 in. from end of girder

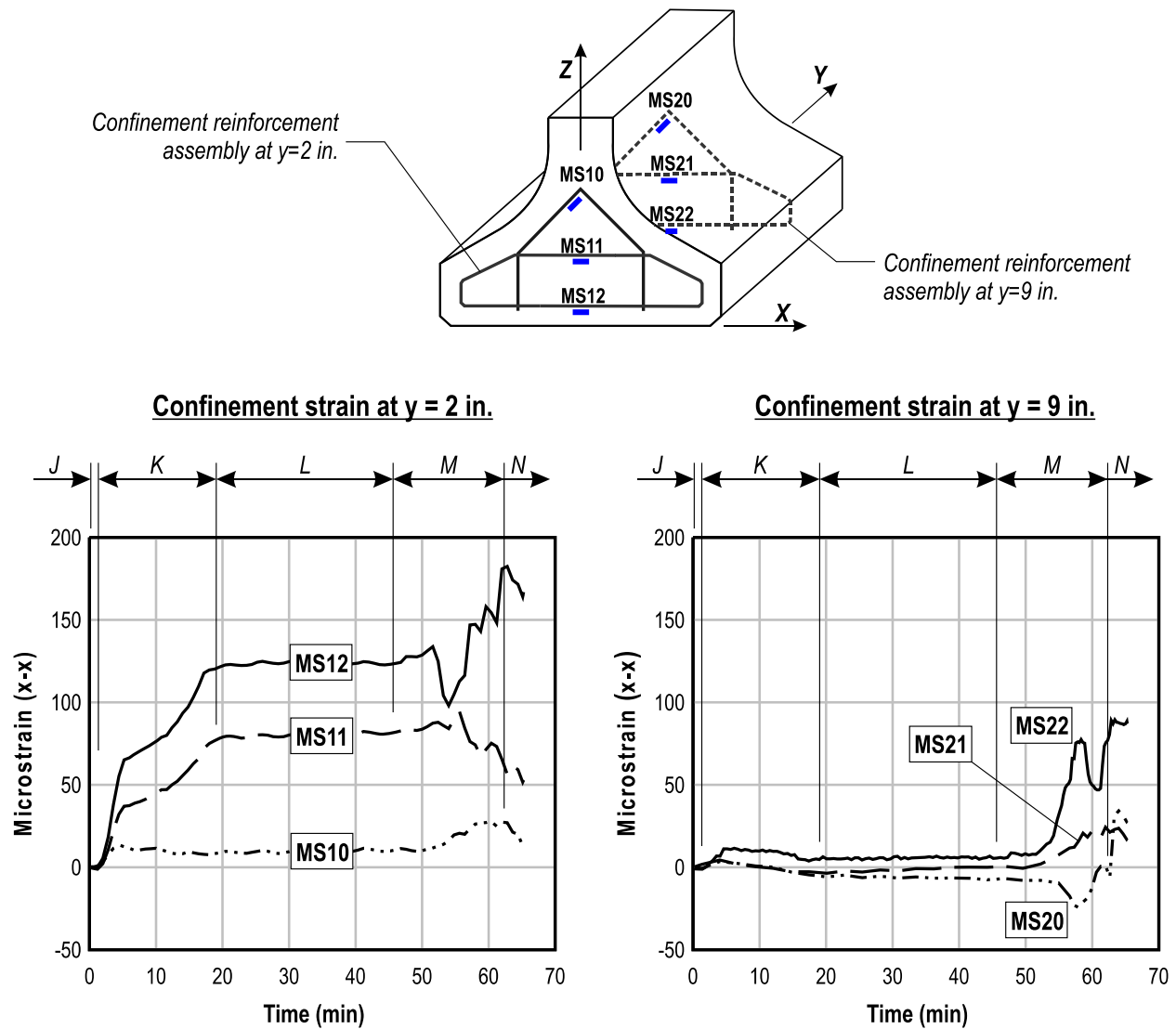


Figure 61–WN Confinement reinforcement strain at 2 in. and 9 in. from end of girder

Specimen FB had fully bonded strands in the outer flange, all of which were cut during stage K. As such, confinement strain in FB (Figure 62) increased during stage K. No fully bonded strands were cut after stage K and the strain did not change in the subsequent stages. Confinement reinforcement was in tension throughout and after the strand cutting process.

Specimen FN had the same strand bond pattern as FB with fully bonded strands located in the outer portion of the flange. Strain behavior in specimen FN (Figure 63) was similar to FB up until the inner strands were released during stage M. During stage M the strain increased rapidly in the bottom (MS12) and middle (MS11) layers of confinement reinforcement. The strain magnitude during stage M suggests that cracking occurred in the nearby concrete. This

result is puzzling because inner strands in specimen FB were shielded for 10ft from the specimen end. It appears that the shielded strands may have induced stresses in the concrete as they expanded after being cut. The thin plastic used to shield the strands may have been insufficient to absorb the strand expansion and prevent normal stresses at the strand-concrete interface. These stresses could have caused the strain changes at gages MS12 and MS11 that occurred during stage M.

Strain data at the end of stage N (all strands cut) is listed in Table 24 for each specimen. Several observations can be made by averaging the stage N strain data (Figure 64). First, strain was greatest in the bottom layer of reinforcement for each test specimen. On average strain in the bottom layer was 1.4 times greater than the middle layer strain and almost 3 times greater than the top layer strain. Second, the largest confinement reinforcement strain occurred in specimens FN and FB in the confinement assemblies 2 in. from the member ends.

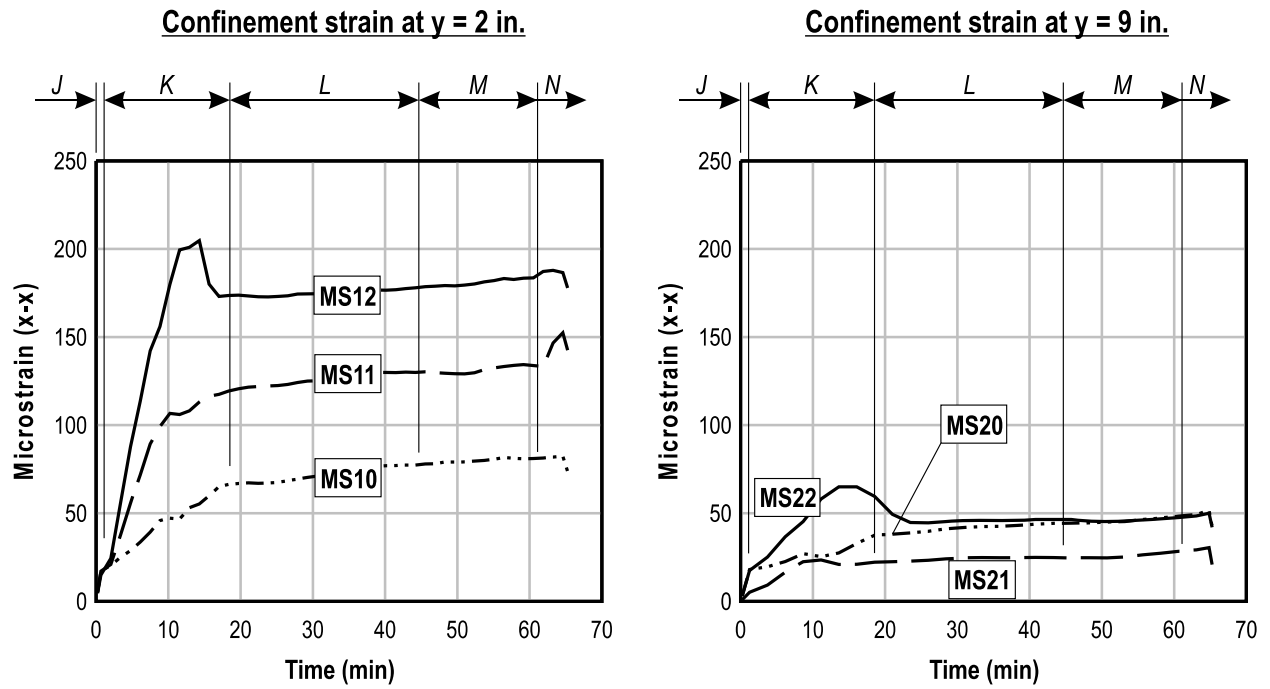
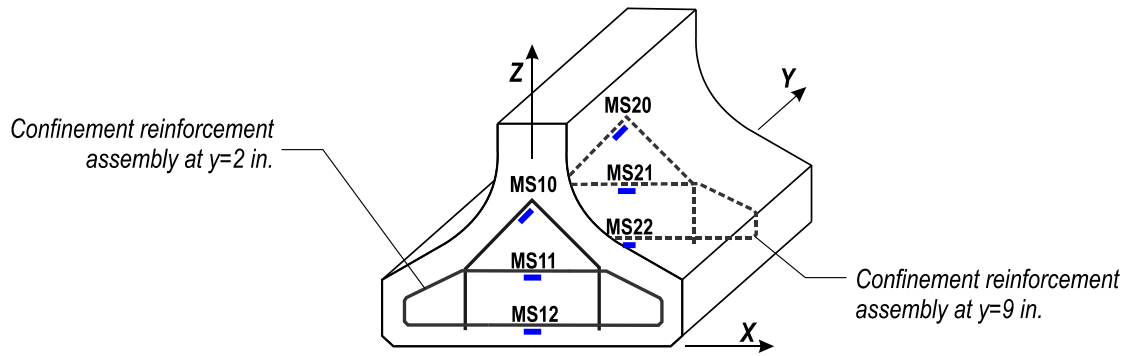


Figure 62–FB confinement reinforcement strain at 2 in. and 9 in. from end of girder

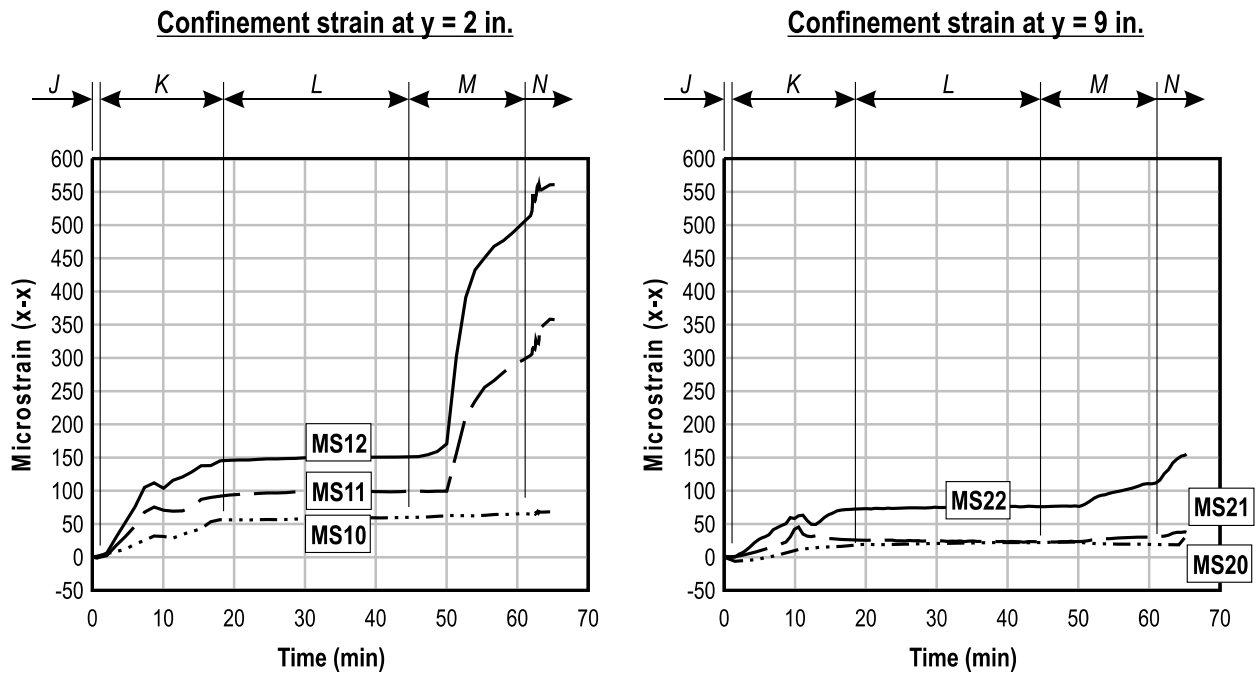
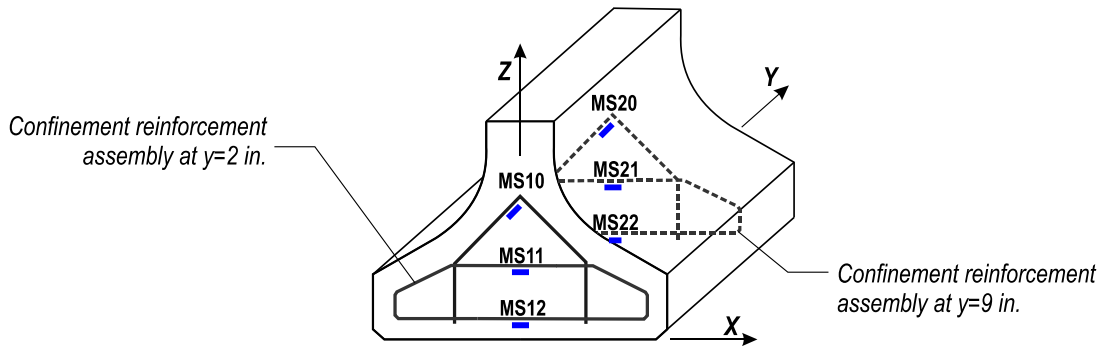


Figure 63–FN Confinement reinforcement strain at 2 in. and 9 in. for end of girder

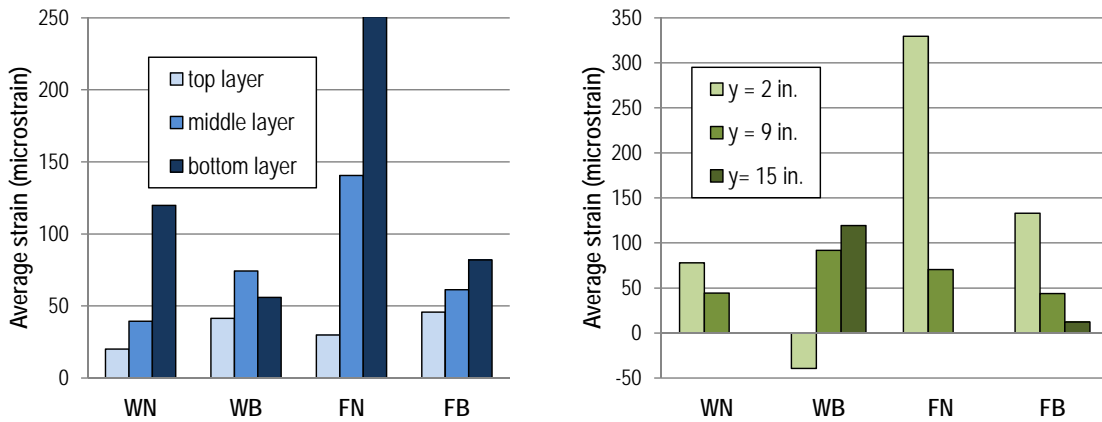


Figure 64–Confinement reinforcement average strain at prestress release

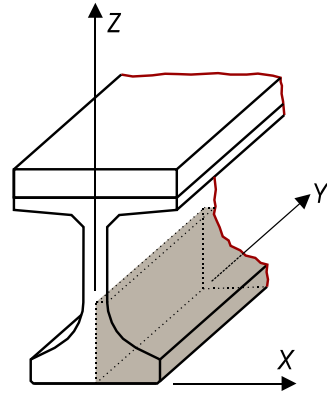
Table 24–Confinement reinforcement strain after prestress transfer

Specimen	Confinement reinforcement layer	Confinement strain (microstrain)		
		y = 2in.	y = 9in.	y = 15in.
WN	Top	7	19	not recorded
	Middle	47	28	not recorded
	Bottom	160	87	not recorded
WB	Top	37	34	53
	Middle	-49	117	155
	Bottom	-106	124	150
FN	Top	70	18	not recorded
	Middle	358	38	not recorded
	Bottom	560	155	not recorded
FB	Top	81	51	5
	Middle	134	30	20
	Bottom	184	50	12

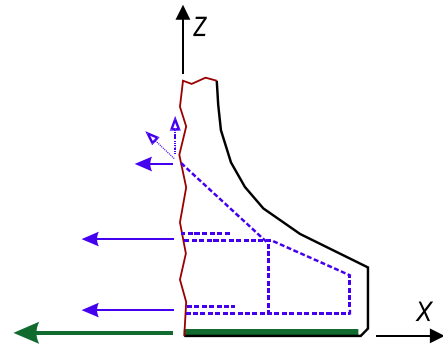
Confinement reinforcement strain at 2 in. from the end of FN and FB was almost 4 times greater on average than confinement strain at 9 in. This is due to the bending behavior of the FN and FB described in Figure 58. Third, confinement strain in specimen FN was typically larger than in FB. The average confinement strain was over 2 times larger in specimen FN than FB. The difference in strain magnitude is attributed to the bearing plate in FB which carried transverse forces thereby reducing the strain in the confinement reinforcement. Finally, the maximum confinement strains in FN and FB were larger than the maximum confinement strains in WN and WB. On average the maximum strain in the FX specimens was 2.6 times greater than the WX specimens

Strain data were used to estimate the total force in each confinement reinforcement assembly after all strands had been cut (stage N). Forces were calculated by multiplying strains from Table 24 by the reinforcement area and steel elastic modulus. Two of five assemblies in specimens WB and FB were not monitored with strain gages. Strains in these assemblies were determined using linear interpolation. In specimens WN and FN three of five confinement assemblies were not monitored. Strains in the unmonitored assemblies were interpolated using the available strain data, or were extrapolated using the available data as well as the relationships between assemblies in specimens WB and FB. Results for each specimen are shown in Figure

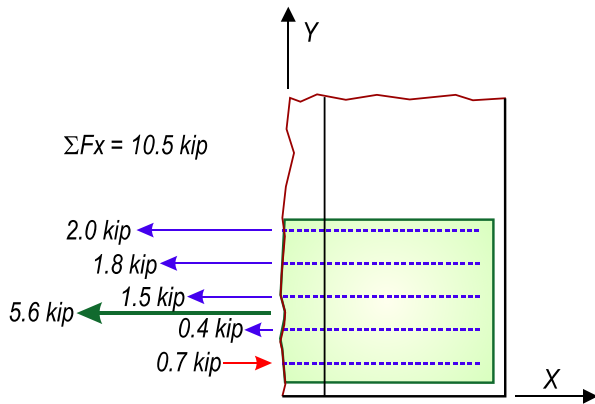
65 along with the estimated forces in the bearing plates. Only the x-direction force component in the inclined top layer of reinforcement was included in the results shown in the figure.



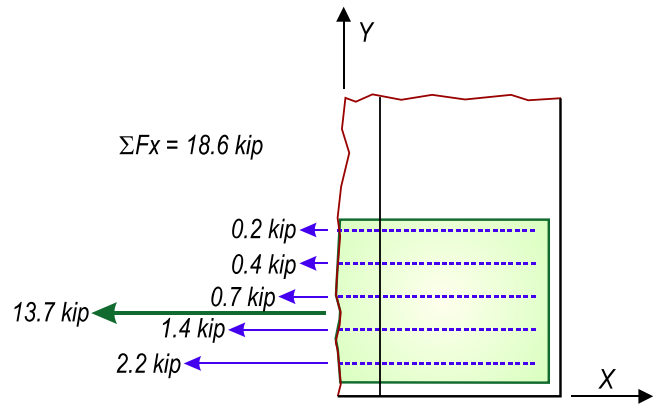
End region
isometric view



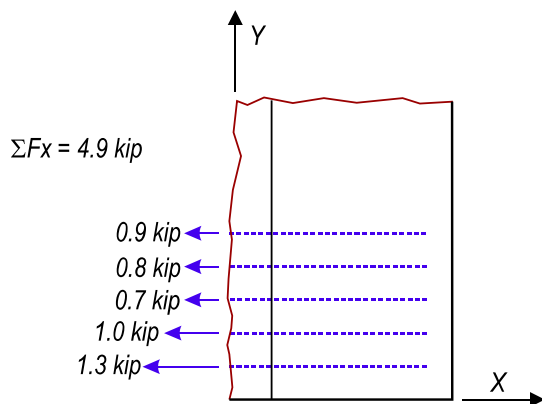
Bottom flange section
end view



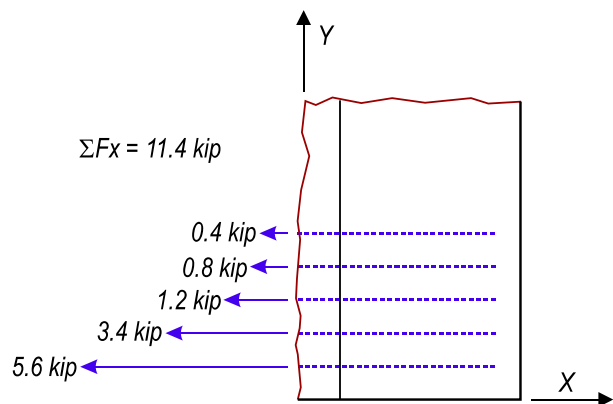
WB bottom flange
partial plan view



FB bottom flange
partial plan view



WN bottom flange
partial plan view



FN bottom flange
partial plan view

Figure 65—Forces in reinforcement and plates after prestress transfer

Total transverse force in the confinement reinforcement and bearing plate (where present) was 63% larger on average in specimens FB and FN than in specimens WB and WN. The additional force is attributed to the strand bond pattern in specimens FB and FN, which placed fully bonded strands in the outer portion of the flange. These fully bonded strands led to additional tension at ends of FN and FB. Most outer strands in specimens WB and WN were partially shielded and did not affect tension at the specimen ends. Transverse forces are compared to the jacking forces in Table 25. Combined transverse forces were equal to 0.6% to 1.7% of the jacking force in the fully bonded strands. Once again, due to the strand bond pattern, the relationship of transverse force to jacking force was larger for FN and FB than for WN and WB.

Data were not collected to estimate confinement reinforcement and bearing plate forces in specimens DC and DM. Strands in these specimens were placed in the ‘design’ strand bond pattern. Fully bonded strands were evenly distributed throughout the bottom flange in this pattern, placing it somewhere between the W_x and F_x specimens in terms of transverse tensile behavior. The transverse force in specimens with the design pattern would likely be smaller than F_x specimens because inner strands in the design pattern relieved tension due to the outer strand. Also, specimens with the design pattern likely had greater transverse force than the W_x specimens because the design pattern included outside strands.

Table 25–Confinement and plate forces

Specimen	Confinement reinforcement transverse force	Bearing plate transverse force	Combined force in reinforcement and plate	Jacking force in fully bonded strands	Transverse force / jacking force
WN	6.2 kip	--	6.2 kip	1070 kip	0.6%
WB	4.3 kip	5.6 kip	9.9 kip	1070 kip	0.9%
FN	11.1 kip	--	11.1 kip	1070 kip	1.0%
FB	4.9 kip	13.7 kip	18.6 kip	1070 kip	1.7%

D.5.1.3 Transfer Length

Longitudinal strains in the bottom flange of I-girders increase through the transfer length as prestress force is transferred from strands to concrete. At locations beyond the transfer length

longitudinal strain is approximately constant. Transfer length in the test girders was experimentally determined by identifying the location at which longitudinal strain in the bottom flange transitioned to constant strain. This was accomplished using strain gages placed at intervals along the bottom flange (Figure 66).

When sufficient data are available, the 95% Average Maximum Strain (AMS) Method is a well-established method for determining transfer length from experimental strain data (Russell and Burns 1993). The available strain data in the current study were insufficient to apply the AMS method, but were still sufficient to estimate the transfer length by other means.

Figure 67 presents strain gage data from the bottom flange of girders H and V immediately after prestress transfer. Blue markers on the figure indicate the strain values reported by individual gages. Values reported by the gages were effectively constant (with some experimental scatter) for the monitored positions along the specimen lengths. This indicates that the gages were placed too far from the end of the girder to capture strain in the transfer length. A bilinear curve representing the apparent strain profile is also shown in Figure 67. The apparent profile shows that the strain must be zero at the end of the girder and must increase to the experimental values recorded at 18in. Beyond 18in. the experimental strains and apparent strain were approximately constant. Thus the transition to constant strain occurred prior to 18in. and it is concluded that the transfer length is not greater than 18in. for girders H and V.

Figure 68 shows experimental strain data from girder F. As before, the blue markers on the figure are data points from individual gages. A piecewise linear curve representing the apparent strain profile is also shown in the figure. Girder F had fully bonded strands in the outer portion of the flange. Strands below the web were shielded for 10ft from the end. Gages were placed near the end of the girder and 10ft from the end in order to evaluate the transfer length of both fully bonded and partially shielded strands.



Figure 66–Strain gages for measuring transfer length

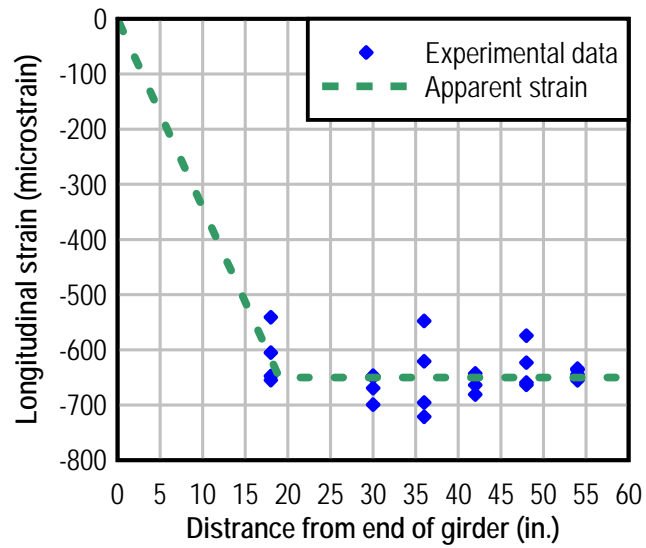


Figure 67–Transfer length in girders H and V

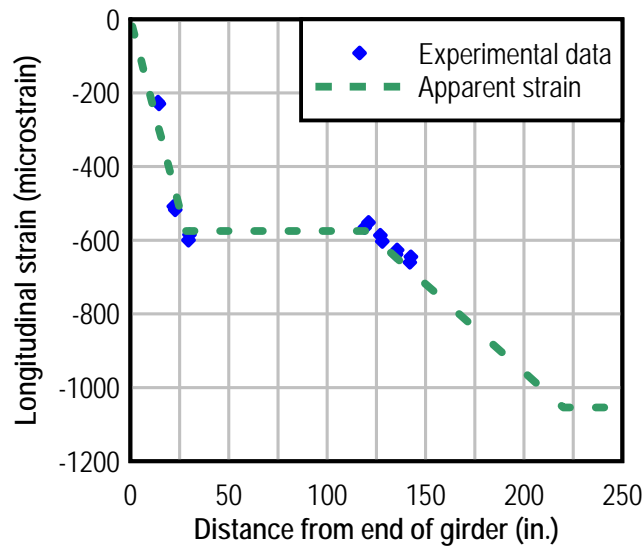


Figure 68–Transfer length in girder F

Gages placed near the ends of girder H reported increasing strain indicative of the transfer length. Beyond 30in. the strain was approximately constant until 120in. at which point the partially shielded strands began to transfer prestress force. Thus the change to constant strain occurred approximately 30in. from the girder end indicating that transfer length for the fully bonded strands was also approximately 30in.

Gages placed between 120in. and 144in. from the end reported increasing strain along the girder length. This indicates that they were within the transfer length of the partially shielded strands. Data were not available beyond 144in. and the transition to constant strain was not observed. As such transfer length of the partially shielded strands cannot be obtained directly from the available data. Transfer length can be estimated by assuming linear-elastic behavior of the concrete and strands. The 24 fully bonded strands affected a microstrain of 575 at the end of their transfer length. The 20 partially shielded strands should have added a proportional amount of strain, resulting in 1054 microstrain at the end of their transfer length. Slope of the apparent strain profile is based on the available data points. Extending the strain profile along this slope shows that the apparent strain intersects 1054 microstrain at a distance 220in. from the member end. Prestress transfer of the partially shielded strands is thus estimated to have occurred between 120in. and 220in. from the member end. The estimated strand transfer length is 100in. This is significantly longer than the transfer length of the fully bonded strands. Additional data

are necessary, though unavailable, for making a more accurate determination of transfer length in the partially shielded strands.

Transfer length was not measured in the other phase two girders (W and D) due to constraints with the data acquisition system. The transfer lengths in girders W and D were likely similar to girder F because the same strand and concrete materials were used for all phase two girders.

Measured transfer length for girders H and V was different from girder F. This difference is attributed to the different strand and concrete materials used in phase one (girder H and V) and phase two (girder F). Measured transfer lengths for fully bonded strands in both phases were less than the AASHTO LRFD calculated transfer length of 36in. Differences between experimental and code values may partially be due to the fact that strain data collected immediately after prestress transfer were used to determine the experimental transfer lengths. Barnes et al. (1999) observed that the transfer length grows by 10% to 20% in the weeks following prestress transfer.

Gages used to measure transfer length were placed at the outside edge of the bottom flange. Longitudinal strain at this location occurred due to axial shortening of the girder and due to shear lag from prestressing forces in the outer stands. Because of the shear lag component, the apparent transfer lengths measured by the gages were likely somewhat longer than the effective transfer length. This effect would be greatest near the end of the girder. Barnes et al. (1999) used finite element modeling to quantify the effect of shear lag on transfer length measurements in AASHTO Type I girders. For fully bonded stands and an apparent transfer length of 18in. Barnes et al. calculated that the effective transfer length would be 16.5 in. For the test girders, the shear lag component of the strain will be affected by the relatively slender and wide bottom flange of the FIB. Thus the correction due to shear lag in the test girders would likely be slightly larger than calculated by Barnes et al.

D.5.2 Crack Data

Girders were inspected periodically during the time between form removal and load testing. When observed crack lengths and widths were measured and documented. Crack widths were determined using a microscope that was precise to +/- 0.001in. Crack lengths were

determined by visual inspection with the naked eye. Three types of cracks were observed in the test girders:

- Top flange flexural cracks
- Web splitting cracks
- Flange splitting cracks

Top flange cracking was due to flexural stresses generated by the vertically eccentric prestressing and is outside the scope of this end region research. Web splitting (Figure 69) cracks were also due to eccentricity of prestressing. Vertical tension stress formed in the web at the end of the specimens as the prestress force was distributed to the cross-section. Flange splitting cracks are of primary interest in the current investigation of confinement reinforcement and were caused by horizontal eccentricity of prestressing, Hoyer expansion of strands, and self-weight reaction of the test girders. Transverse tensile stress formed in the bottom flange as prestressing forces were distributed through the cross-section from eccentric strands in the outer portion of the flange. Additional tensile stresses formed due to the Hoyer effect, in which strand expansion after cutting was restrained by the concrete. Self-weight caused tensile stresses above the support due to Poisson and flange bending effects. Cracks in the top flange, web, and bottom flange occurred when the tensile stresses described above exceeded the concrete strength.



Figure 69–Web splitting and flange splitting cracks

Presentation of crack data is divided according to the two phases of construction. This was done because the materials properties, construction procedures, and curing conditions varied between the construction phases. Within each phase, crack data were further divided between flange splitting cracks and web splitting cracks.

Cracking was quantified and compared in terms of total crack length, total crack area, and maximum crack width. Total crack length was calculated by summing the length of individual cracks for a specimen. Total crack area was calculated by summing the length of each crack multiplied by its representative width. Representative widths were determined from microscope measurements taken at selected points along cracks. Maximum crack width was determined from the microscope readings.

As part of an NCHRP research project, Tadros et al. (2010) recommended criteria for acceptance, repair, and rejection of girders with web splitting cracks. Criteria are based on laboratory data and from field data from Nebraska and Virginia. More stringent criteria may be warranted in aggressive environments such as along Florida coasts. Nevertheless, the recommendations shown in Table 27 and were used as a benchmark for evaluating crack widths in the test specimens.

In general, cracking behavior differed between the two phases of construction. Cracks were first observed in phase one girders (H and V) in the days following prestress transfer, whereas cracks were first observed in phase two girders (W, F, and D) during prestress transfer. Another difference was that cracks in the phase one girders typically did not grow after they were first observed. Cracks in the phase two girders continued to grow in length during the weeks after they were first observed. It is not clear why this occurred. Cracks appearing after some time may be due to tensile creep. If so, then differing environments, plant practices, and mixture properties would have an effect on this behavior.

D.5.2.1 Girders H and V

Girders H and V were fabricated together during the first phase of construction. Girders were inspected for cracking ten times between form removal and load testing (Table 26). Figure 70 shows web and flange splitting cracks observed during inspections. Flexural cracking in the top flange cracking is not shown in the figure.

Cracks were first observed in girders H and V nine days after prestress transfer. The day that cracks formed is unknown because girders H and V were not inspected during the days

immediately following prestress transfer. Web splitting cracks were observed in each specimen. Flange splitting cracks were only observed in specimens without confinement reinforcement (HU and VU). At the end of these specimens the flange cracks intersected with the outermost strand in the third row (Figure 71). Strands at this location had 2.5 in. of clear cover to the top surface of the flange, which was the least amount of top cover for any strand in the test girders.

Table 26–Girders H and V construction events and inspection dates

Event	Date	Days after prestress transfer	Notes
Form Removal	September 7, 2010	--	No cracks observed
Prestress Transfer	September 8, 2010	0	No cracks observed
Lifting and setting on dunnage	September 8, 2010	0	No cracks observed
Girders in storage	September 17, 2010	9	Splitting cracks observed (all specimens)
Girders in storage	September 23, 2010	15	Additional web splitting crack observed (HC)
Girders in storage	October 10, 2010	49	No additional cracks
Girders in storage	January 7, 2011	121	No additional cracks
Trucking	February 23, 2011	167	No additional cracks
Casting deck	April 6, 2011	204	No additional cracks
Begin load tests	May 5, 2011	237	No additional cracks

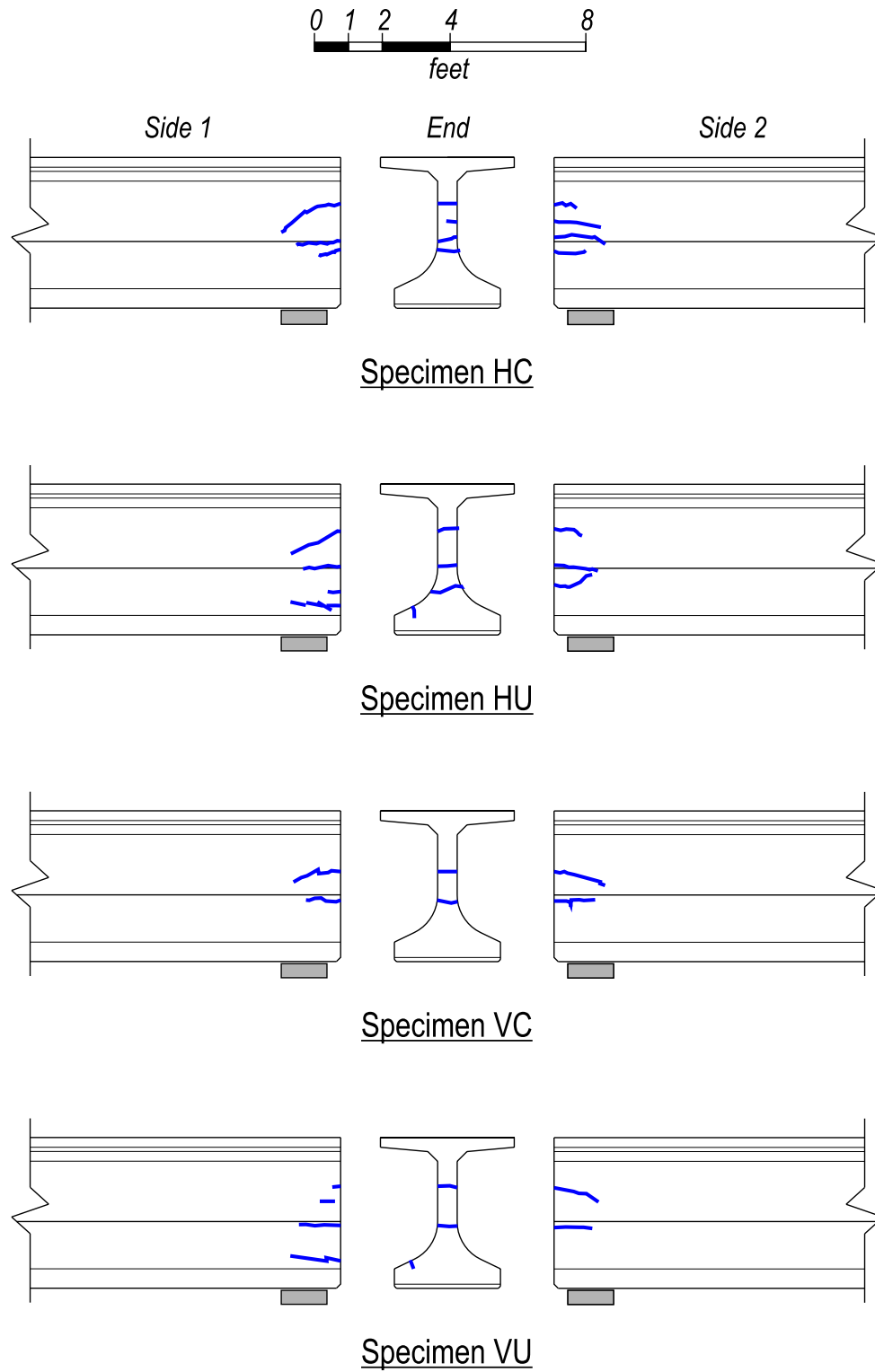


Figure 70–Girder H and V cracks prior to load tests

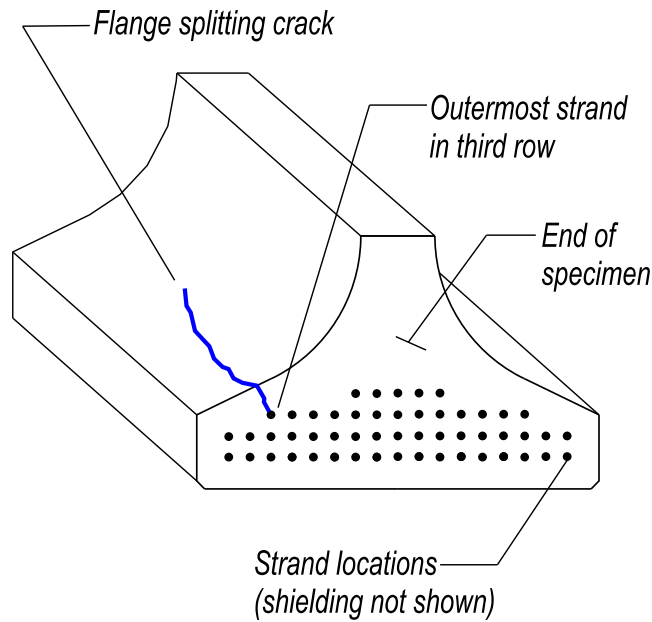


Figure 71–Flange splitting crack intersecting outer strand

Cracks in specimens H and V changed little after they were first observed. An additional web splitting crack was observed in specimen HC during an inspection fifteen days after prestress transfer. No other significant changes in crack quantity, width or length were observed during subsequent inspections of girders H and V.

Web splitting cracks in specimens with the greater amount of end region reinforcement (HC and HU) were an average of 72% longer than the cracks in specimens with less reinforcement (VC and VU)(Figure 72). One possible reason that web cracks were longer in HC and HU was that horizontal bars at the ends of these specimens created a path where horizontal cracks could form and propagate. Web cracks in HC and HU always occurred at the location of horizontal bars.

Although the additional reinforcement increased the total web crack length, it was also more effective in controlling web crack widths. The maximum web splitting crack width was 0.008in. in specimens HC and HU, whereas maximum crack widths were 0.012in. and 0.02 in. in VC and VU, respectively (Figure 73). The additional vertical bars in specimens HC and HU appear to have increased the post-cracking stiffness thereby reducing maximum crack width relative to VC and VU.

For girders H and V the maximum crack widths were typically less than 0.012 in., which according to the criteria in Table 27 do not require repair. Only specimen VU had a crack with a

width greater than 0.012 in. One of the web splitting cracks in this specimen had a maximum width of 0.02 in. According to the criteria in Table 27 this crack would require repair by filling with cementitious material and application of a sealant to the girder end.

Total crack area (Figure 72) was derived from both length and width data, and provides a quantitative comparison of end cracking. Web cracks in specimens HC and HU were longer but narrower than web cracks in VC and VU. Because of this, there is less variation in total web crack area than was observed in total web crack length and maximum web crack width. Variation in total web crack area varied by 24% between HX and VX specimens.

Flange splitting cracks only occurred in specimens HU and VU, which did not have confinement reinforcement. The total length and area of flange cracks were similar between HU and VU (Figure 74). The maximum width of flange splitting cracks was 0.004 in (Figure 73). Presumably, confinement reinforcement in HC and VC controlled the formation and propagation of flange cracks in those specimens.

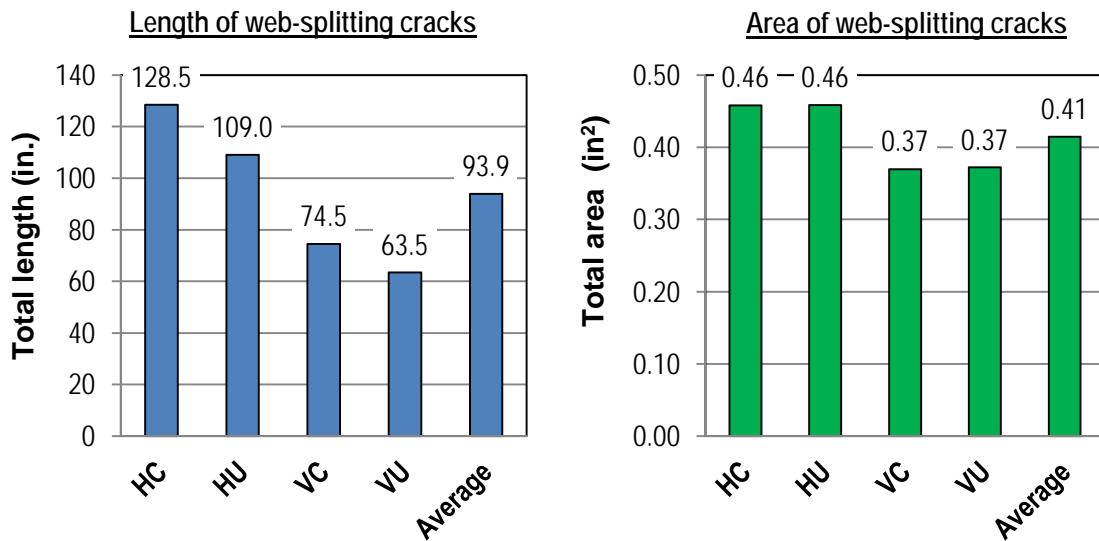


Figure 72–Web splitting cracks in specimens H and V

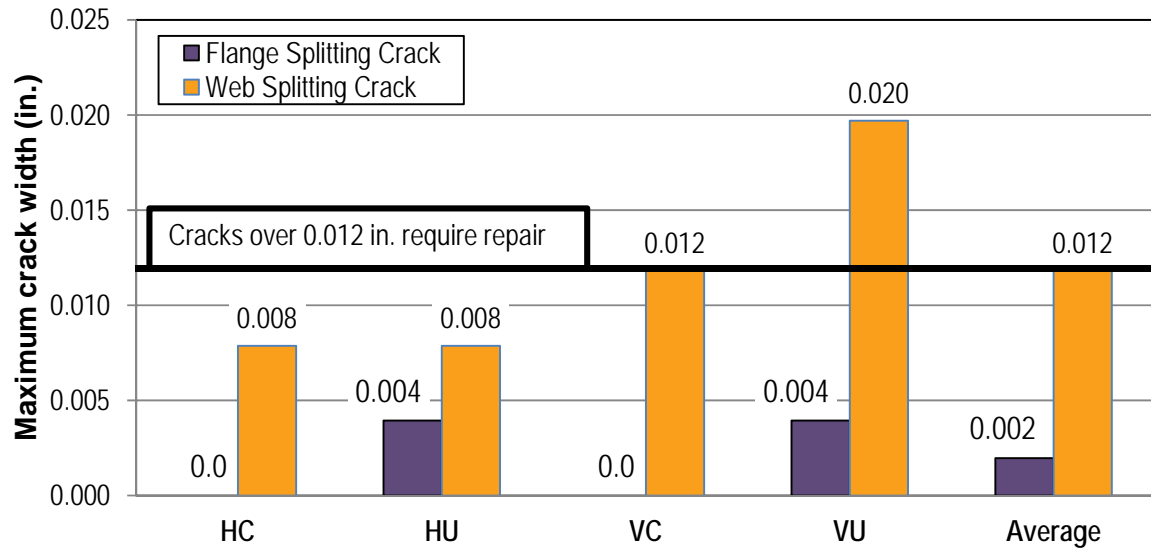


Figure 73–Maximum crack widths in girders H and V

Table 27–Recommended action for web splitting cracks (Tadros et al. 2010)

Crack Width (in.)	Required Action
Less than 0.012	None
0.012 to 0.025	Fill cracks with cementitious material and apply surface sealant to end 4 ft of girder
0.025 to 0.05	Fill cracks with epoxy and apply surface sealant to end 4 ft of girder
Greater than 0.05	Reject girder unless shown by detailed analysis that structural capacity and long-term durability are sufficient

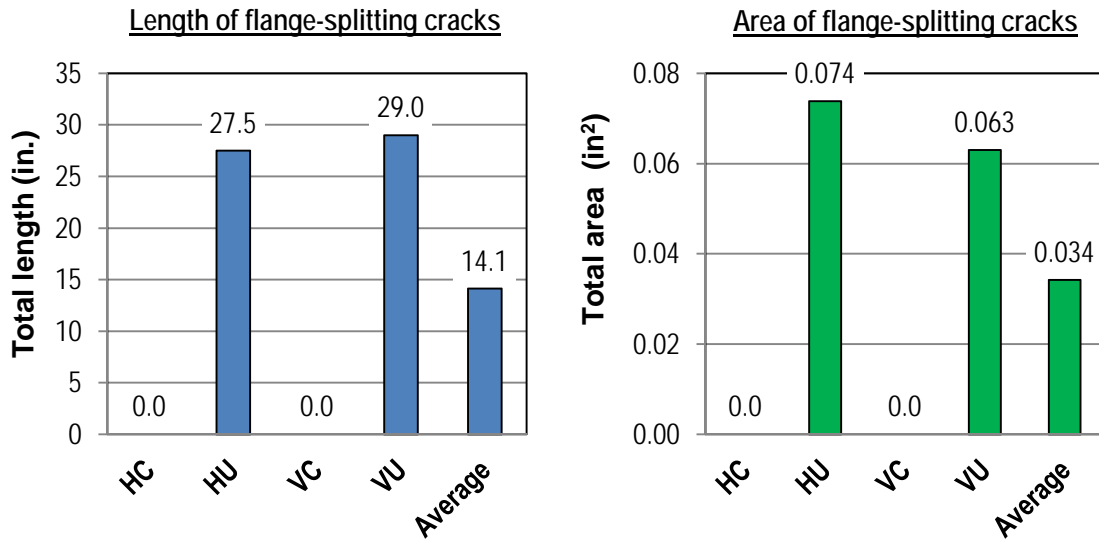


Figure 74—Flange splitting crack data in girders H and V

D.5.2.2 Girders W, F, and D

Girders W, F, and D were fabricated together during the second phase of construction. Construction events, inspection dates, and notes from girders W, F, and D are listed Table 28. Flange and web splitting cracks were first observed in these girders after the outer strands had been cut during prestress transfer. Cracks grew in quantity and length in the days and weeks following prestress transfer. Figure 75 shows the web and flange splitting cracks observed prior to load testing. Flexural cracks in the top flange are not shown.

Steel bulkheads were used during construction of girders W, F, and D. A portion of the bulkhead covering the end of the bottom flange (Figure 76) remained with each test girder for approximately two weeks after prestress transfer. Bottom flange ends covered by the bulkheads were inspected for the first time 30 days after transfer. Cracks were observed at the girder ends during this inspection. Because the ends were previously covered, it is not known when splitting cracks at the end of the bottom flanges first formed.

The location of cracks shown in Figure 75 can be understood by considering the strand bond patterns in the test specimens. For example, specimens WN and WB had flange splitting cracks located 10ft from their ends. These cracks formed within the transfer length of partially shielded strands. Strands in WN and WB were 45% partially shielded, with all shielding located

in the outer portion of the flange. It is believed that the flange cracks in WN and WB occurred due to Hoyer stresses and lateral-splitting stresses associated with the partially shielded strands.

Table 28—Girders W, F, and D construction events and inspection dates

Event	Date	Days after prestress transfer	Notes
Form Removal	February 20, 2012	--	No cracks observed
Prestress Transfer	February 21, 2012	0	First cracks observed after outer strands released.
In storage immediately after lifting	February 22, 2012	1	Additional splitting cracks and extension of previous cracks observed.
In storage	February 23, 2012	2	Additional splitting cracks and extension of previous cracks observed.
In storage	February 24, 2012	3	Additional splitting cracks and extension of previous cracks observed.
In storage	March 6, 2012	14	Additional splitting cracks and extension of previous cracks observed.
In storage	March 22, 2012	30	Additional splitting cracks and extension of previous cracks observed. Bottom flange at ends examined for first time. Previously the bulkhead plates were covering the flange end.
In storage	April 9, 2012	48	Additional splitting cracks and extension of previous cracks observed.
Trucking	April 30, 2012	69	Additional splitting cracks and extension of previous cracks observed.
Casting deck	May 7, 2012	76	No additional cracking observed.
Begin load testing	May 23, 2012	92	Bottom of girder inspected for first time. Flange splitting cracks observed prior to load tests.

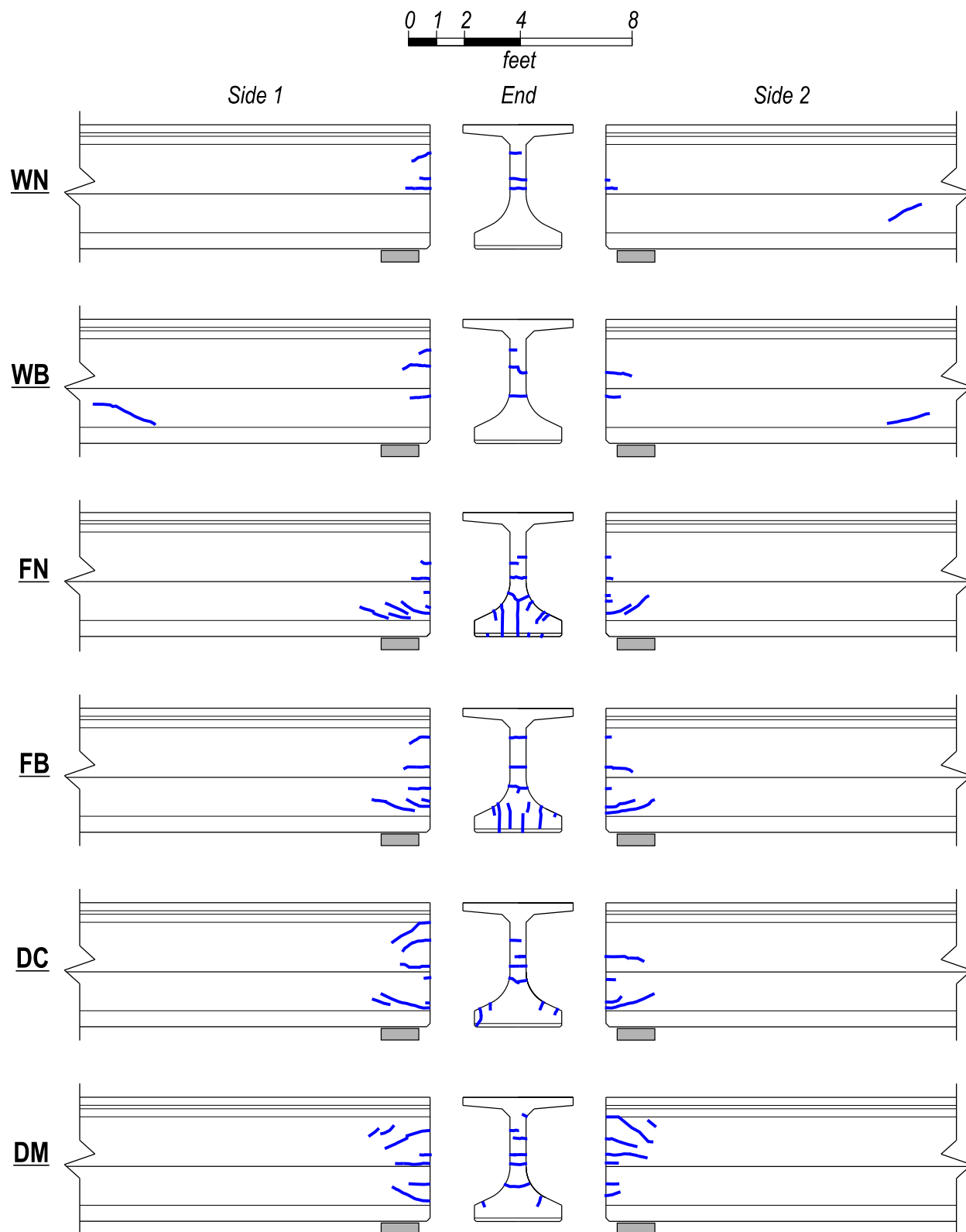


Figure 75–Girders W, F, and D web and flange splitting cracks



Figure 76–End of bottom flange covered by portion of steel bulkhead

Strands in specimens FN and FB were also 45% shielded, with all shielding located below the web and all shielding terminating 10ft from the specimen ends. This pattern placed fully bonded strands in the outer portion of the flange and led to tensile stresses in the bottom flange as illustrated by Figure 58. Flange splitting cracks formed when tension stresses at the end of the flange exceeded the concrete tensile strength. Flange cracks at the ends of FN and FB intersected strands (Figure 77) suggesting that the Hoyer effect also contributed to the tensile stresses and crack formation. Flange splitting cracks in FN and FB were greater in total length and in total area than all other specimens (Figure 78). The maximum width of flange splitting cracks was also greater for FN and FB (Figure 79) than other specimens.

Specimens DC and DM had the largest number of fully bonded strands (39) in the phase 2 test girders. As such the web stresses and web splitting cracks were greatest in DC and DM. All other specimens had only 24 fully bonded strands. The total length of web splitting cracks in specimens DC and DM were 132 in. and 179 in., respectively (Figure 80). The maximum width of web splitting cracks was 0.008 in. specimens DC and DM (Figure 79).

Specimens DC and DM had flange splitting cracks (Figure 81) in addition to web cracks. At the end of these specimens the flange splitting cracks intersected strands, suggesting that the Hoyer effect contributed to crack formation. In specimen DC the cracks intersected the outermost strands in the second and third rows.

The maximum crack width in girders W, F, and D was 0.008 in. This width does not warrant repair using the criteria from Table 27.

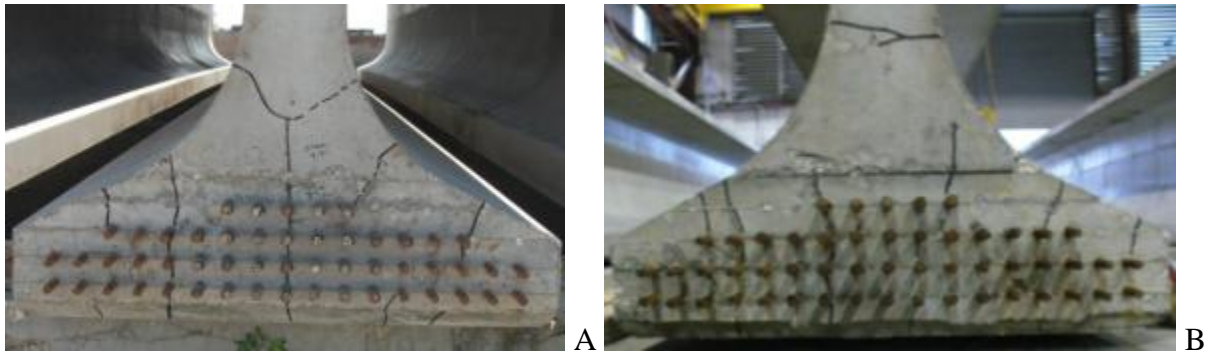


Figure 77–Girder F flange splitting cracks in A) specimen FN and B) specimen FB

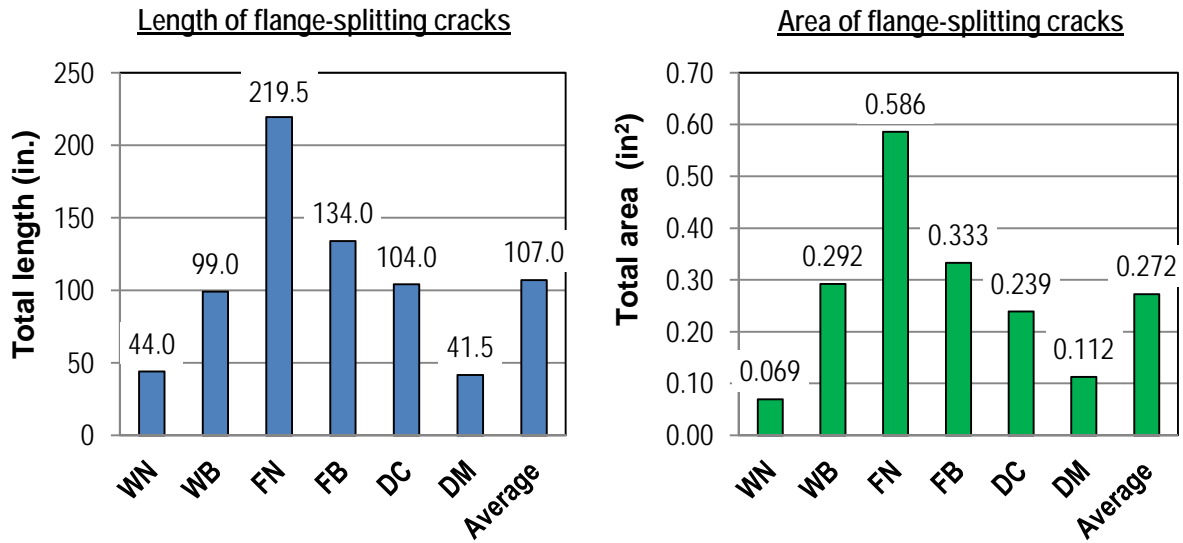


Figure 78–Flange splitting cracks in girders W, F, and D

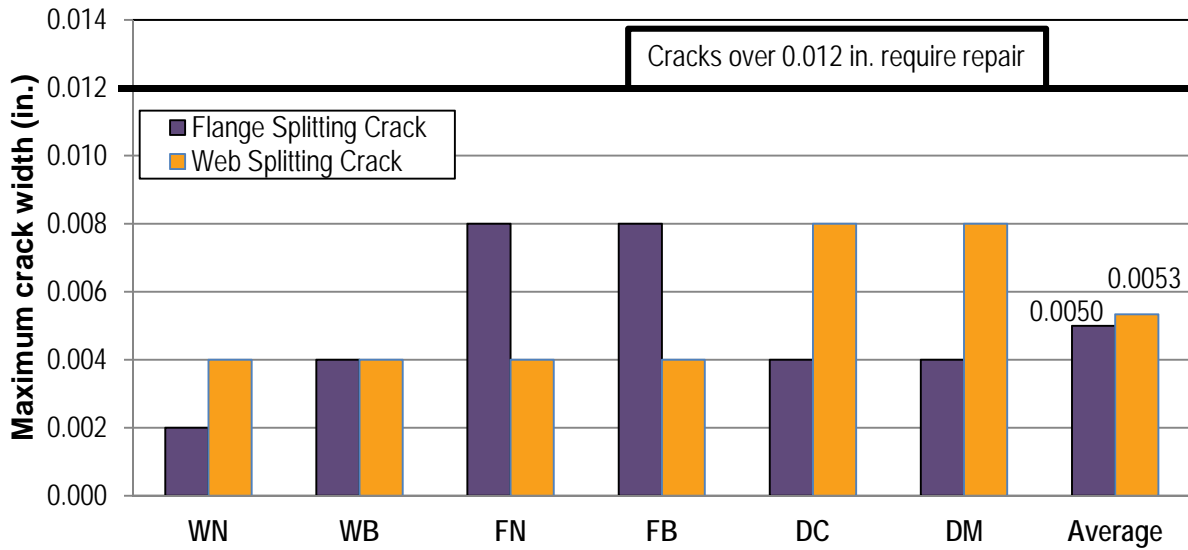


Figure 79–Maximum crack widths in girders W, F, and D

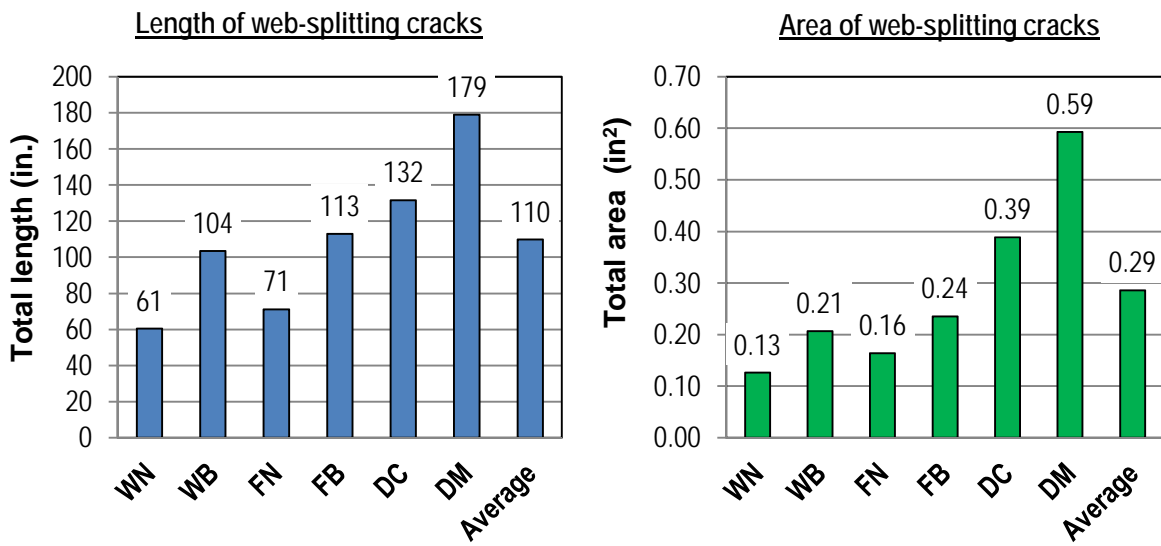


Figure 80–Web splitting cracks in girders W, F, and D

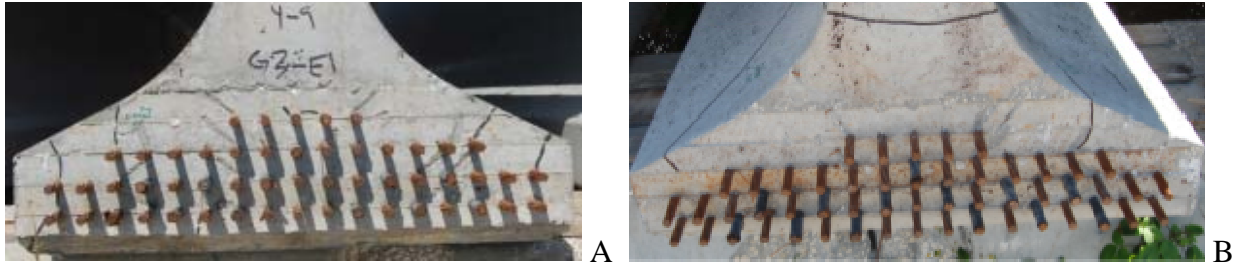


Figure 81–Girder D flange splitting cracks in A) specimen DC and B) specimen DM

D.5.3 Prestress Loss

Vibrating wire gages were placed near mid-span of each girder to monitor prestress losses. Null values were taken just prior to prestress transfer. Additional data were taken from these gages at discrete intervals throughout fabrication, storage, and deck construction. Elastic and long term loss losses were calculated using the strain data. Experimentally calculated loss values are listed in Table 29 and Table 30 along with code estimated losses from the AASHTO and PCI methods using the specified material properties. Experimental and code estimated losses vary between girders with different magnitudes of prestress force.

Table 29–Prestress losses girders F and W.

Prestress Losses	Experimental		Code	
	F	W	AASHTO	PCI
Elastic Losses (%)	14.0%	16.9%	13.4%	10.4%
Long Term Losses (%)	10.1%	13.2%	14.1%	24.3%
Total Losses (%)	24.1%	30.1%	27.5%	34.6%
Measurement Period (days)	76	76	-	-
Initial Prestress (kip)	2002			

Table 30–Prestress losses girder H, V, and D.

Prestress Losses	Experimental			Code	
	H	V	D	AASHTO	PCI
Elastic Losses (%)	14.6%	13.9%	12.4%	13.5%	10.5%
Long Term Losses (%)	11.9%	11.0%	9.2%	14.3%	24.4%
Total Losses (%)	26.5%	24.9%	21.6%	27.8%	34.9%
Measurement Period (Days)	242	242	76	-	-
Initial Prestress (kip)	2046				

The estimated prestress losses from the AASHTO and PCI methods were generally higher than the experimentally determined losses. One possible reason for the difference is that

the experimental losses occurred over a few months, whereas long the AASHTO and PCI methods assume longer time periods. The PCI method predicted higher losses than the AASHTO method.

D.5.4 Variable Comparison and Discussion

This section compares crack behavior across specimens and variables. Trends identified in the test specimens will be useful in detailing end regions to prevent and control cracking during and after prestress transfer.

Flange splitting cracks (Figure 74) formed in phase one specimens without confinement reinforcement (HU and VU) but not in specimens with confinement (HC and VC). This result suggests that confinement reinforcement controls flange splitting cracks that form due to prestressing. It is presumed that confinement reinforcement in HC and VC prevented flange splitting cracks from opening and propagating.

The quantity of bonded strands affected the total length and area of web splitting cracks. This is evident from Figure 80 which compares specimens DC and DM (39 strands each) with specimens WN, WB, FN, and FB (24 strands each). On average the total crack length and total crack area were 78% and 168% larger, respectively, in specimens with 39 fully bonded strands than in the specimens with only 24 strands. The maximum web crack width was twice as large in specimens with 39 fully bonded strands as in those with 24. These results indicate that reducing the quantity of fully bonded strands through partial shielding can successfully control the length, area, and maximum width of web splitting cracks.

The location of shielded strands within the bottom flange (inner flange or outer flange) was not a factor in length, area, or maximum width of web splitting cracks. Web splitting cracks in specimens with shielded stands placed in the outer portion of the flange (WN and WB) had similar total length, total area (Figure 80), and maximum width (Figure 79) as comparable specimens with shielded strands placed below the web (FN and FB).

The effect of confinement reinforcement and bearing plates on web splitting cracks is not obvious from the test data. Comparing total crack areas for girder H and V (Figure 72), it can be seen that specimens with confinement reinforcement had similar crack area but longer lengths than specimens without confinement. Specimens WN and FN without bearing plates had more crack length and area (Figure 79 and Figure 80) as specimens WB and FB with bearing plates.

One possible explanation for the greater amount of cracking in FB and WB is that bottom flange confinement provided by the bearing plates resulted in shorter transfer lengths and higher end stresses than in specimens without bearing plates.

Specimens FN and FB had the worst flange cracking and had all bonded strands placed in the outer portion of the flange. Severity of flange cracking specimens FN and FB is attributed to this strand bond pattern. The total length and total area (Figure 78) of flange cracks in FX specimens were both 2.5 times greater on average than the same metrics in the other phase 2 specimens. Similarly, the maximum flange crack width (Figure 79) was twice as large in FX specimens as in the other phase 2 specimens. Based on these results it is recommended that strands be placed as near to the centerline of the bottom flange as practical in order to maximize cover and minimize flange splitting cracks.

Six of the ten specimens had flange splitting cracks at the member end. In five of the six with flange cracks at the end, flange cracking intersected the outermost strand in the third row (Figure 71). Strands at this location had only 2.5 in. of clear cover to the top of the bottom flange. This was the least amount of cover of any strand in the test specimens. It is recommended that this location be avoided when designing strand patterns. Furthermore it is recommended that strand patterns be designed with the maximum amount of top cover.

Flange cracks were observed within the transfer length of the partially shielded strands in specimens WB and WN. Approximately 45% of strands in these specimens were partially shielded, and all shielding terminated at the same section 10 ft from the specimen ends. Both the overall shielding percentage and the termination of shielding violated AASHTO LRFD requirements. Flange cracks were not observed within the transfer length of partially shielded strands in specimens that complied with the AASHTO requirements.

Similar to specimens WB and WN, specimens FB and FN also violated the AASHTO requirements for total percentage of shielded strands and quantity of strand shielding that terminated at a section. Unlike specimens WB and WN, however, specimens FB and FN had partially shielded strands placed below the web and did not have flange cracks within the transfer length of the partially shielded strands. This demonstrates that the overall percentage of shielded strands was not a factor in flange cracking. The location of shielding was more critical to flange cracking than was the percentage of strand shielding that terminated at a given section.

Flange cracking in specimen end regions extended up to 30 in. from the member end. This length is 6 in. shorter than the code calculated transfer length of 36in. The similarity between these values suggests that code specified transfer length may be a good estimate of flange splitting crack lengths and that the code transfer length is a reasonable guideline for placement of confinement. The correlation between flange splitting crack length and transfer length is attributed in-part to the Hoyer effect which causes tensile splitting stresses within the transfer length.

Embedded steel bearing plates were excluded from specimens WN and FN. Absence of a bearing plate in specimen FN led to 64% greater total crack flange crack length and 76% greater total crack area when compared to specimen FB which had a bearing plate. Both specimens had fully bonded strands placed only in the outer portion of the flange.

Absence of a steel bearing plate did not adversely affect cracking in specimen WN relative to WB which had a bearing plate. Neither specimen had flange cracks at the member end. Thus presence of a bearing plate had the beneficial effects of reducing crack length and area, but only in specimens with fully bonded strands placed in the outer portion of the flange.

Configuration of confinement reinforcement can be compared using results from specimens DC and DM. Specimen DC had #3 confinement reinforcement as currently specified by FDOT. DM had #4 confinement reinforcement, but had fewer total confinement bars than DC. Specimen DC had 151% greater total flange crack length, and 113% greater total flange crack area than did specimen DM. Average flange crack width was not significantly different between the specimens. These results suggest that the modified confinement reinforcement performed better at controlling flange splitting cracks than the FDOT configuration. This is attributed to the fact that specimen DM had more reinforcement placed closer to the end than did specimen DC.

D.5.5 Summary and Conclusions

Cracking and strain data were collected in pretensioned FIB girders during multiple stages of construction including: prestress transfer, lifting, storage, transport, and deck construction. Each end of each girder had a different set of variables. Variables included: the quantity or lack of confinement reinforcement, the presence or lack of a steel bearing plate, and the strand bond pattern. Two of the tested strand bond patterns were intentionally designed to

violate current AASHTO LRFD requirements. Strain data from the reinforcement and bearing plates were used to estimate the transverse forces developed during prestress transfer. The following conclusions are made based on results from the strain data:

- Transverse tensile strains were observed in the bottom flange, confinement reinforcement and embedded bearing plates during and after prestress transfer. Tensile strains are attributed to prestressing forces, the Hoyer effect and girder self-weight and are thought to have caused flange splitting cracks.
- Transverse tensile strains are greatest in sections with fully bonded strands placed only in the outer portions of the bottom flange. Bonded strands in the outer flange are eccentric with the resultant internal force, thereby inducing bending in the bottom flange and associated transverse tension at the girder end.
- Transverse tensile strains are smaller in sections with fully bonded strands placed below the web than in sections without fully bonded strands below the web. This is because prestress forces from the inner (below the web) strands counteract the transverse tension caused by prestress forces from strands in the outer portions of the flange.
- Confinement reinforcement can be effective in controlling transverse tensile strain and associated splitting cracks in the bottom flange during and after prestress transfer. Specimens without confinement reinforcement had average transverse tensile strains in the bottom flange concrete that were 3.4 times greater than specimens with confinement reinforcement.
- The greatest strain in confinement reinforcement typically occurs in the lowest layer of reinforcement. In the test specimens, the bottom layer of confinement had strains 1.4 times greater on average than the middle layer.
- Confinement strains are largest near the end in members with fully bonded strands placed in the outer portion of the flange. In test specimens with fully bonded outer strands the strain was 4 times larger in bars 2in. from the end than in bars 9in. from the end.
- Transverse tensile forces in confinement reinforcement and bearing plates were approximately 50% larger on average in members with bonded strands in the

outer flange only, as compared to members with bonded strands in the inner flange only.

- The combined transverse tensile force in confinement reinforcement and bearing plate was estimated (based on strain data) to be between 0.6% and 1.7% of the total jacking force in fully bonded stands. These values represent lower and upper bounds for extreme strand bond patterns.
- Lifting of test girders and placement on dunnage had little effect on the transverse and vertical strain in the end region. The maximum change in strain during this process of 25 microstrain.

Cracking was monitored in test specimens from the time forms were removed until the time of load testing. The following conclusions are made based on results from the crack data:

- In some cases web and flange splitting cracks occur during and immediately following prestress transfer. In other cases cracking occurs during the days or weeks following transfer.
- Length and width of web and flange cracks were affected by detailing of the end region, even in specimens having the same cross-section.
- Flange splitting cracks in test specimens had maximum widths between 0.002 in. and 0.008 in. These cracks widths would not warrant repair according to the criteria set forth by Tadros et al. (2010).
- Flange splitting cracks extended up to 30 in. from the test specimens ends. This length is comparable to the code calculated transfer length of 36 in. (30 strand diameters) suggesting that the code transfer length is a reasonable extent for the placement of confinement reinforcement to control flange splitting cracks.
- Confinement reinforcement appeared to have effectively controlled flange splitting cracks in specimens HC and VC based on the splitting cracks that were observed in comparable specimens (HU and VU) without confinement reinforcement.
- Absence of a steel bearing plate affected the lengths and widths of flange splitting cracks in specimens with fully bonded strands placed only in the outer portion of the flange. For example, the total flange crack length was 64% greater and total

flange crack area 76% greater in specimen FN (no plate) than in specimen FB (with plate).

- The total length and area of flange splitting cracks were dependent on the strand bond pattern. Specimens with bonded strands placed only in the outer flange had 2.5 times greater total flange crack length and area than specimens with bonded strands distributed throughout the bottom flange. Splitting cracks did not occur in the end region in specimens where bonded strands were placed only in the inner portion of the flange.
- Flange splitting cracks formed within the transfer length of partially shielded strands in two specimens. These cracks were affected by the placement of shielded strands in the outer portion of the flange, and the quantity of shielding that terminated at a same section. The total percentage of shielded strands did not affect cracking.
- Flange splitting cracks were not observed in the transfer length of shielded strands in specimens complying with AASHTO LRFD requirements for quantity of shielding that can terminate at a given section.
- Splitting cracks in the bottom flange typically intersected the outermost strand in the third row from the bottom. This strand location had the least amount of top cover of any location in the test girders.
- Length and area of web splitting cracks was a function of the quantity of fully bonded strands. Web splitting cracks in specimens with 39 fully bonded strands were 78% longer and had 168% more area than web cracks in specimens with 24 fully bonded strands.
- Position of fully bonded strands in the bottom flange did not affect the length, area, or width splitting cracks in the web.

D.6 Results and Discussion: Load Tests

Five 54 in. deep Florida This chapter presents the results of load testing conducted on ten FIB-54 specimens. Test results are presented in terms of superimposed shear, which is referred to as shear in this chapter. Superimposed shear is defined as the shear force due to the applied load acting at the support nearest the load point. Self-weight is not included in the superimposed shear.

Displacement results are presented as the vertical displacement occurring at the load point. Displacement at the load point was calculated as the average of the displacements reported by LVDTs that were placed on either side of the load. The effect of bearing pad displacement has been removed.

Strand slip data are presented as the average slip from all monitored fully bonded strands. Displacement data from partially shielded strands are not included. Locations of monitored strands are presented in Chapter D.5.

D.6.1 Failure Modes

Three different modes of failure were observed in the test program: Web-shear, lateral-splitting and bond-shear. This section defines each type of failure and discusses the characteristics associated with each failure mode.

Web-shear failure is distinguished by crushing of the concrete web at peak load. This type of failure is controlled by the capacity of the web to carry diagonal compression between the top and bottom flanges. A post-peak characteristic of web-shear failure includes sliding of the top portion of the girder relative to the bottom along a shear plane through the web (Figure 82). This type of failure mode is considered in the shear design provisions of AASHTO LRFD and ACI 318.

Lateral-splitting failure is characterized by longitudinal cracks in the bottom flange and by peeling (outward) movement at the edges of the bottom flange (Figure 83.) Peeling movement of the bottom flange is caused by eccentricity between prestressing forces in the outer flange and the resultant equal and opposite force centered in the web (Figure 84.) This condition creates a moment which opens bottom flange cracks, and peels the edges of the bottom flange outward. In specimens with sufficient bottom flange confinement, peeling movement and longitudinal cracks are restrained, and peeling failure is mitigated.

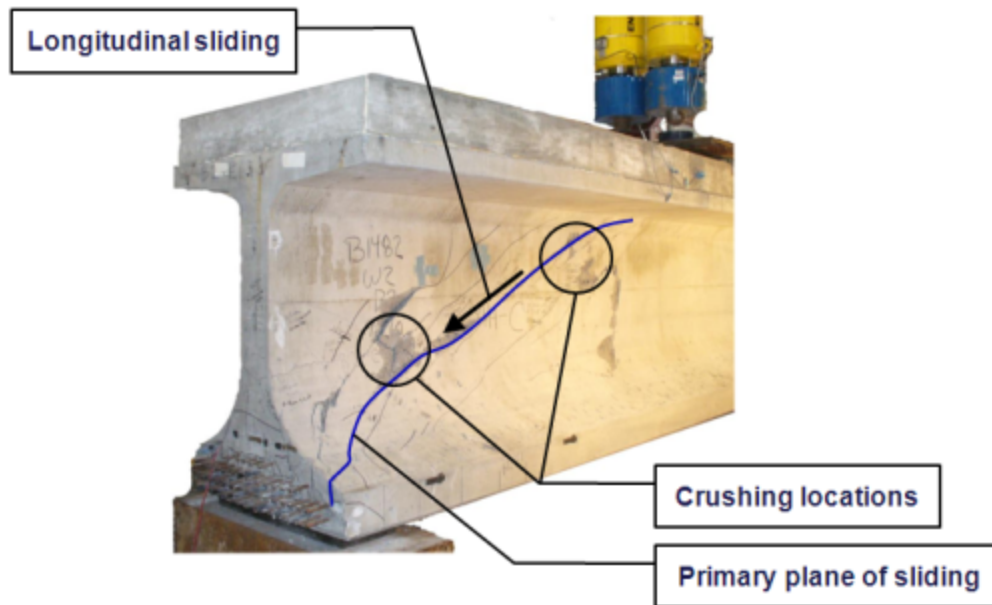


Figure 82–Web-shear failure

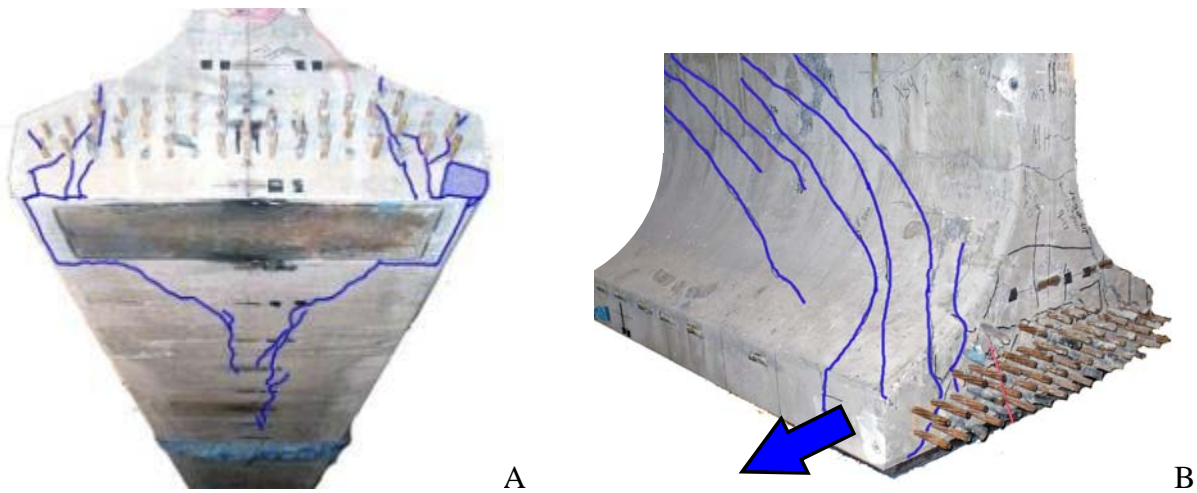


Figure 83–Lateral-splitting failure A) bottom view and B) side-end view

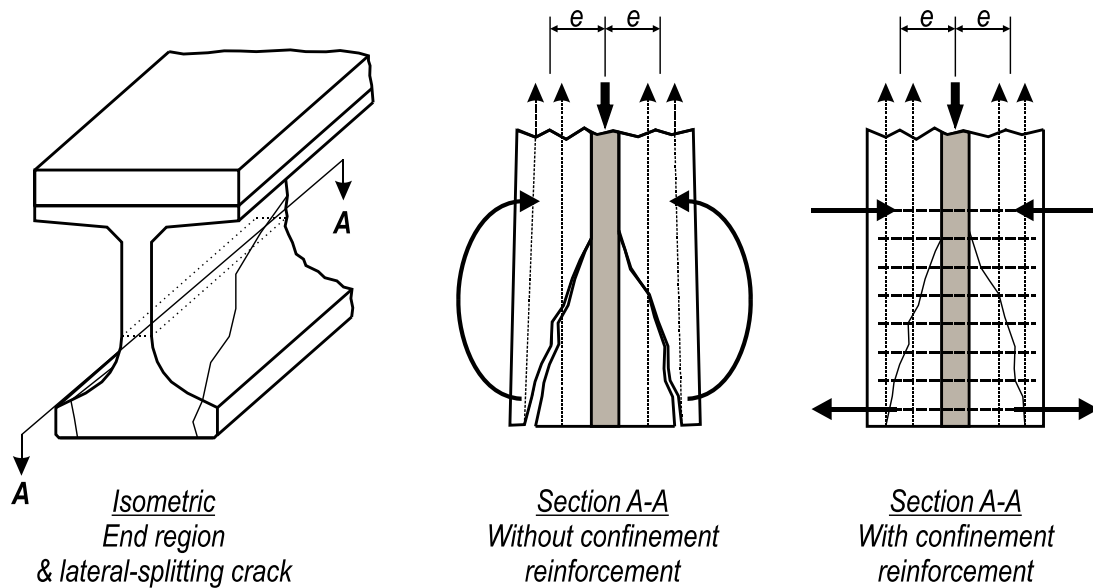


Figure 84–Lateral-splitting failure mechanics

Strand slip is observed in some specimens failing in lateral-splitting mode. Flange splitting cracks are a precursor to strand-slip in lateral-splitting failures. Once strands start to slip cracks open wider and capacity is lost in a sudden manner.

Longitudinal cracking along the specimen bottom (Figure 83) is also a characteristic of lateral-splitting failure. Cracks on the bottom are another manifestation of lateral-splitting cracks on the top surface of the bottom flange.

Bond-shear failure is characterized by strand-slip at peak load. This type of failure is governed by concrete-strand bond capacity and by specimen propensity for cracking within the strand development length. Cracking in the development length is always a precursor to strand slip (Figure 85). Cracks interrupting strand development reduce the embedment length to the distance between the crack and the girder end. After strands start slipping the cracks opened wider and new cracks form. An abrupt slip event occurs at peak load followed by a subsequent loss of capacity. Longitudinal splitting cracks can also be observed on the bottom of specimens that failure in bond-shear (Figure 85).

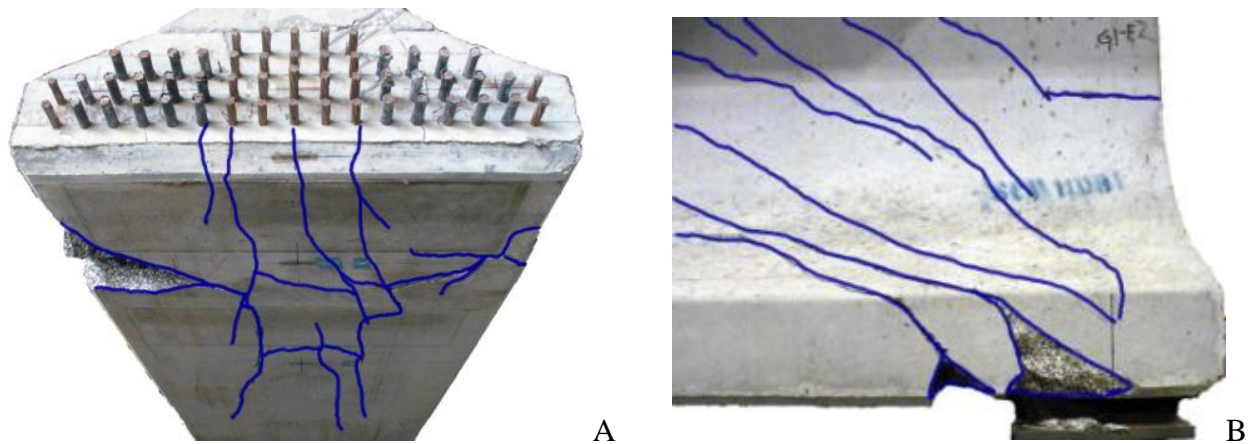


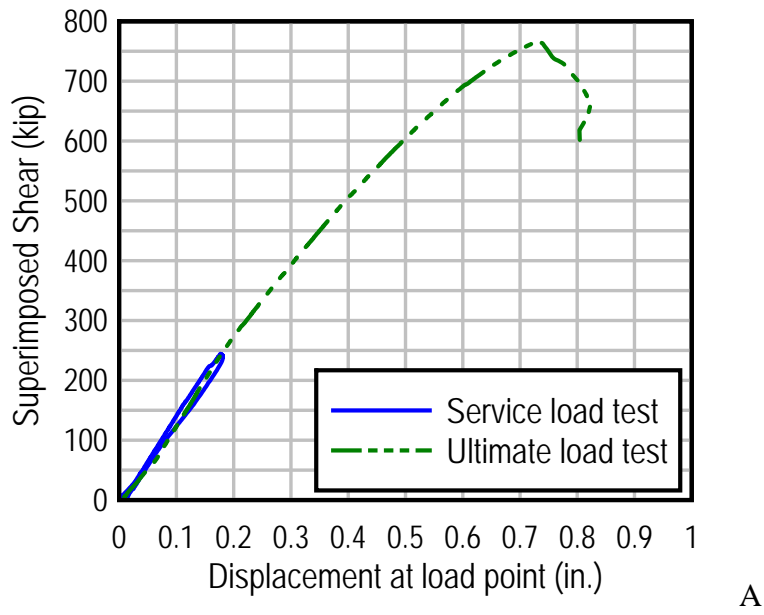
Figure 85–Bond-shear failure A) bottom view and B) side view

As described above, similar characteristics are associated with lateral-splitting and bond-shear failures. One subtle difference between these failure modes is the cause of cracking in the bottom flange. In lateral-splitting failures bottom flange cracking is caused by shear forces and transverse tensile forces due to eccentric prestressing. Bottom flange cracking in bond-shear failures are caused primarily by shear forces. Magnitude of strand slip is a more obvious distinction between bond-shear and lateral-splitting failures. In the test program, specimens failing in bond-shear reported maximum average strand slip over 0.25in. When slip was observed in specimens failing in later-splitting maximum the average slip was less than 0.1in.

D.6.2 Load Test Results

D.6.2.1 HC

Detailing of specimen HC (Figure 10) was effectively identical to the 2008 FDOT Interim Design Standards (FDOT, 2008). Variables in specimen HC included FDOT specified confinement reinforcement and bearing plate in the bottom flange, horizontal reinforcement in the end region, and the ‘design’ strand bond pattern (Figure 9) which had (39) fully bonded strands. Specimen HC failed in web-shear mode. Shear-displacement and crack pattern are shown in Figure 86.



Release cracks not shown.
 Initial cracks shown bold in red
 Final cracks shown blue.

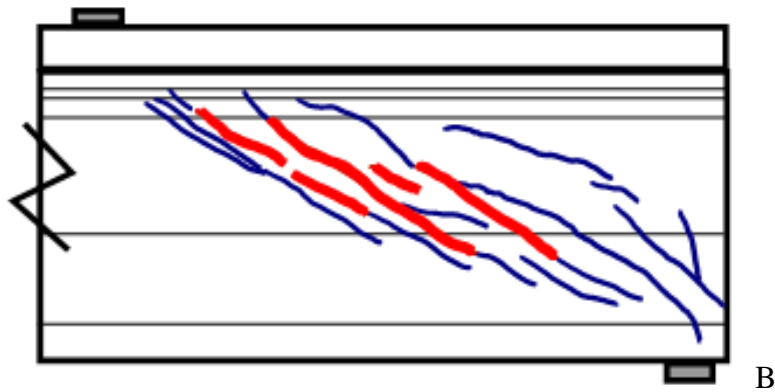


Figure 86–Specimen HC load test summary A) shear-displacement and B) crack pattern

Cracks in HC were first observed during the service load test at a shear of 225 kip. Inclined web cracks between the load point and support were the first to be observed. The service load test reached a peak shear of 244kip. Cracks partially closed during the unloading stage of the service load test. Web cracks in specimen HC had a maximum width of 0.004 in. at a shear of 244kip, and 0.002 in. after load was removed.

Following service load testing specimen HC was loaded to ultimate capacity. Stiffness decreased gradually as load increased beyond the level of the service load tests. Because flexural cracks were not observed, loss in stiffness is attributed to formation and growth of diagonal cracks. Ultimate capacity was signaled by web crushing followed immediately by sliding movement of the specimen's top portion relative to the bottom. Sliding movement occurred along the inclined cracks in the web. Areas of the web surface spalled off at the peak load (Figure 87). Spalling near the load point was a secondary effect, occurring immediately after the load had dropped. No splitting cracks were observed on the bottom of the girder.

Failure of HC is classified as a web-shear failure. Loss of capacity after the web-shear failure was abrupt. Specimen HC supported a maximum shear of 766 kip, the most of any specimen in the test program.

Strand slip data are not presented in Figure 86. LVDT data indicate that strand slip was negligible at lower loads. At higher loads cracks caused shifting of the frame holding the LVDTs thereby compromising the strand slip data. Specimens DC and DM used the same strand bond pattern as HC, but used different strand slip instrumentation that did not shift during testing. Slip data from the DC and DM suggest that strand slip was not a factor in the failure mode of specimens (such as HC) with the design strand pattern. The lack of slip observed in the specimens with this pattern is attributed to the relatively large quantity of fully bonded strands.

After the test the wood frame holding the LVDTs was removed, revealing cracks at the end of HC that intersected most of the strands (Figure 89). These cracks are believed to have occurred at or subsequent to the peak load.

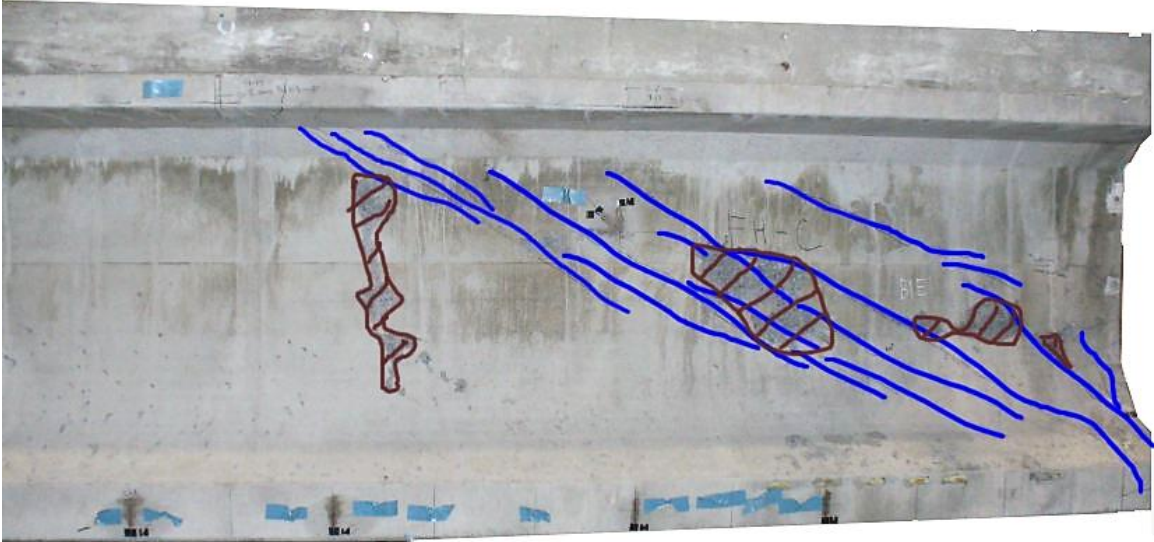


Figure 87–HC after load testing (cracks shown blue; spalling in brown)

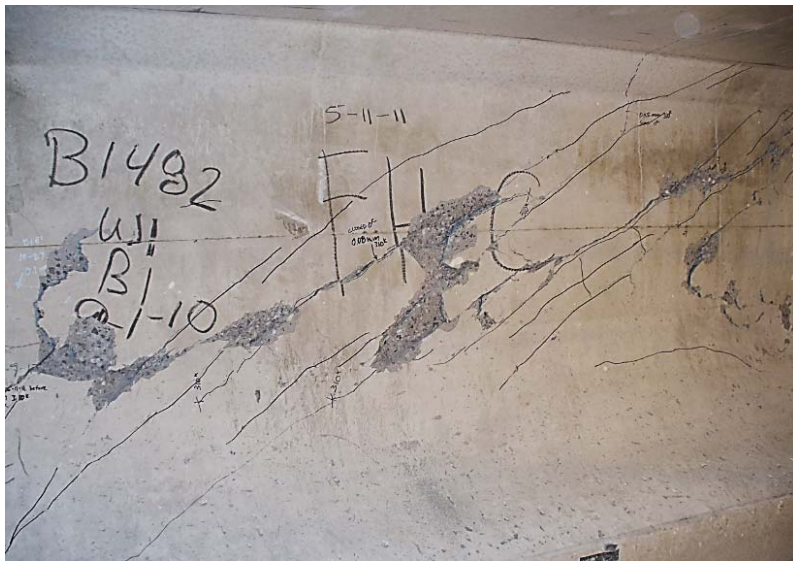


Figure 88–Close-up of web crushing and spalling

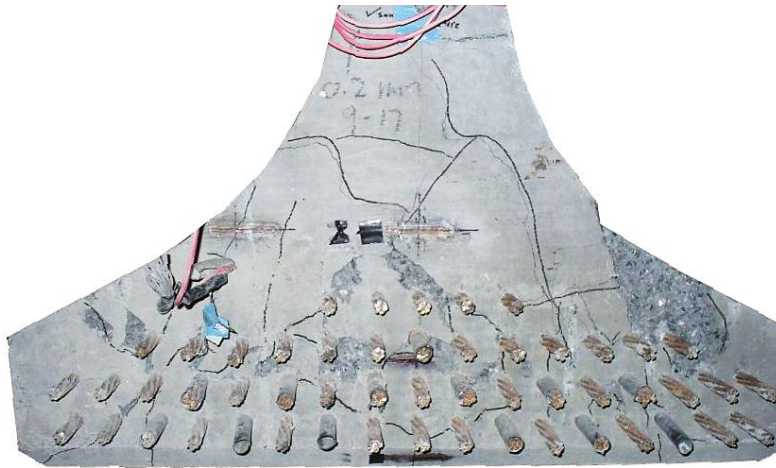


Figure 89–Cracks at end of HC after testing

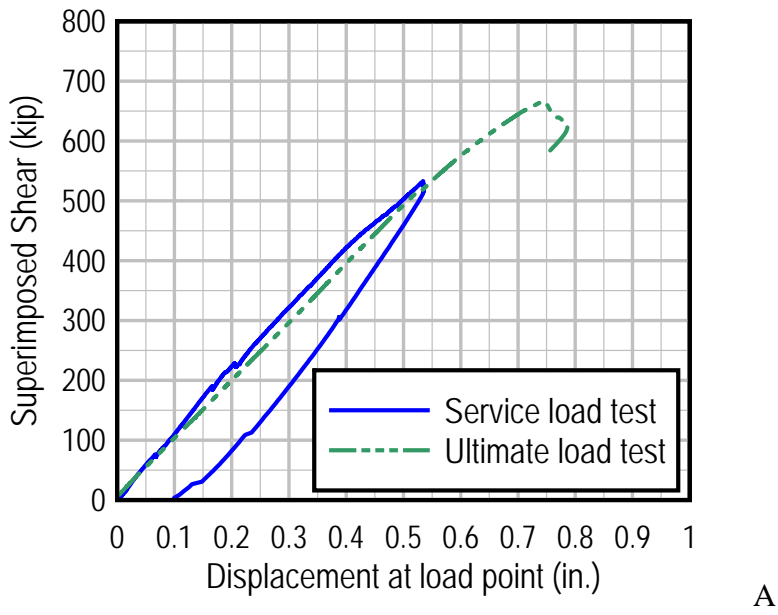
D.6.2.2 HU

Detailing of specimen HC (Figure 10) was effectively identical to the 2008 FDOT Interim Design Standards (FDOT, 2008), with the exception that no confinement reinforcement was placed in the bottom flange. Specimen HU had a bearing plate in the bottom flange, horizontal reinforcement in the end region, and the ‘design’ strand pattern (Figure 9) which included (39) fully bonded strands. Shear-displacement and crack pattern are shown in Figure 90.

Cracks in HU were first observed during the service load test at a shear of 215 kip. The first crack to be observed was a web crack inclined between the load point and support. Web cracks in specimen HU had a maximum width of 0.004 in. at a shear of 230kip, and partially closed to 0.002 in. after load was removed.

Following service load testing specimen HU was loaded to ultimate capacity. Stiffness decreased gradually as load increased beyond the level of the service load tests. Loss in stiffness is attributed to formation and growth of diagonal cracks. Web cracks that formed at lower loads were observed to spread into the bottom flange during the latter stages of testing. Flexural cracks were not observed.

Peak load in specimen HU corresponded to lateral-splitting failure in the bottom flange, which resulted in an abrupt loss of load (Figure 91, Figure 92). Specimen HU supported a maximum shear of 666 kip.



Release cracks not shown.
 Initial crack shown bold in red
 Final cracks shown blue.

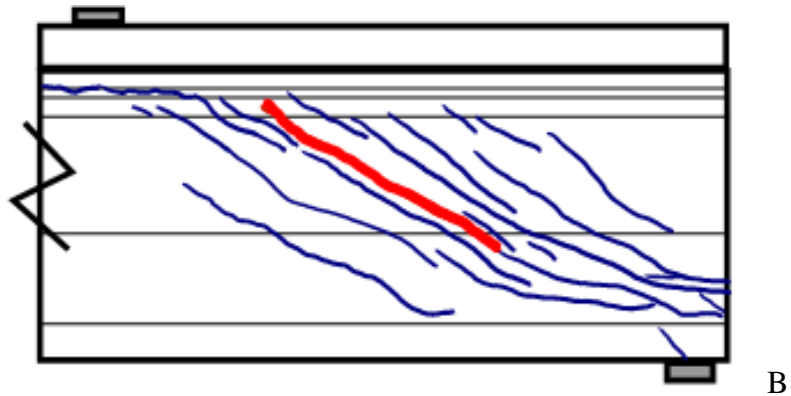


Figure 90–Specimen HU load test summary A) shear-displacement and B) crack pattern

Strand slip data are not shown in Figure 90. LVDT data indicate that strand slip was negligible at lower loads. At higher loads cracks caused shifting of the frame holding the LVDTs thereby compromising the strand slip data. Data from specimens with similar strand bond patterns and better instrumentation suggest that strand slip was not a contributing factor to in the failure of in specimens with the ‘design’ strand bond pattern.

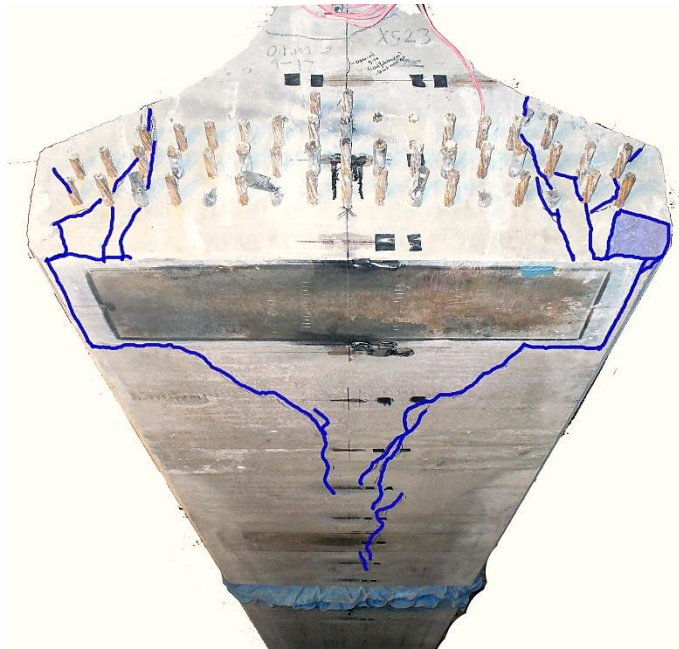


Figure 91–Bottom and end of HU after testing

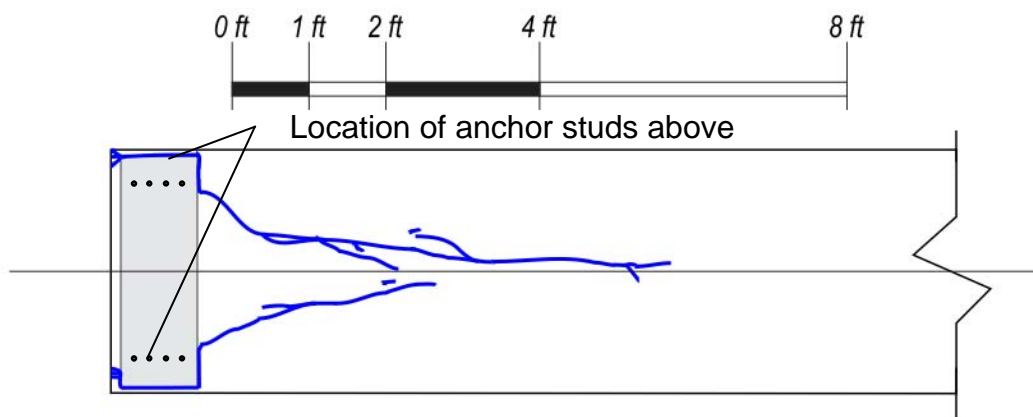
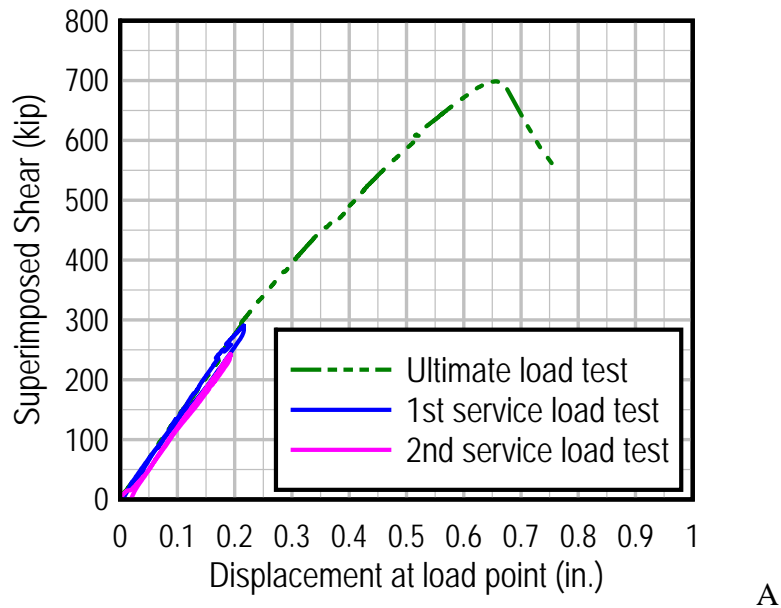


Figure 92–Bottom view of splitting cracks in HU

D.6.2.3 VC

Detailing of specimen VC (Figure 11) was similar to the 2008 FDOT Interim Design Standards (FDOT, 2008), with the exceptions that fewer vertical bars and no horizontal bars were placed in the end region. Other variables in specimen VC included FDOT specified confinement reinforcement and bearing plate in the bottom flange, and the ‘design’ strand bond

pattern (Figure 9) which included (39) fully bonded strands. Specimen VC failed in a web-shear failure mode. Shear-displacement and crack pattern are shown in Figure 93.



Release cracks not shown.
Initial crack shown bold in red.
Final cracks shown in blue.

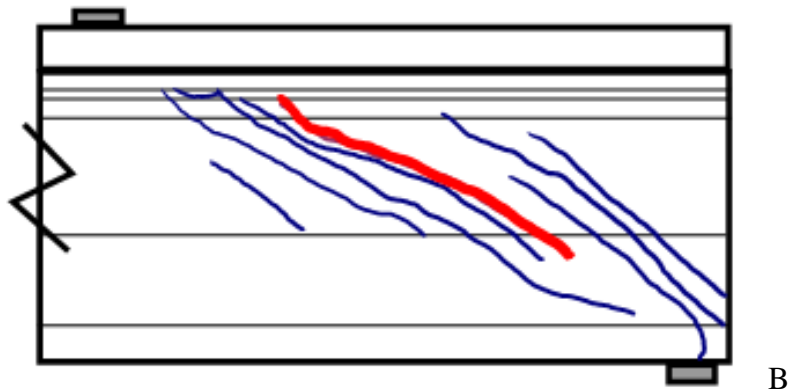


Figure 93–Specimen VC load test summary A) shear-displacement and B) crack pattern

Cracking in VC was first observed during service load testing at a shear of 240 kip. An inclined web crack between the load point and support was the first to be observed. Cracks in specimen VC partially closed during the unloading stage of the service load test. Web cracks in

VC had a maximum width of 0.014 in. at a shear of 290kip, and 0.002 in. after load was removed.

Following the service load testing specimen VC was loaded to ultimate capacity. Stiffness decreased gradually as load increased beyond the level of the service load tests. Because flexural cracks were not observed, the loss in stiffness is attributed to formation and growth of diagonal cracks. Ultimate capacity was signaled by web crushing followed immediately by movement of the portion of the specimen above the inclined cracks relative to that below the inclined crack (Figure 94). Areas of the web surface spalled due to the crushing. Spalling also occurred in the web below the load point, however this was a secondary effect occurring immediately after the load had dropped. No splitting cracks were observed on the bottom of the specimen.

Failure of VC is classified as a web-shear failure. Loss of capacity after the web-shear failure was abrupt. Specimen VC supported a maximum shear of 698 kip.

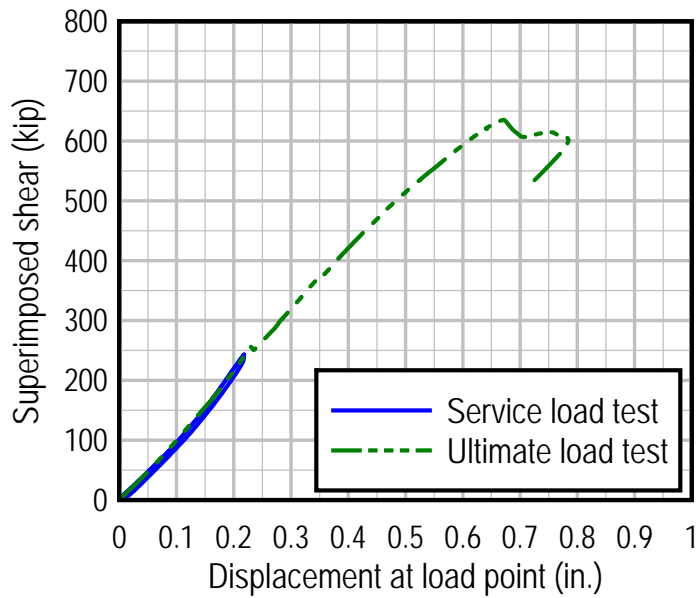
Strand slip data are not shown in Figure 93. LVDT data indicate that strand slip was negligible at lower loads. At higher loads cracks caused shifting of the frame holding the LVDTs thereby compromising the strand slip data. Data from specimens with similar strand bond patterns and better instrumentation suggest that strand slip was not a contributing factor to in the failure of in specimens with the 'design' strand bond pattern.



Figure 94–VC after load test

D.6.2.4 VU

Specimen VU (Figure 11) had the least amount of reinforcement of any specimen in the test program. Variables in specimen VU included no confinement reinforcement, no horizontal reinforcement and reduced vertical reinforcement in the end region. Specimen VU had a bearing plate in the bottom flange and had the ‘design’ strand bond pattern (Figure 9) which included (39) fully bonded strands. Shear-displacement and crack pattern are shown in Figure 95.

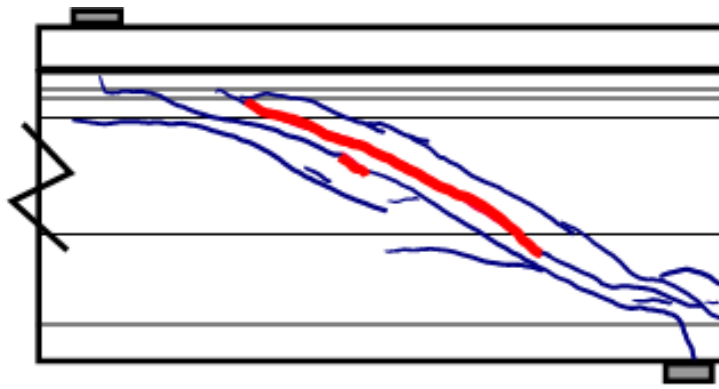


A

Release cracks not shown.

Initial cracks shown bold in red.

Final cracks shown blue.



B

Figure 95–Specimen VU load test summary A) shear-displacement and B) crack pattern

Cracks in VU were first observed during the service load test at a shear of 243 kip. The first crack to be observed was a web crack inclined between the load point and support. Web cracks in specimen VU had a maximum width of 0.001 in. at a shear of 243kip, and did not change in width as load was removed after the service load test.

Following service load testing specimen VU was loaded to ultimate capacity. Stiffness decreased gradually as load increased beyond the level of the service load tests. Loss in stiffness

is attributed to formation and growth of diagonal cracks. Web cracks that formed at lower loads were observed to spread into the bottom flange during the latter stages of testing. Flexural cracks were not observed.

Peak load in specimen HU corresponded to lateral-splitting failure in the bottom flange, which resulted in an abrupt loss of load (Figure 96). Specimen VU supported a maximum shear of 635 kip.

Strand slip data are not shown in Figure 95. LVDT data indicate that strand slip was negligible at lower loads. At higher loads cracks caused shifting of the frame holding the LVDTs thereby compromising the strand slip data. Data from specimens with similar strand bond patterns and better instrumentation suggest that strand slip was not a contributing factor to in the failure of in specimens with the ‘design’ strand bond pattern.

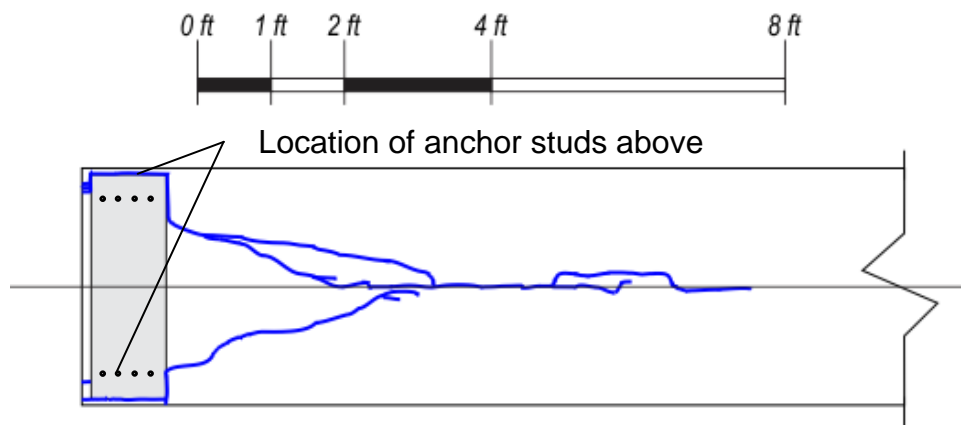
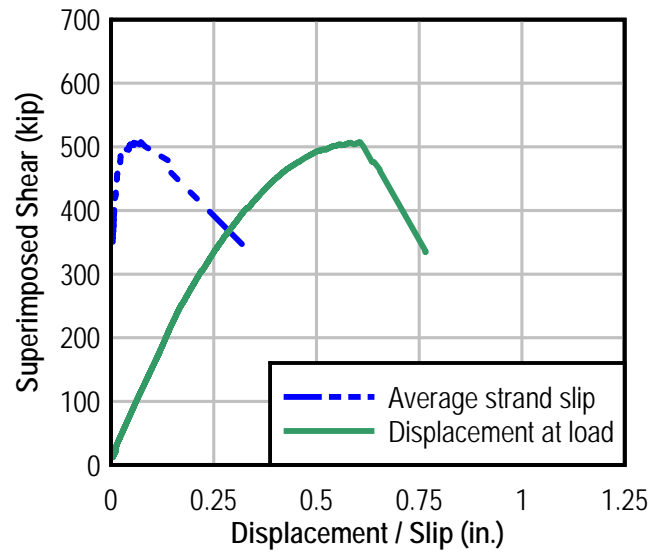


Figure 96–Bottom view of splitting cracks in VU

D.6.2.5 WN

The primary features of specimen WN (Figure 21) were the lack of an embedded bearing plate and the ‘web’ strand bond pattern (Figure 9) that placed (20) fully bonded strands below the web. Four additional strands were fully bonded at the edges of the flange, resulting in a total of (24) fully bonded strands. Other variables in WN included no horizontal bars in the end region and modified confinement reinforcement. The modified confinement scheme had fewer, but larger, bars than specified by the FDOT. Shear-displacement, shear-slip and crack pattern results for specimen WN are shown in Figure 97.

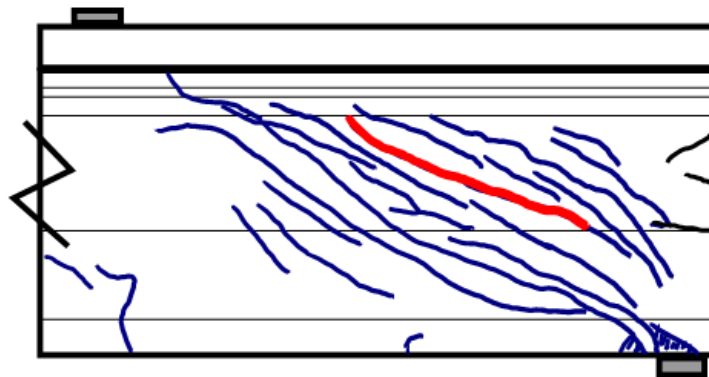


A

Release cracks shown black.

Initial crack shown bold in red.

Final cracks shown blue.



B

Figure 97–Specimen WN load test summary A) shear-displacement/slip and B) crack pattern

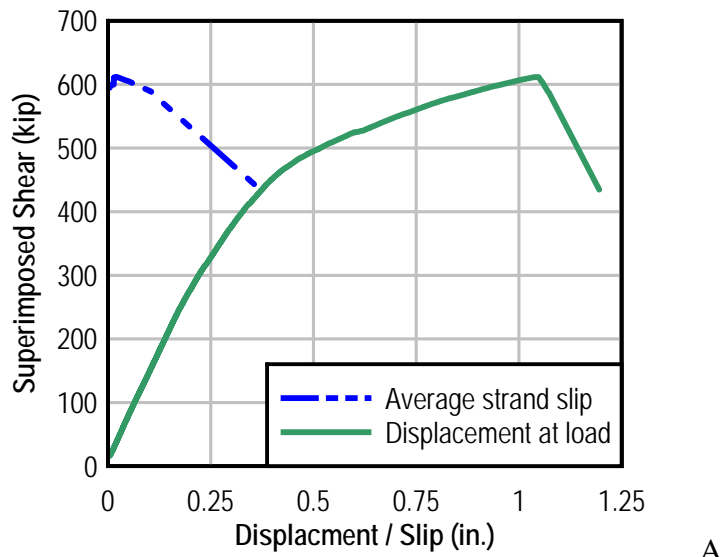
Cracking in WN was first observed during service load testing at a shear of 198 kip. An inclined web crack between the load point and support was the first to be observed. Cracks widths in specimen WN partially closed during the unloading stage of the service load test.

Following service load testing specimen WN was loaded to ultimate capacity. Stiffness decreased gradually as load increased beyond the level of the service load tests. Loss of stiffness is attributed primarily to flexural cracks which were first observed at a shear of 435 kip. Strand-slip initiated at approximately the same load. Popping sounds indicative of strand slip were

heard with increasing frequency as the load approached a peak shear of 507 kip. At peak shear, the strands slipped suddenly resulting in opening of the crack in front of the bearing pad and a subsequent loss of load. Capacity of WN was limited by strand-concrete bond, and failure of WN is labeled as a bond-shear failure.

D.6.2.6 WB

The primary feature of specimen WB (Figure 21) was the ‘web’ strand bond pattern (Figure 9) that placed (20) fully bonded strands below the web. Four additional strands were fully bonded at the edges of the flange, resulting in a total of (24) fully bonded strands. Other variables in WN included presence of an embedded bearing plate, and modified confinement reinforcement. The modified confinement scheme had fewer, but larger, bars than specified by the FDOT. Shear-displacement, shear-slip and crack pattern results for specimen WB are shown in Figure 98.



Release cracks shown black.
 Initial crack shown bold in red.
 Final cracks shown blue.

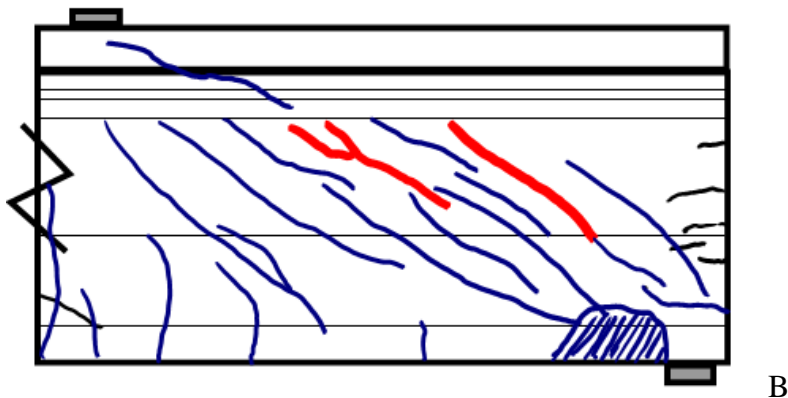


Figure 98–Specimen WB load test summary A) shear-displacement/slip and B) Crack pattern

Cracking in WB was first observed during service load testing at a shear of 175 kip. An inclined web crack between the load point and support was the first to be observed. Cracks widths in specimen WB partially closed during the unloading stage of the service load test.

Following service load testing specimen WB was loaded to ultimate capacity. Stiffness decreased gradually as load increased beyond the level of the service load tests. Loss of stiffness

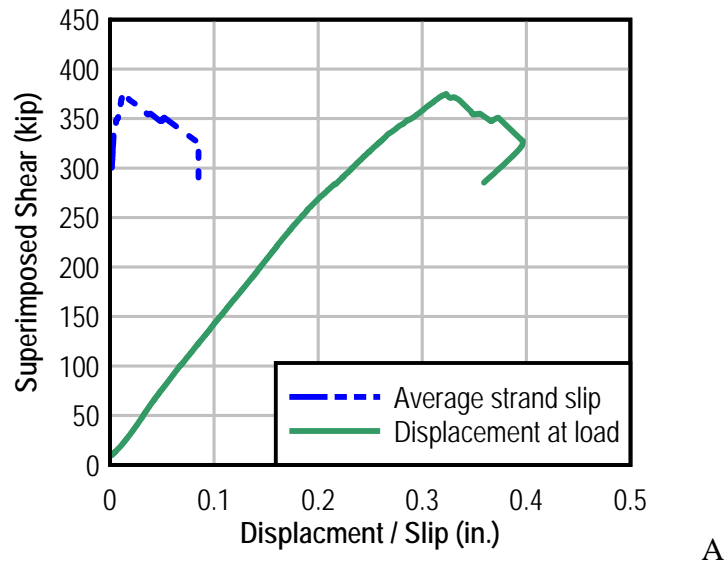
is attributed primarily to flexural cracks which were first observed at a shear of 380 kip. The first flexural crack occurred below the load and intersected cracks in the flange that had formed prior to load testing due to prestress transfer. Additional flexural cracks were observed at a shear of 494 kip.

Specimen WB had the greatest ductility and reached the largest displacement of any test specimen. The displacement at peak load was approximately 1.05in. Peak shear for WB was 612 kip. At peak shear the strands slipped abruptly and the crack in front of the bearing pad opened suddenly. Strand slip and cracking resulted in a sudden loss of load.

The bearing plate and confinement reinforcement in specimen WB maintained the structural integrity of the bottom flange above the bearing throughout load testing. Because the bottom flange held together above the bearing, the strand-concrete bond was also maintained at high load levels in WB. Capacity of the WB was governed by strand-concrete bond, and failure of WB is labeled as a bond-shear failure.

D.6.2.7 FN

The primary features of specimen FN (Figure 22) were lack of an embedded bearing plate and the 'flange' strand bond (Figure 9) pattern that placed (24) fully bonded strands in the outer portions of the bottom flange. Other variables in FN included no horizontal bars in the end region and modified confinement reinforcement. The modified confinement scheme had fewer, but larger, bars than specified by the FDOT. Shear-displacement, shear-slip and crack pattern results for specimen FN are shown in Figure 99.



Release cracks shown black.
 Initial crack shown bold in red.
 Final cracks shown blue.

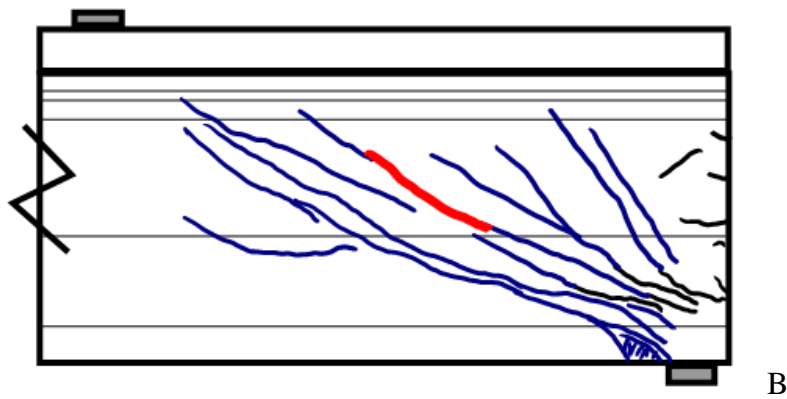


Figure 99–Specimen FN load test summary A) shear-displacement/slip and B) crack pattern

Cracking in FN was first observed during service load testing at a shear of 174 kip. An inclined web crack between the load point and support was the first to be observed. Additional inclined cracks formed and intersected splitting cracks in the bottom flange that had formed prior to load testing due to prestress transfer. Shear in the service load test reached 237kip, but for safety reasons the load was immediately removed and cracks were marked after the specimen was unloaded. The concern with specimen FN was that the strand bond pattern and lack of a

bearing plate could affect a sudden failure. Cracks widths in specimen FN partially closed during the unloading stage of the service load test.

Following service load testing specimen FN was loaded to ultimate capacity. Stiffness decreased as load increased beyond the level of the service load tests, but not to the degree observed with other specimens. Loss of stiffness is attributed to formation and growth of diagonal cracks. Web cracks that formed at lower loads were observed to spread into the bottom flange during the latter stages of testing. Flexural cracks were not observed.

Specimen FN reached a peak shear of 375 kip. This was the smallest peak of any specimen in the test program. At peak shear the strands slipped suddenly and the crack in front of the bearing opened. Slip and cracking was accompanied by a subsequent drop in load. Failure of specimen FN is labeled as a lateral-splitting failure because failure occurred in large part due to transverse splitting cracks in the bottom flange.

Failure of specimen FN can be understood by considering the strut-and-tie model shown in Figure 100. During latter stages of the ultimate load test, shear load was carried through the web into the bottom flange by concrete compression struts. Once in the bottom flange the load split into three separate load paths. The two outer paths connected to nodes at the fully bonded outer stands. The inner path was in the same plane as the web and connected to an inner node above the centerline of the bearing pad. At outer nodes equilibrium in the y-direction was maintained by tie forces in the strands. Y-direction equilibrium at the inner node was maintained by tension force in the concrete. At peak load strands at the outer nodes slipped and the crack in front of the bearing pad propagated into the center of the bottom flange thereby cutting the concrete tie (Figure 101).

The strut-and-tie concept shown in Figure 100 is supported by strain data from the confinement reinforcement which formed the transverse tie between the outside nodes. Strain in the confinement reinforcement increased after peak load. Once the concrete tension tie failed at peak load, force from the inner load path transferred to the outer load paths. Accordingly, additional force was generated in the confinement reinforcement to maintain x-direction equilibrium at the outer nodes. This additional force is responsible for the post-peak increase in strain observed in the confinement reinforcement (Figure 102).

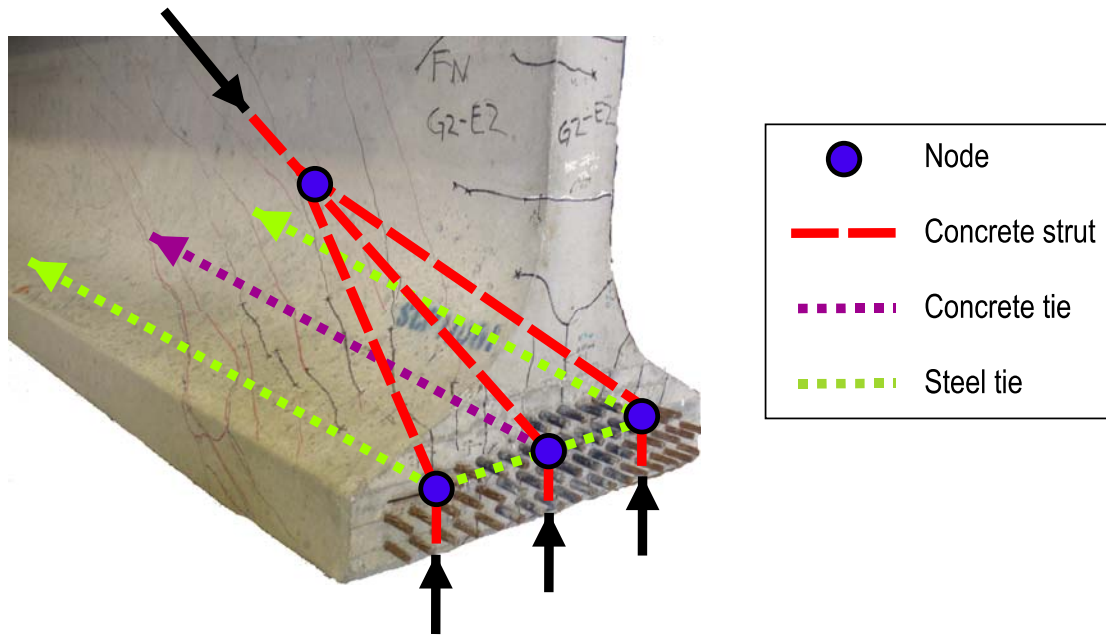


Figure 100–Strut and tie behavior specimen FN

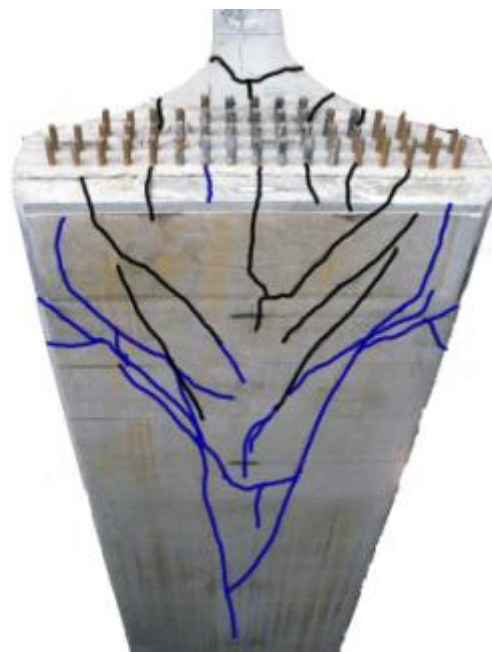


Figure 101–Longitudinal splitting cracks on bottom of specimen FN (release cracks shown black; final cracks shown blue)

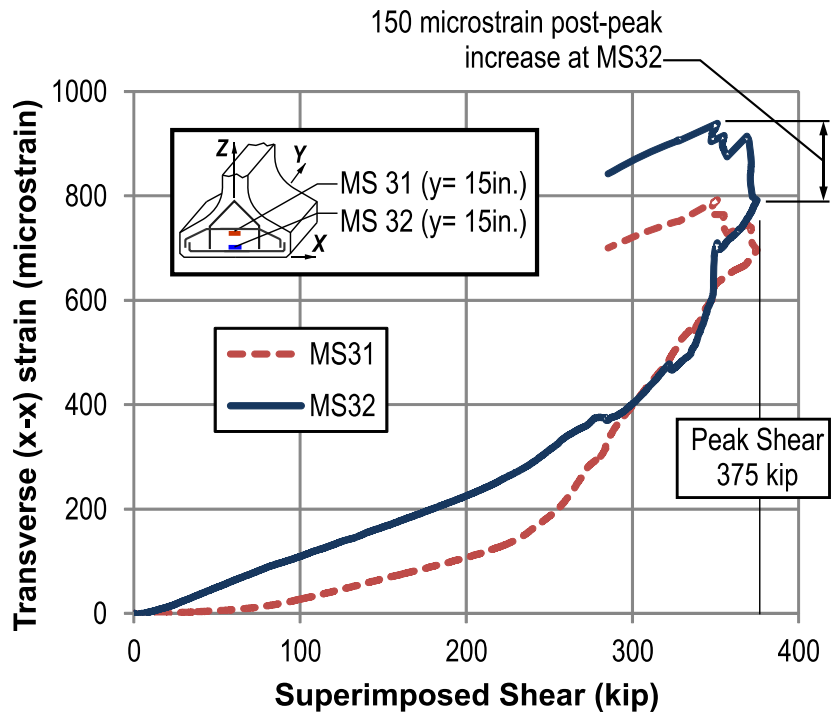


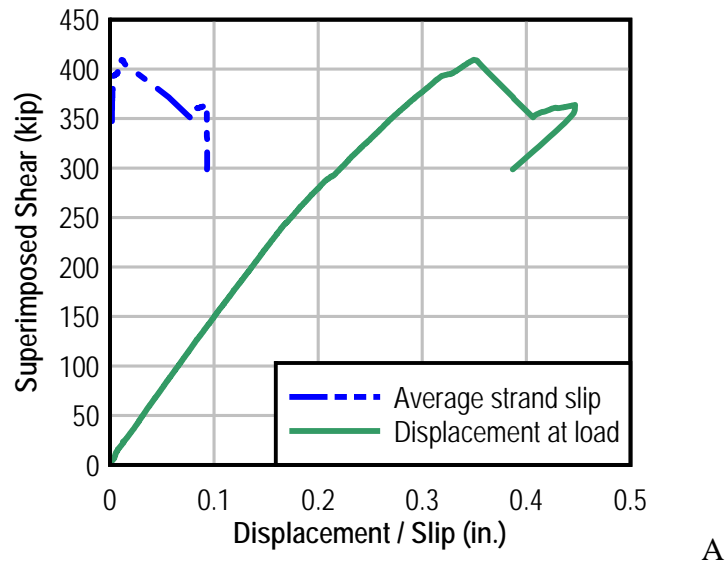
Figure 102–Confinement reinforcement strain specimen FN

D.6.2.8 FB

The primary features of specimen FB (Figure 22) were an embedded bearing plate and the ‘flange’ strand bond pattern (Figure 9) that placed (24) fully bonded strands in the outer portions of the bottom flange. Other variables in FB included no horizontal bars in the end region and modified confinement reinforcement. The modified confinement scheme had fewer, but larger, bars than specified by the FDOT. Shear-displacement, shear-slip and crack pattern results for specimen FB are shown in Figure 103.

Cracking in FB was first observed during service load testing at a shear of 158kip. An inclined web crack between the load point and support was the first to be observed. Cracks widths in specimen FB partially closed during the unloading stage of the service load test.

Following service load testing specimen FB was loaded to ultimate capacity. Specimen FB reached a peak shear of 409 kip. Failure of FB is categorized as a later-splitting failure. Circumstances and failure behavior of specimen FB were the same as those reported for specimen FN. As such, a detailed description of the failure mode is not repeated here.



Release cracks shown black.
 Initial crack shown bold in red.
 Final cracks shown blue.

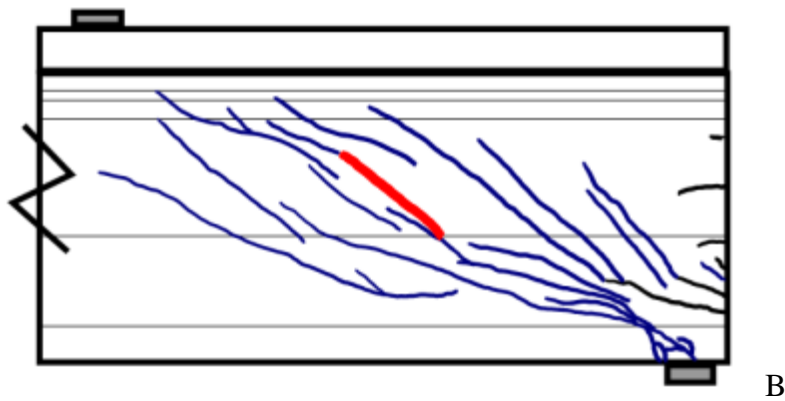


Figure 103–Specimen FB load test summary A) shear-displacement/slip and B) crack pattern

D.6.2.9 DC

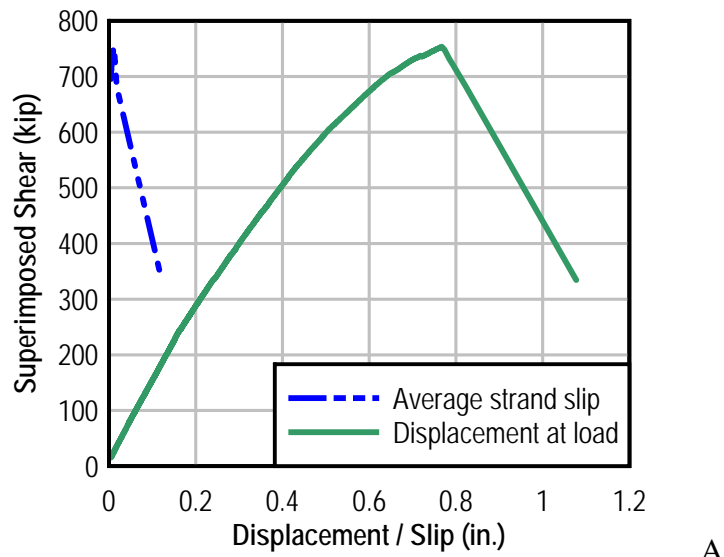
Specimen DC (Figure 23) was detailed according to the 2010 FDOT Interim Design Standards (FDOT, 2010). Variables in specimen DC included FDOT specified confinement reinforcement and bearing plate in the bottom flange, no horizontal reinforcement in the end region, and the ‘design’ strand pattern (Figure 9) which had (39) fully bonded strands. Shear-displacement, shear-slip, and crack pattern are shown in Figure 104.

Cracks in DC were first observed during the service load tests at a shear of 174 kip. Inclined web cracks between the load point and support were the first to be observed. Cracks partially closed during the unloading stage of the service load test.

Following service load testing specimen DC was loaded to ultimate capacity. Stiffness decreased gradually as load increased beyond the level of the service load tests. Because flexural cracks were not observed, the loss in stiffness is attributed to formation and growth of diagonal cracks.

Ultimate capacity was signaled by web crushing followed immediately by movement of the portion of the specimen above the inclined cracks relative to that below the inclined crack. This failure is classified as a web-shear failure. Loss of capacity after the web-shear failure was abrupt. Specimen HC supported a maximum shear of 753 kip.

Figure 104 shows that strand slip in specimen DC was negligible prior to the peak load. Strand slip reported in the figure after peak load was likely exaggerated by cracking of the bottom flange at the end of the load test. Lack of slip observed in DC and other specimens with the 'design' strand bond pattern is attributed to the relatively large quantity of strands.



Release cracks shown black.
 Initial crack shown bold in red.
 Final cracks shown blue.

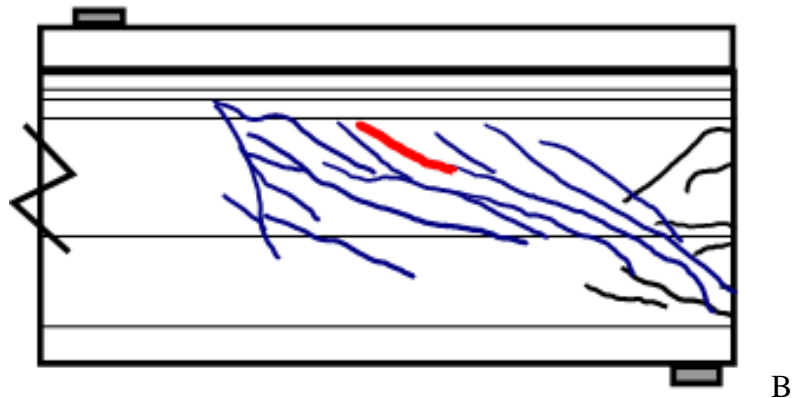


Figure 104–Specimen DC load test summary A) shear-displacement/slip and B) crack pattern

D.6.2.10 DM

Detailing of specimen HC (Figure 23) was effectively identical to the 2010 FDOT Interim Design Standards (FDOT 2010), with the exception that the modified confinement reinforcement scheme was used in the bottom flange. Modified confinement had fewer, but larger, bars than specified by the FDOT. Other variables in specimen DM included a bearing plate in the bottom flange, no horizontal reinforcement in the end region, and the ‘design’ strand

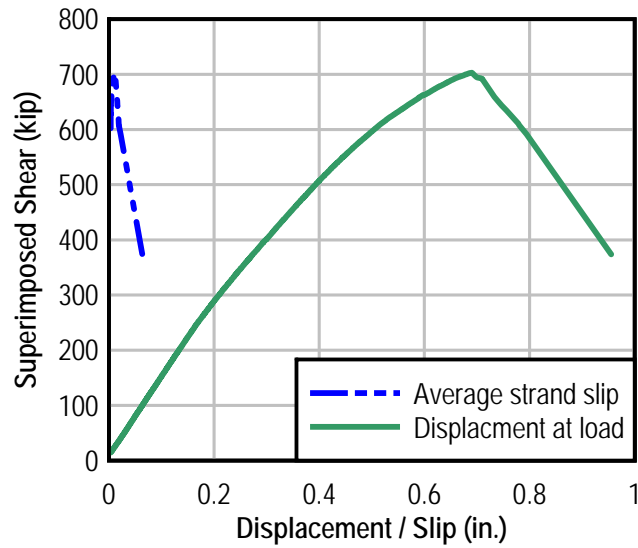
pattern (Figure 9) which had (39) fully bonded strands. Shear-displacement, shear-slip and crack pattern results for specimen DM are shown in Figure 105.

Cracks in DM were first observed during the service load tests at a shear of 166 kip. Inclined web cracks between the load point and support were the first to be observed. Cracks partially closed during the unloading stage of the service load test.

Following service load testing specimen DM was loaded to ultimate capacity. Stiffness decreased gradually as load increased beyond the level of the service load test. Because flexural cracks were not observed, the loss in stiffness is attributed to formation and growth of diagonal cracks.

Failure of specimen DM was a hybrid between lateral-splitting and web-shear. At peak load one of the inclined cracks had a suddenly increased in width. The load dropped approximately 5 kip after the crack opened. Opening of the crack and loss in load occurred in-part due to peeling movement of the bottom flange. Loading continued for approximately 15 sec until the web crushed and the load fell abruptly. After web crushing the top portion of the specimen slid along the cracking plane relative to the lower portion. Concrete spalled away from the web on both sides of the specimen during the web failure. Specimen DM supported a maximum shear of 703 kip. Longitudinal splitting cracks were observed on the bottom of DM after testing, indicative of lateral-splitting failure.

Figure 105 shows that strand slip in specimen DM was negligible prior to the peak load. Strand slip reported in the figure after peak load was likely exaggerated by cracking of the bottom flange at the end of the load test. Lack of slip observed in DM is attributed to the relatively large quantity of strands.

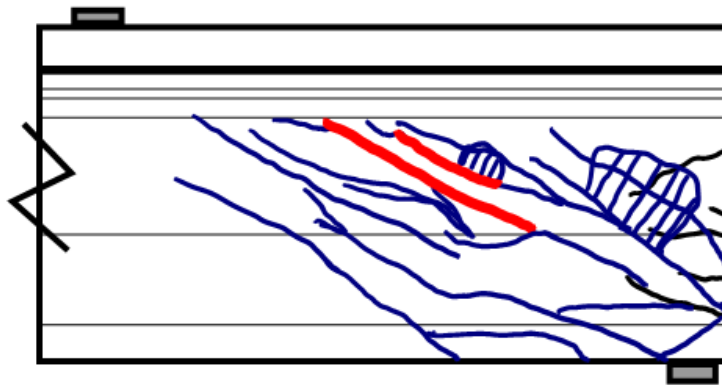


A

Release cracks shown black.

Initial crack shown bold in red.

Final cracks shown blue.



B

Figure 105–Specimen DM load test summary A) shear-displacement/slip and B) crack pattern

D.6.3 Confinement Reinforcement and Bearing Plates

Strain gages were used to monitor bearing plates and select confinement reinforcement assemblies during load testing. Strain data were then used to calculate stresses and forces in the confinement reinforcement and bearing plates. Stresses and forces were calculated at a shear of 375 kip and at each specimen’s maximum capacity. Analyses were conducted at a shear of 375 kip because this force corresponds to the maximum capacity of specimen FN. It is also near the factored shear force in the prototype bridge from which some the specimens were designed.

D.6.3.1 Girders W and F

Confinement reinforcement strain in specimens WN, WB, FN, and FB was monitored during prestress transfer and during load testing. Bearing plate strain was also monitored in WB and FB. Strain from prestress transfer and load testing were superimposed to determine total strain in the confinement reinforcement and bearing plates. It was assumed that strain did not change between prestress transfer and load testing. Although it is unlikely that strain was constant, it is necessary to make this assumption in order to estimate total strain.

Specimens WN, WB, FN, and FB each had the modified confinement reinforcement scheme (Figure 15) which placed five assemblies of confinement reinforcement above the bearing. Three of the five assemblies in each specimen were instrumented with gages (Figure 106). Gages were placed to measure the transverse (x-x) strain.

Combined strain from prestress transfer and load testing was multiplied by the steel modulus of elasticity to determine stress in the confinement reinforcement. Data indicate that confinement stresses were typically less than yield stress. One bar in specimen FN and one bar in WN had reached yield stress as ultimate load. Average stresses for each specimen at a shear force of 375 kip are shown in Figure 107. Figure 108 shows average stresses at ultimate capacity.

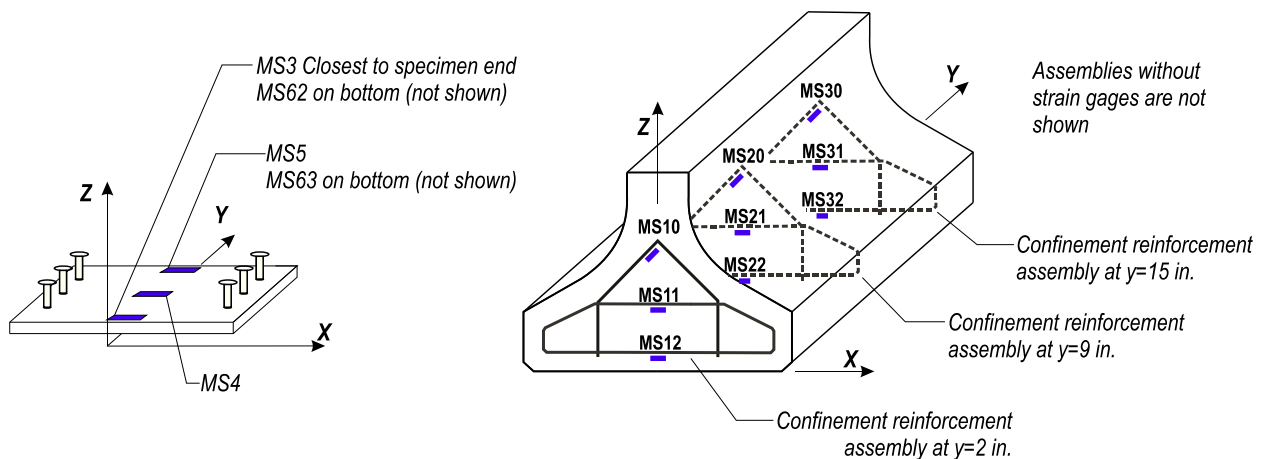


Figure 106–Strain gage placement girders W, F, and D

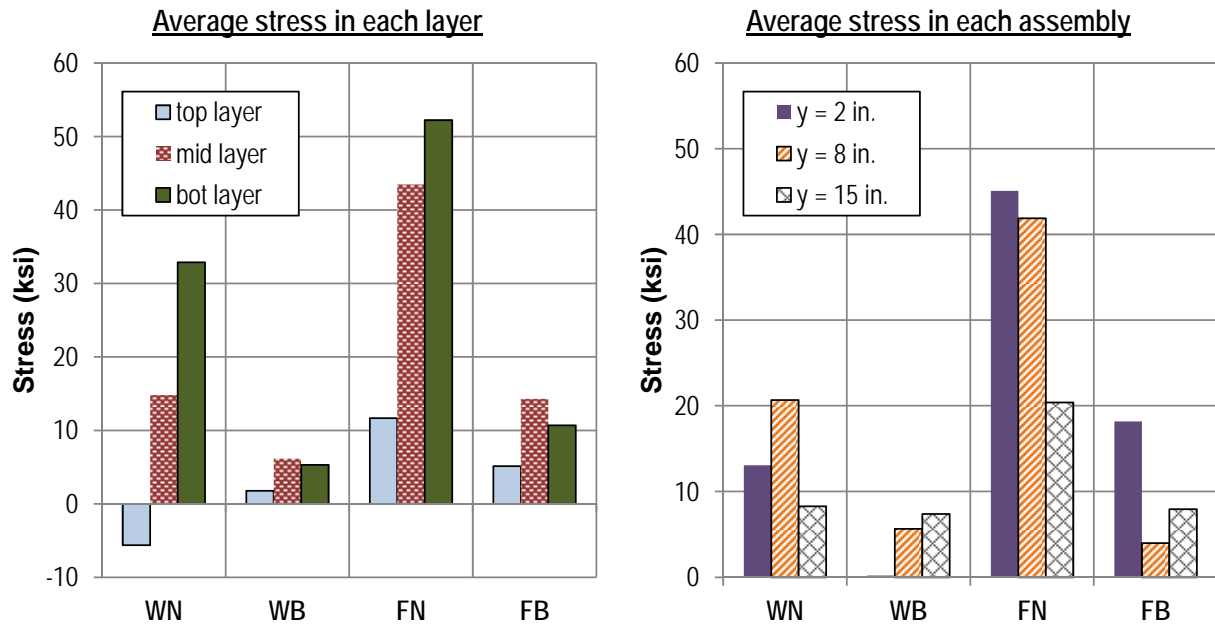


Figure 107–Confinement stress at shear = 375 kip

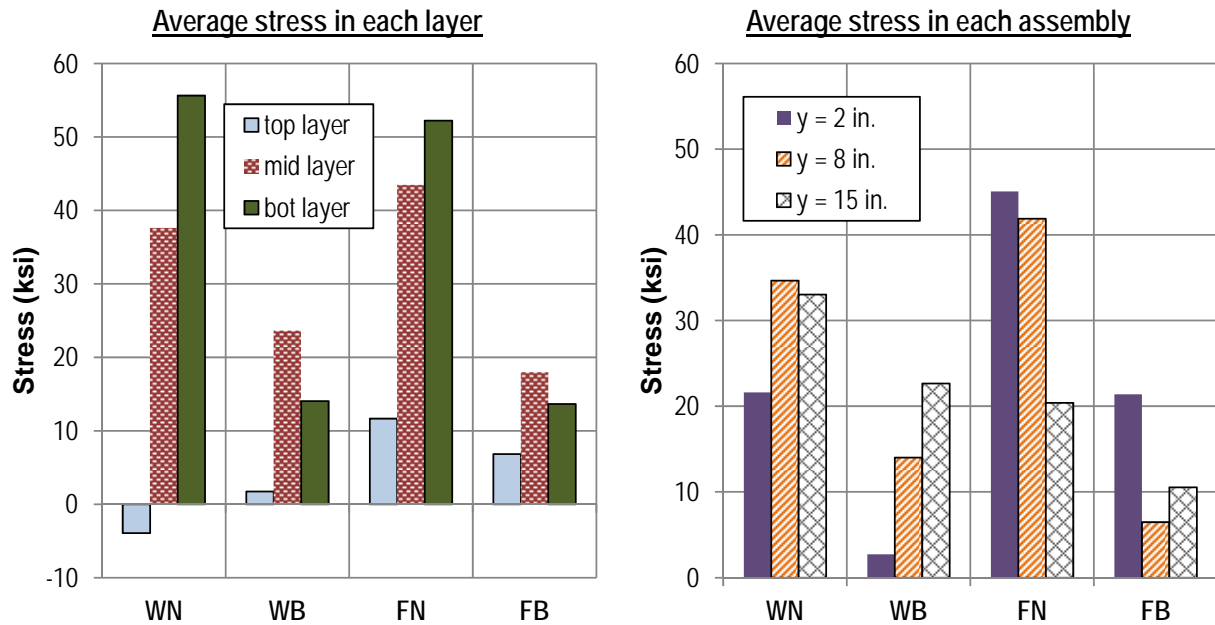


Figure 108–Confinement stress at ultimate capacity

The largest stresses occurred in specimens WN and FN, which did not have bearing plates. At a shear of 375 kip, the average confinement stress in WN and FN was 3.5 times

greater than the average stress in the specimens with bearing plates (WB and FB). At ultimate load the average stress in WN and FN was 2.5 times greater than WB and FB. These differences in stress are attributed to the presence of the steel bearing plate in WB and FB. The stiffness of the plate attracted transverse forces thereby reducing the forces (and stress) in the confinement reinforcement.

Average confinement stress varied according to the reinforcement layer. Average stresses in the middle and bottom layers were 6 to 8 times greater than stress in the top layer. It is believed that tension formed in the bottom flange as shear was delivered from the relatively narrow web to the wider bearing pad. This tension was likely the cause of the greater stress in the bottom and middle layers of confinement. Analytical modeling is presented in Chapter 8 to explore this effect.

Stress distribution in the confinement reinforcement also varied in the y-direction. For specimens with fully bonded strands placed below the web (WN and WB) the average stress in reinforcement at 8in. and 15in. was 1.6 to 2.1 times greater than the stress in reinforcement at 2in. The opposite trend was observed in specimens with fully bonded strands placed in the outer flange (FN and FB). Average stress in reinforcement 2in. from the end of FN and FB was typically 2 times greater than average stress in reinforcement placed at 15in. Similar trends were noted in confinement behavior at prestress transfer as discussed in Chapter D.6. The mechanics presented in Figure 58 and Figure 59 are believed to be culpable in the stress changes observed in stress in the y-direction. Discussion of these mechanics can be found in Chapter D.6 and are not repeated here.

Strand bond pattern also affected the magnitude of the average stresses. At a shear of 375 kip, confinement reinforcement in specimens FN and FB had an average stress that was 2.5 times greater than the average stress in WN and WB. The additional stress in FN and FB is attributed to strand bond pattern which placed fully bonded strands in the outer portion of the flange. This pattern caused transverse tension as described in Figure 84.

Transverse forces in confinement reinforcement and bearing plates (WB and FB only) were estimated by multiplying transverse stresses by the respective cross-sectional areas. Linear interpolation was used to estimate forces in the confinement assemblies that were not monitored with gages. Results are presented in Table 31. Forces from reinforcement with compressive

stress were not included in the results. Only the x-direction components of forces in the top layer were included.

Total transverse force between specimens WN and WB was consistent, suggesting that the presence of a bearing plate did not change the transverse force demand in these specimens.

Transverse forces in specimens FN and FB were not consistent. The bearing plate specimen (FB) had approximately 50% less transverse force. The difference in force between FB and FN is attributed to the bearing plate mechanics in specimen FB. Experimental data indicate that the bearing plate in FB carried an in-plane bending moment during loading. This behavior resulted in tensile and compressive forces in the bearing plate (Figure 109). The causes of the in-plane moment are the force and eccentricity of the outside strands (Figure 84). By carrying in-plane moment, the plate reduced the magnitude of transverse forces typically associated with the outer strands. In-plane bending of the plate in Specimen WB was not observed.

Table 31–Transverse forces in W and F specimens

		WN (kip)	WB (kip)	FN (kip)	FB (kip)
Shear of 375 kip	Confinement reinforcement	50	15	107	27
	Bearing plate	0	36	0	30
	Total	50	51	107	58
Ultimate load	Confinement reinforcement	95	40	107	35
	Bearing plate	0	70	0	30
	Total	95	111	107	65

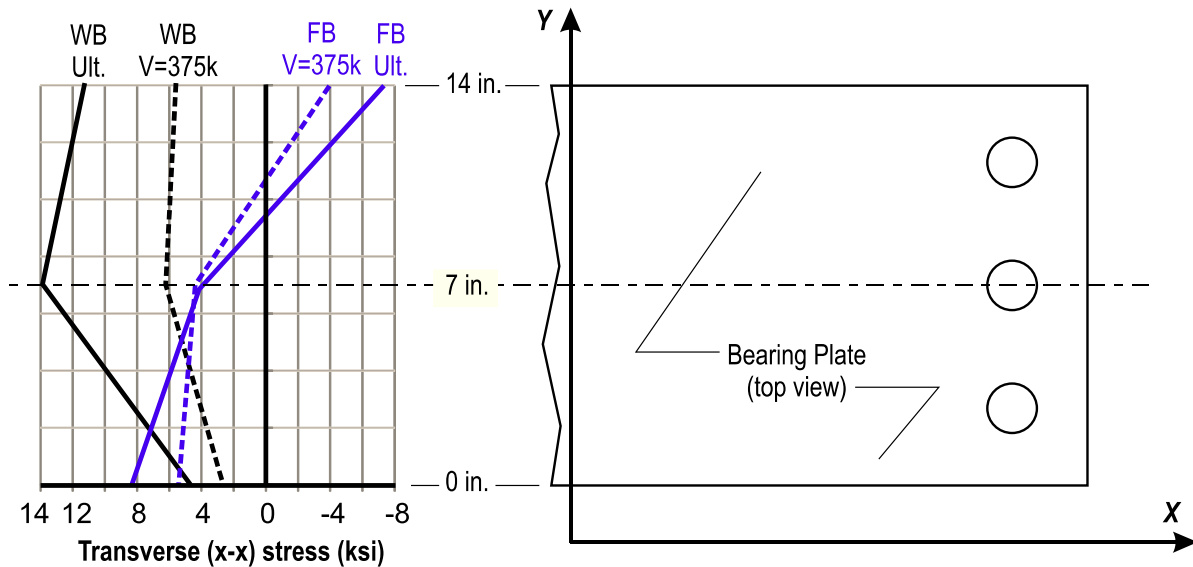


Figure 109–Transverse (x-x) stress profiles at bearing plate centerline

D.6.3.2 Girders H and V

Strain gages were placed on confinement reinforcement and bearing plates in specimens HC and VC to monitor strain during loading (Figure 110). Stresses and forces in these elements were estimated in the same manner as was done for specimens in girders W and F. Forces at ultimate load are shown in Figure 111, and are due to applied load only. Confinement strain data were not collected during prestress transverse in specimens VC and HC, and the effects of transfer are not included in Figure 111. In calculating the forces it was assumed the total strain in the confinement and plates was less than the yield strain. This assumption appears valid for HC and VC because yielding was only reached in two of the 36 bars that were monitored in girders W and F, and because the yielded bars occurred in specimens without bearing plates.

The estimated tensile force carried by all confinement reinforcement was 25.7 kip and 30.3 kip for specimens HC and VC, respectively. These forces equate to approximately 4% of the reaction at ultimate load. The largest confinement reinforcement forces occurred near the end of the specimens. At locations farther away from the end, the confinement reinforcement carried compressive forces, thus confirming the theoretical behavior presented in Figure 84.

The transition from tensile to compressive action in the confinement reinforcement is estimated to have occurred at distances approximately 40in. and 50in. from the specimen ends (Figure 111). The flexural depth (d) of the non-composite member was 49in. Comparing the distribution of confinement forces with the flexural depth shows that all tension in the

confinement reinforcement occurred within d of the member end. Current AASHTO LRFD requirements specify that confinement reinforcement must extend at least $1.5d$ from the member end. The experimental results suggest that this requirement is conservative, and that more effective placement of confinement reinforcement is possible. Other researchers (Tadros et al. 2010) have also suggested that the required distribution of confinement reinforcement should be reduced to less than $1.5d$.

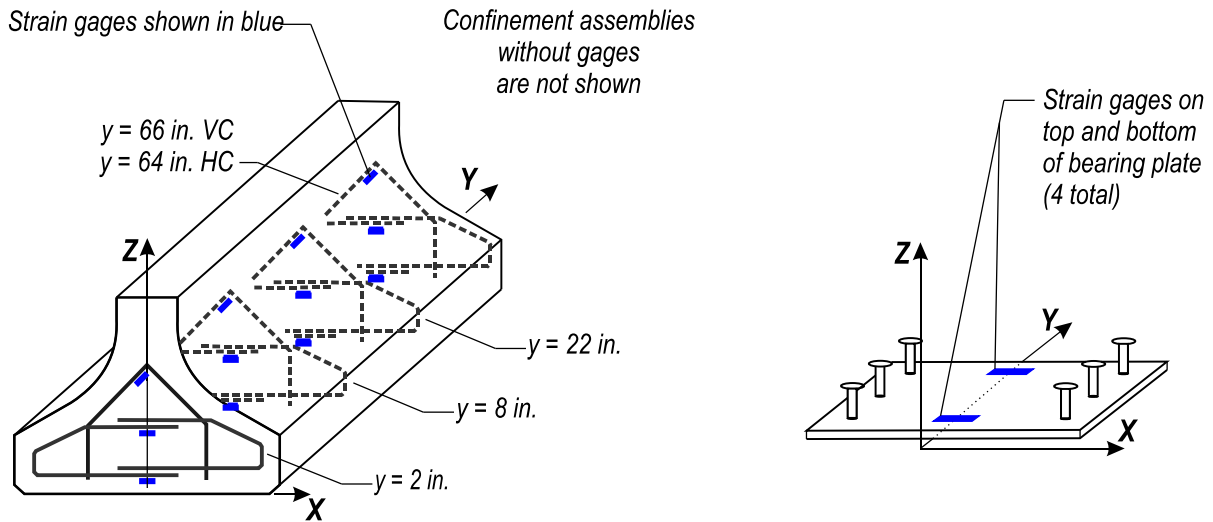
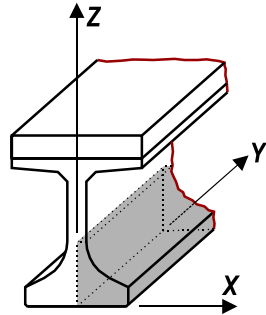
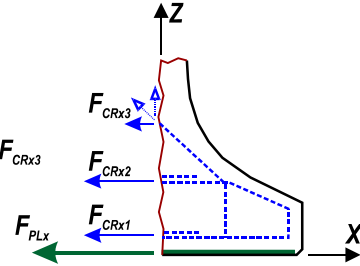


Figure 110—Strain gage placement girders H and V

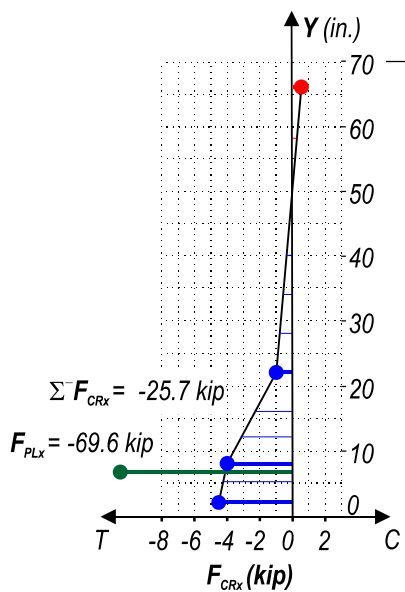


End region
isometric view

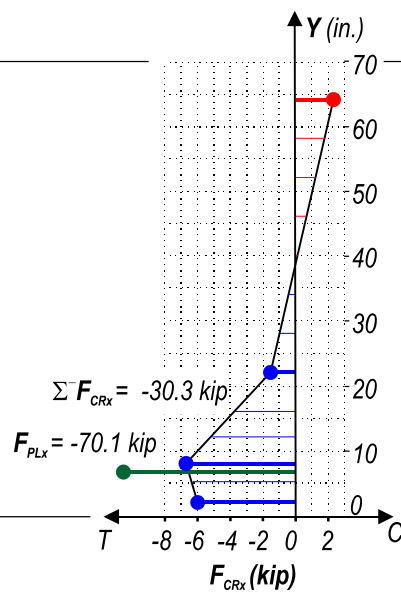
$$F_{CRx} = F_{CRx1} + F_{CRx2} + F_{CRx3}$$



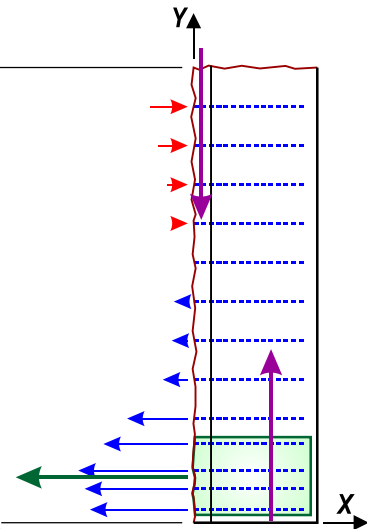
Bottom flange section
end view



Bottom flange forces
specimen HC



Bottom flange forces
specimen VC



Bottom flange section
partial plan view

Figure 111—Specimens HC and VC confinement reinforcement and bearing plate transverse (x-x) forces due to maximum applied load

D.6.3.3 Bearing Plates

Eight of the ten experimental specimens had embedded steel bearing plates. Strain in each bearing plate was monitored during load testing. Average stresses in the bearing plates were calculated by multiplying the average experimental strain by the elastic modulus. Bearing plate stresses due applied load (effects of prestress transfer not included) are presented in Figure 112. At ultimate load the average stresses ranged from 2.4 ksi (FB) to 10.6 ksi (VU). The

relatively low average stress in specimen FB was due to in-plane bending of the plate as discussed previously.

Bearing plate forces were calculated by multiplying the average stresses by the cross-section areas (Figure 113). Net tension force in the bearing plates at ultimate load ranged from 96.2 (VU) to 16.5 kip (FB). The average tension force at ultimate load was 62.9 kip.

Tension forces in the bearing plates are compared to the total transverse force in Figure 114. For this figure the total transverse force is defined as the combined transverse force in the bearing plate plus confinement reinforcement. Forces in Figure 114 are due to applied loads only. On average the bearing plates carried 60% to 71% of the total transverse force due to the applied load.

The portion of transverse force carried by the bearing plates at prestress transfer was evaluated using data from specimens WB and FB. As shown in Figure 115, contribution of the bearing plate at prestress transfer was affected by the strand bond pattern. The bearing plate in specimen FB (bonded strands in outer flange) carried almost 77% or the total transverse force at prestress transfer, whereas the plate in specimen WB (inner strands bonded) carried 52% of the transverse force at transfer.

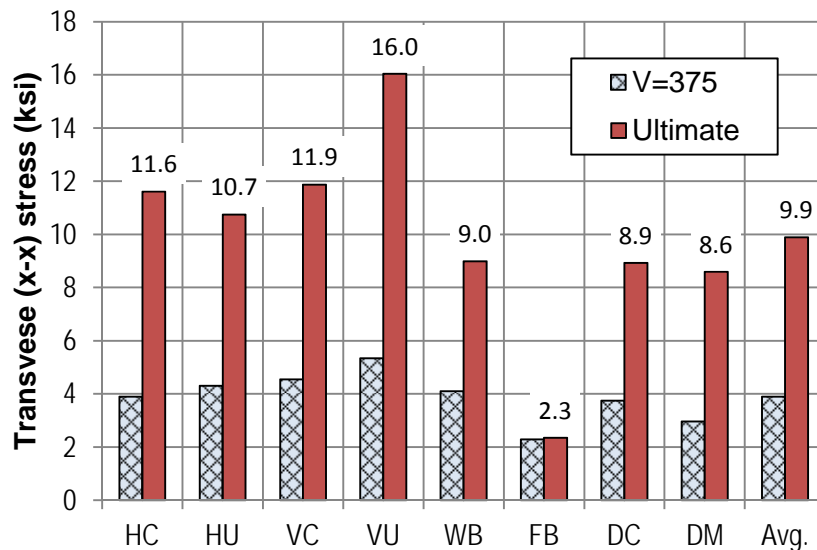


Figure 112–Bearing plate stress due to applied load

Experimental data presented in this section indicate that bearing plates in FIB girders will typically carry more than 50% of transverse splitting forces. Thus for purposes of designing

confinement reinforcement it is conservative to assume that the bearing plate will carry no more than 50% of transverse force.

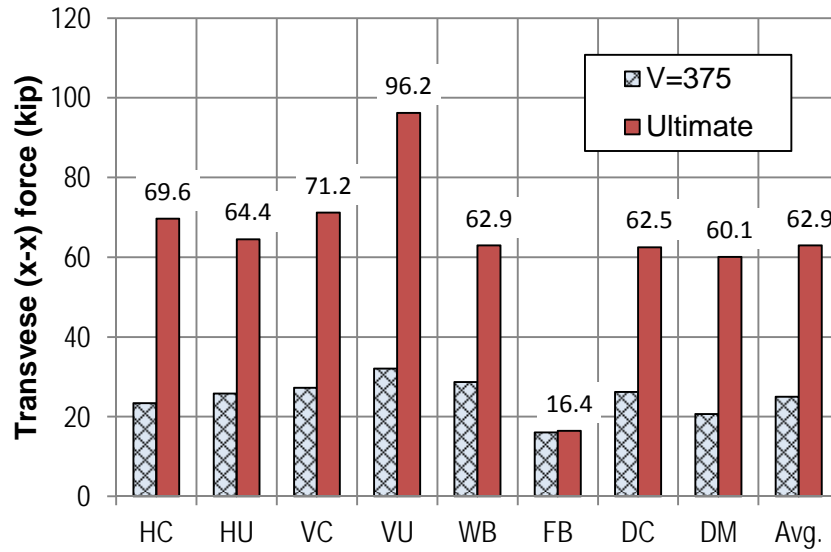


Figure 113–Bearing plate force due to applied load

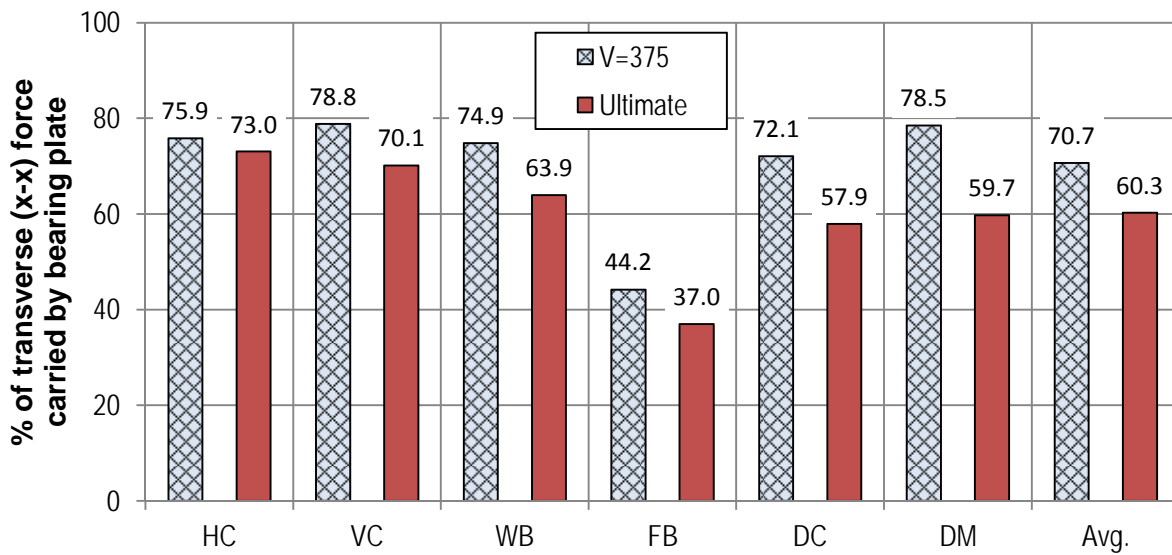


Figure 114–Percent of transverse force due to applied loads carried by bearing plate

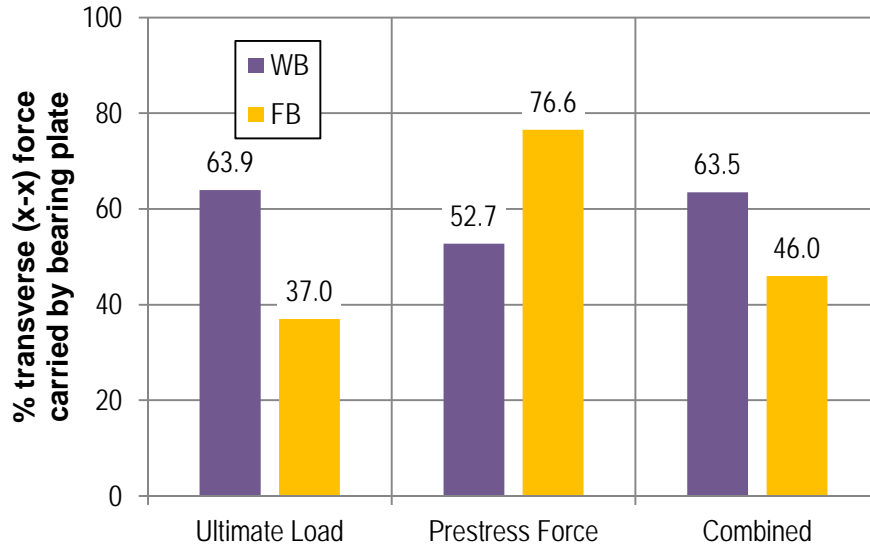


Figure 115–Percent of transverse force carried by bearing plate in WB and FB

D.6.4 Variable Comparisons

Maximum superimposed shear for each specimen are reported in Figure 116 and Table 32. Values ranged from a high of 766 kip (HC) to a low of 375 kip (FN), with an average of 612 kip. The large degree of variation in these results is a testament to the effect that detailing can have on end region behavior and capacity, even for members having the same cross-section and materials properties. Effects of the variables are discussed below and are summarized in Table 33.

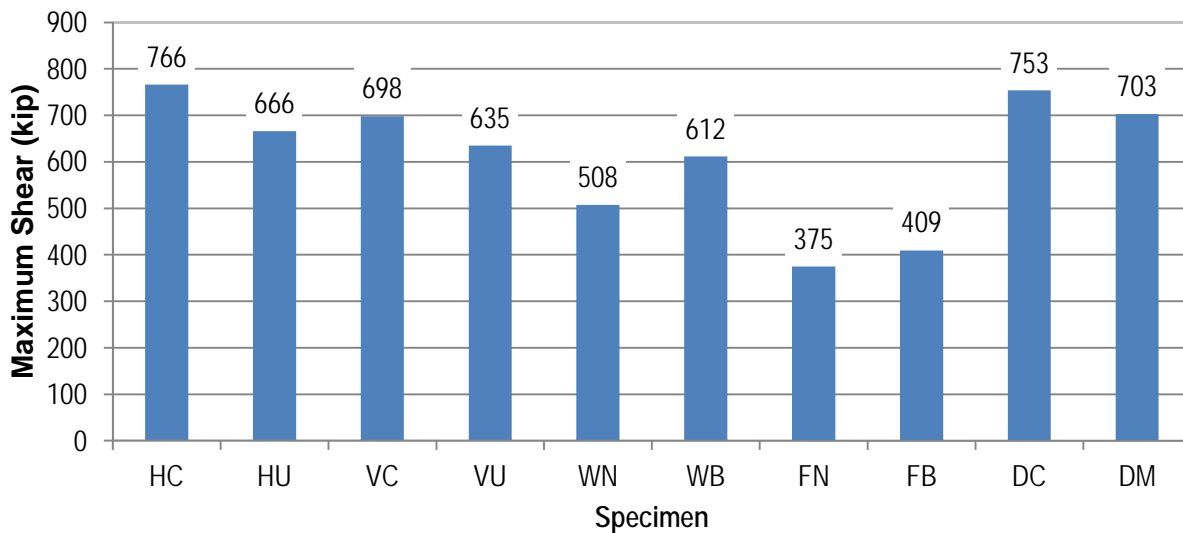


Figure 116–Maximum superimposed shear

Table 32–Maximum superimposed shear

Specimen	Maximum superimposed shear (kip)	Maximum shear / average shear
HC	766	1.25
HU	666	1.09
VC	698	1.14
VU	635	1.04
WN	507	0.83
WB	612	1.00
FN	375	0.61
FB	409	0.67
DC	753	1.23
DM	703	1.15
Average	612	1.00

Table 33–Variable comparisons

Variable	Relevant specimens	Result
Horizontal reinforcement	HC, DC	Negligible effect on end region capacity in specimens failing in web-shear
Bearing plate	WN, WB, FN, FB	9% to 21% capacity increase from bearing plate
FDOT vs. no confinement reinforcement	HC, HU, VC, VU	13% capacity increase from FDOT confinement reinforcement
FDOT vs. modified confinement reinforcement	DC, DM	7% capacity increase from FDOT confinement reinforcement
Strand quantity	All	Average capacity increase of 18.4 kip / bonded strand
Strand placement	WN, WB, FN, FB	43% capacity increase for strands placed near centerline relative to strands placed in outer flange

D.6.4.1 Horizontal Reinforcement

The 2008 FDOT interim standard for FIB-54 girders (FDOT 2008) called for horizontal bars to be placed in girder end regions. For reasons unrelated to the current test program, this detail was changed such that the 2010 FDOT interim design standard (FDOT 2010) eliminated horizontal bars. Effects of the horizontal reinforcement can be evaluated using results from specimens HC and DC. Specimens HC and DC were effectively identical with the exception of horizontal reinforcement placed in HC. Failure loads of these specimens were within 2% of each other, and both specimens failed in a web-shear mode. This result suggests that the relatively small amount of horizontal reinforcement placed in specimen HC had negligible effect on behavior or capacity.

Previous research by the authors (Ross et al. 2011) has shown that horizontal reinforcement improves ductility in girders having a critical failure mode of bond-shear. Specimens HC and DC failed in web-shear, thus indicating that horizontal reinforcement had negligible impact when web-shear was the critical failure mode.

D.6.4.2 Embedded Steel Bearing Plate

FDOT details call for embedded steel plates to be placed at the end of I-girders above the bearing location. Inclusion of the plates in the FDOT detail was based on recommendations by Cook and Reponen (2008), and was implemented to prevent cracks at the bottom corner of girders during fabrication. Embedded steel bearing plates were included as a variable in the current test program to evaluate the effects of bearing plates on bottom flange confinement.

Specimens WB and WN had identical detailing with the exception of the bearing plate which was excluded from specimen WN. Specimen WB had a bearing plate and a capacity of 612 kip. This was 21% greater than the 507 kip capacity of WN. Both specimens failed in bond-shear mode. The additional capacity in specimen WB is attributed to the confining effect of the bearing plate that helped maintain structural integrity of the bottom flange above the bearing. Because the bottom flange held together, strand-concrete bond in WB was maintained at loads beyond which specimen WN (no bearing plate) lost strand-concrete bond.

Specimens FB and FN also had identical detailing with exception of the bearing plate which was excluded from FN. Specimen FB had a bearing plate and a capacity of 409 kip. This was 9% larger than the 375 kip capacity of specimen FN. Both specimens failed in laterally-splitting mode. The additional capacity of specimen FB is attributed to the bearing plate, however the effect of the bearing plate was not as pronounced as the effect between specimens WN and WB.

D.6.4.3 Confinement Reinforcement

Three different confinement reinforcement schemes (Figure 15) were used in the test specimens. The current FDOT confinement scheme was used in specimens HC, VC, and DC. A modified confinement scheme was used in specimens WN, WB, FN, FB, and DM. The modified confinement scheme had fewer but larger bars than the FDOT scheme. Specimens HU and VU had the final scheme, in which confinement reinforcement was totally omitted.

FDOT vs. No Confinement. Specimens HC, VC, HU, and VU contained comparable variables and can be used to evaluate FDOT confinement relative to specimens with no confinement. HC and VC had FDOT confinement reinforcement and failed in a web-shear mode. The capacity of HC and VC was on average 13% larger than the capacity of HU and VU which had no confinement reinforcement. HU and VU failed in a later-splitting mode. Thus omission of confinement reinforcement allowed lateral-splitting failure of the bottom flange and

decreased capacity by 13%. Or, conversely, the presence of confinement reinforcement forced failure away from the bottom flange, thereby increasing capacity by an average of 13%.

FDOT vs. Modified Confinement. Detailing of specimens DC and DM (Figure 13) was identical with the exception of confinement reinforcement. DC had FDOT confinement reinforcement and a capacity of 753 kip, whereas DM had modified confinement reinforcement and a capacity of 703 kip. Failure mode was different between these specimens. In specimen DC the FDOT confinement reinforcement was sufficient to prevent lateral-splitting failure, thereby forcing a web-shear failure. Confinement reinforcement in DM was insufficient to prevent lateral-splitting of the bottom flange. Thus the current FDOT detail for confinement provides more effective confinement at ultimate load than the modified scheme. One reason that the FDOT scheme was superior is because it placed confinement bars in front of the bearing where they can act as stirrups. Confinement reinforcement as stirrups was postulated by Csagoly (1991). Confinement bars were not provided away from the bearing in the modified scheme. This allowed propagation of cracks in front of the bearing of specimen DM (Figure 117).

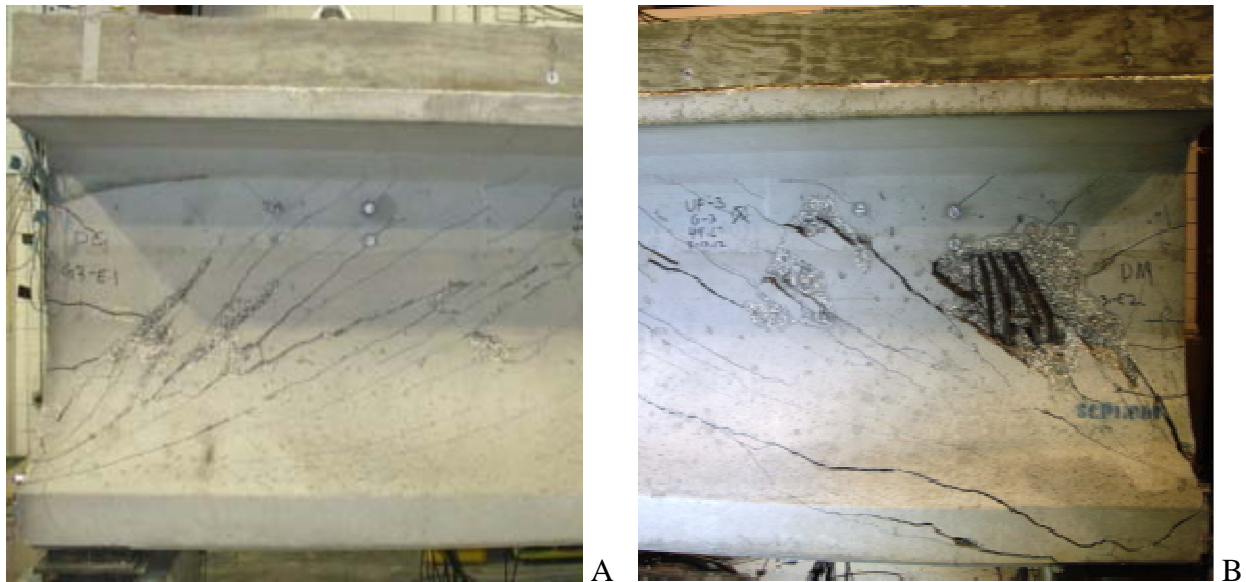


Figure 117–Girder D bottom flange cracking A) specimen DC with limited bottom flange cracking in front of bearing and B) specimen DM with severe bottom flange cracking in front of bearing

D.6.4.4 Strand Quantity

Strand quantity had a greater effect on specimen capacity than any other variable in the test program. Average capacity of specimens with (39) fully bonded strands was 48% greater than the average capacity of specimens with only (24) fully bonded strands. The relationship between strand quantity and experimental capacity is described in Figure 118. The figure shows a linear trend line that was fit to the experimental data. The trend line has an R^2 value of 0.69, indicating a reasonable degree of correlation between experimental capacity and strand quantity.

Current AASHTO LRFD requirements limit the quantity of partially shielded strands to 25% of the total strand count. Providing limits on strand shielding is considered good practice in light of the experimental results. Based on experimental data, every strand that was shielded resulted in a roughly proportional decrease in capacity. The data also suggest, however, that the means by which AASHTO LRFD limits strand shielding can be improved. Rather than limiting shielding to an arbitrary percentage, it is more rational to limit shielding according to the total number of bonded strands required to provide the necessary end region capacity. If sufficient strands are available to support the required capacity, than shielding of the remaining strands can reasonably be permitted. As will be discussed later, the minimum longitudinal reinforcement requirements of AASHTO section 5.8.3.5 can be employed to determine the necessary strand quantity for a given load demand.

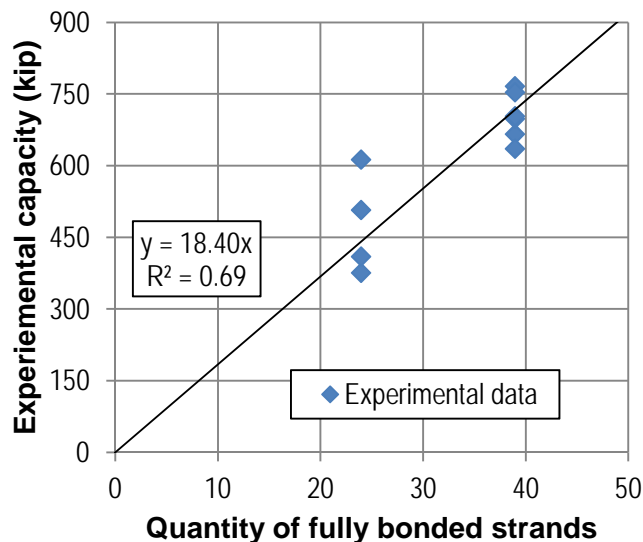


Figure 118—Relationship between strand quantity and end region capacity

D.6.4.5 Strand Placement

Strand placement can be evaluated using results from WN, WB, FN, and FB. Fully bonded strands in WN and WB were placed primarily in the center of the bottom flange below the web. In FN and FB, fully bonded strands were placed in the outer portions of the flange (Figure 9). Specimens WN and WB (strands below the web) failed in a bond-shear failure mode and at an average load that was 43% greater than specimens FB and FN (fully bonded strands in the outer flange). Specimens FB and FN failed in lateral-splitting mode. Crack patterns associated with the different strand patterns and failure modes are shown in Figure 119.

To maximize end region capacity and prevent lateral-splitting failures it is desirable to place strands as close to the cross-section centerline as practical. Doing so minimizes the horizontal eccentricity between prestressing forces and the equal but opposite internal force. This in-turn reduces the propensity for lateral-splitting in the bottom flange.



Figure 119–Comparison of FB (left) and WB (right)
(release cracks shown black; final cracks shown blue)

D.6.5 Code Comparisons

Experimental moments and shears in this section include both the applied load *and* self-weight of the specimens. Experimental moment is denoted as M_{exp} and is defined as the maximum moment occurring during testing at the section below the point load. Experimental shear is denoted as V_{exp} and is defined as the maximum shear occurring during testing at the near support.

Nominal capacities were calculated using the material properties listed in Table 34. These values are representative of the tested properties of materials in the experimental girders. The following paragraphs explain the calculation procedures used to determine nominal capacities.

Table 34—Material properties for capacity calculations

Property	Value
Prestressing strands ultimate strength	285 ksi
Vertical reinforcement yield strength	68 ksi
Concrete deck compressive strength	6500 psi
Concrete girder compressive strength	11000 psi

Nominal Moment Capacity. None of the experimental specimens failed in flexure; however nominal moment capacities were still calculated for reference purposes. Capacity was calculated using principals of strain compatibility and equilibrium. Typical assumptions for concrete in flexure were applied. Nominal moment capacity is denoted as M_n . Shear associated with nominal moment is denoted as V_{Mn} .

AASHTO LRFD Nominal Shear Capacity. Concrete contribution to shear capacity was calculated using the General Procedure from section 5.8.3.4.2 of AASHTO LRFD (2007). This procedure is based on the modified compression field theory (MCFT). Steel contribution was calculated using AASHTO LRFD Equation 5.8.3.3-4. AASHTO LRFD nominal shear capacity is denoted as V_{nLRFD} .

ACI Nominal Shear Capacity. Concrete contribution was calculated using section 11.3.3 of ACI 318 (2011). Provisions in this section are commonly referred to as the ACI detailed method. Steel contribution was calculated using the provisions of section 11.4.7. ACI nominal shear capacity is denoted as V_{nACI} .

Nominal Tie Capacity (Minimum longitudinal reinforcement). Nominal tie capacity calculations are based on the minimum longitudinal steel requirement in AASHTO LRFD 5.8.3.5. Equation 5.8.3.5-2 requires that sufficient longitudinal reinforcement be provided to carry tie forces at the bearing. Bond-shear failure is likely when the tie is insufficient. Procedures from Ross et al. (2011) were used to calculate the shear force that accompanies the nominal tie capacity. These procedures encompass the AASHTO LRFD requirements, but were derived for application to test specimens. Shear associated with nominal tie capacity is denoted as V_{nT} . In making the tie calculations, an available development of 22 in. was assumed. Forces in the strands were then calculated using the bi-linear relationship from AASHTO LRFD for strand development.

For each specimen the experimental moment was less than the calculated nominal moment capacity (Table 35). This result is in agreement with experimental specimens, in which no flexural failures were observed. Most specimens carried experimental moments that were between 60% and 75% of their nominal moment capacity.

Table 35–Experimental moments and nominal moment capacities

Specimen	M_{exp} (kip-ft)	M_n (kip-ft)	V_{exp} (kip)	V_{Mn} (kip)	M_{exp}/M_n
HC	7384	10295	793	1098	0.72
HU	6478	10295	697	1098	0.63
VC	6746	10295	725	1098	0.66
VU	6155	10295	662	1098	0.60
WN	4954	6570	534	700	0.75
WB	5939	6570	639	700	0.90
FN	3716	6720	402	716	0.55
FB	4035	6720	436	716	0.60
DC	7262	10295	780	1098	0.71
DM	6793	10295	730	1098	0.66

Nominal and experimental shear capacities are compared in Table 36. The AASHTO LRFD and ACI nominal shear capacities are based on web-shear failure, which was only observed in four of ten specimens. Bond-shear failure, the assumed failure mode of the AASHTO tie capacity, was only observed in two of the ten specimens. Because of

inconsistencies between code-assumed and experimentally observed failure modes, the comparisons shown in Table 36 are useful for relative comparisons only.

Table 36–Experimental shear and nominal shear capacities

Specimen	V_{exp} (kip)	AASHTO Shear		ACI Shear		AASHTO Tie	
		V_{nLRFD} (kip)	V_{exp} / V_{nLRFD}	V_{nACI} (kip)	V_{exp} / V_{nACI}	V_{nT} (kip)	V_{exp} / V_{nT}
HC	793	590	1.34	490	1.62	754	1.05
HU	697	590	1.18	490	1.42	754	0.92
VC	725	590	1.23	490	1.48	658	1.10
VU	662	590	1.12	490	1.35	658	1.01
WN	534	528	1.01	454	1.18	553	0.97
WB	639	528	1.21	454	1.41	553	1.16
FN	402	528	0.76	454	0.89	563	0.71
FB	436	528	0.83	454	0.96	563	0.77
DC	780	590	1.32	490	1.59	754	1.03
DM	730	590	1.24	490	1.49	754	0.97
Average			1.12		1.34		0.97

Although inconsistent with failure modes, calculated nominal capacities were typically conservative relative to the experimental results. ACI shear calculations were the most conservative, and resulted in nominal capacities 34% less on average than the experimental results. AASHTO shear capacity was an average of 12% less than the experimental results. AASHTO tie nominal capacity was an average of 3% greater than the ultimate strength.

Specimens FN and FB were the only specimens with calculated nominal capacities significantly greater than the experimental shear forces. These specimens failed in lateral-splitting. This type of failure is not explicitly considered in ACI or AASHTO code provisions. Because ACI and AASHTO codes do not account for lateral-splitting failure, code-based capacities for specimens FN and FB were unconservative (i.e. greater than experimental capacity). This result demonstrates the need for code provisions that account for lateral-splitting failure.

The nominal tie method was the most accurate method for calculating end region capacity of the experimental specimens. Average strength calculated by the nominal tie method was 3% greater than the average of the experimental capacities. It must be noted, however, that nominal capacity calculated by the tie method is highly dependent on the values that are assumed for the required and available development lengths. The AASHTO LRFD code does not give

specific requirements for selecting these values. Rather the code states, “Any lack of full development length shall be accounted for.” In spite of the ambiguity in code language, the agreement shown between experimental and nominal tie capacities demonstrate the utility of this method for designing I-girder end regions. In particular, this method is useful in determining the number of bonded strands required at the girder end to preclude a bond-shear failure.

D.7 Summary and Conclusions

Ten uniquely detailed FIB-54 specimens were load tested in three-point bending at a shear span-to-depth (a/d) ratio of 2.0. Variables in the test program included:

- Presence/absence of confinement reinforcement
- Quantity and configuration of confinement reinforcement
- Presence/absence of horizontal reinforcement
- Quantity of vertical reinforcement
- Presence/absence of embedded steel bearing plates
- Strand quantity
- Strand placement

The following conclusions are made:

- Differences in detailing have significant effect on the end region capacity, even for members having the same cross-section. All test specimens used the FIB-54 cross-section, yet experimental capacities ranged from a maximum of 766 kip to a minimum of 375 kip.
- Horizontal reinforcement in the end region has negligible effect on the capacity of members failing in web-shear. The test specimen with horizontal reinforcement had no significant increase in capacity relative a comparable specimen without horizontal reinforcement.
- Embedded steel bearing plates provide confinement to the bottom flange, thereby improving end region capacity. Test specimens with bearing plates had 9% to 21% greater capacity relative to comparable specimens without bearing plates.
- Confinement reinforcement can be used to mitigate lateral-splitting failure, thereby improving end region capacity. Test specimens with confinement reinforcement per current FDOT specifications failed in web-shear mode and at an average load 13% higher than comparable specimens without confinement. Specimens without confinement failed in lateral-splitting.
- To mitigate lateral-splitting failure confinement reinforcement must have sufficient quantity and effective placement. Lateral-splitting failure was observed

in specimens with confinement reinforcement placed only above the bearing. A comparable specimen with confinement placed throughout the strand transfer length failed in web-shear and at a 7% higher load.

- Bearing plates carry a significant portion of transverse splitting forces. Up to 79% of the transverse tension was carried by bearing plates in the test program.
- For purposes of designing confinement reinforcement it is conservative to assume that bearing plates carry 50% or less of the transverse splitting force.
- Girders with fully bonded strands in the outer flange have greater transverse splitting forces than due girders with fully bonded strands placed below the web. In the test program, transverse force in confinement reinforcement was up to 2.5 times larger in specimens with strands in the outer flange relative to those with strands below the web.
- Strand quantity had the greatest effect on end region capacity of any variable in the test program. Specimens with 39 fully bonded strands had an average capacity that was 43% greater than specimens with 24 fully bonded strands.
- There was a reasonable degree of correlation ($R^2=0.69$) between quantity of fully bonded strands and experimental end region capacity. As such, design of strand shielding based on longitudinal tie capacity appears to be a rational design approach. This approach may give better results than the arbitrary shielding limits imposed by current AASHTO LRFD specifications.
- There is need for code provisions that explicitly address lateral-splitting failure. Current shear and longitudinal tie provisions resulted in nominal capacities that were unconservative (too large) for some specimens failing in lateral-splitting.